DEVELOPING SIGNAL PROCESSING AND FEATURE EXTRACTION METHODS FOR BRAIN COMPUTER INTERFACE

A Thesis

Submitted in fulfillment of the requirements for the award of the degree of

DOCTOR OF PHILOSOPHY

In

Electronics and Communication Engineering

By

Tanvi Dovedi
Regn. No: 901806015

Under the supervision of

Dr. Rahul Upadhyay (Associate Professor, ECED)
Dr. Vinay Kumar (Associate Professor, ECED)

Department of Electronics and Communication Engineering

Thapar Institute of Engineering & Technology

(Deemed to be University)

Patiala-147004, India

May, 2024

…dedicated to my parents

Declaration

I, **Tanvi Dovedi**, hereby certify that the work being presented in the thesis, entitled **"Developing signal processing and Feature Extraction methods for Brain Computer Interface,"** submitted in Thapar Institute of Engineering and Technology, Patiala, in fulfillment of the requirement for the award the degree of Doctor of Philosophy in Electronics and Communication Engineering, is an authentic record of my own research work carried out during the period of August 2018 to February 2024 under the supervision of **Dr. Rahul Upadhyay and Dr. Vinay Kumar**.

I have also cited the reference about the text(s)/ figures(s)/ tables(s) from where they have been taken. The matter presented in this thesis has not been submitted elsewhere for the award of any other degree or diploma from any institution.

Date: 14/05/2024

Tanvi Dovedi
Candidate

This is to certify that the above statement made by the candidate is correct to the best of my knowledge.

Date: 14/05/2024

Dr. Rahul Upadhyay
Associate Professor, ECED

Dr. Vinay Kumar
Associate Professor, ECED

Acknowledgment

Completing this Ph.D. thesis has been an incredibly fulfilling journey, and I owe my deepest gratitude to a multitude of individuals who have been instrumental in making this achievement possible. I begin by expressing my profound gratitude to my esteemed supervisors, Dr. Rahul Upadhyay and Dr. Vinay Kumar. Their guidance, expertise, and unwavering commitment to my intellectual growth have been the cornerstone of this research. I am grateful for their patience, constructive criticism, and endless support throughout the doctoral process. Dr. Upadhyay, you transcended the traditional role of a supervisor and became more like a family. You were the one who stood by me and motivated me whenever I felt low, reminding me of the strength within. I will always cherish our discussions, your insightful guidance, and the trust you placed in me.

I extend my deepest gratitude to my parents, whose unwavering love, encouragement, and emotional support have been my constant motivation and the bedrock of my academic pursuits. I will always cherish the memory of conversations with my mother, where her wisdom and comforting words eased every challenge. My father's unwavering belief in me, even during my moments of self-doubt, provided the strength to persevere. Together, you have been my guiding stars, and I dedicate this achievement to you with all my heart.

I would also like to extend my heartfelt thanks to Dr. Kulbir Singh, Head of the ECE department, for his leadership and support in creating an environment conductive to research and academic growth. Furthermore, I express my gratitude to the members of my doctoral committee, Dr. Rinkle Rani, Dr. Sanjay Kumar, and Dr. Ashutosh Singh, for their invaluable insights and suggestions, which significantly elevated the quality of my work. I want to acknowledge the academic environment at Thapar Institute of Engineering and Technology. The resources, opportunities, and academic community provided here have been essential in shaping my research and personal growth. I am also indebted to CSIR-HRDG for their financial support through the SRF fellowship, which allowed me to fully immerse myself in my research without financial constraints. I extend special recognition to my friends and colleagues, who have shared the joys and challenges of this journey. My dear friend Pulkit Sharma deserves a special mention. Your unwavering support, insightful conversations, and countless moments of laughter have lightened the academic load and made my journey more memorable.

Abstract

Brain Computer Interface (BCI) systems represent a revolutionary advancement in neural output manipulation, empowering individuals to interact with their environment solely through brain signals, bypassing conventional neuromuscular pathways. These systems primarily aim to facilitate control over assistive devices like speech synthesizers and robotic wheelchairs, facilitating seamless interaction with the surroundings. At the core of BCI systems lie preprocessing and feature extraction modules, which play pivotal roles in enhancing system performance.

To this end, this work endeavors to pioneer novel techniques in both preprocessing and feature extraction for BCI systems. Beginning with the preprocessing phase, our focus centers on refining artifact removal from Electroencephalogram (EEG) data. We propose an automated approach leveraging Independent Component Analysis (ICA) guided by Sparse Entropy, effectively identifying and eliminating artifactual Independent Components without manual intervention. Furthermore, the methodology amalgamates Preconditional ICA for real data with Time-Reassigned Multisynchrosqueezing Transform, amplifying EEG artifact correction performance while preserving valuable neurological signals intertwined with artifacts. This correction-centric approach ensures a robust foundation for neuroscientific exploration and clinical applications by retaining pertinent neural activity.

Transitioning to feature extraction, we introduce an innovative method tailored for Motor Imagery (MI) EEG signals within BCI systems. By integrating Multivariate Variational Mode Decomposition with Phase Space Reconstruction, we address the complexity of multivariate oscillatory patterns in MI-EEG signals, enhancing system accuracy and reliability. This method strategically utilizes data from a minimal set of EEG channels, optimizing computational efficiency without compromising performance. By reconstructing modes derived from Multivariate Variational Mode Decomposition into a 2D phase space, we gain deeper insights into the dynamic evolution of MI-EEG signals, facilitating comprehensive feature extraction encompassing statistical metrics and nonlinear characteristics. Remarkably, this method achieves high classification accuracy in both binary and multi-class tasks using five EEG channels, underscoring its viability for real-time BCI applications.

In a further advancement, we propose a novel feature extraction method focusing on MI-EEG signals, combining Local Maximum Synchrosqueezing Transform with Non-Negative Matrix Factorization. This approach presents substantial improvements in BCI technology, integrating a channel selection technique to enhance real-time feasibility while reducing computational burden and eliminating redundant information. The Local Maximum Synchrosqueezing Transform extracts temporal and spectral information from selected channels, transforming MI-EEG signals into time-frequency representations with enhanced resolution. Non-Negative Matrix Factorization further refines these representations, capturing meaningful patterns and reducing dimensionality for precise signal classification. By incorporating statistical and nonlinear features, this method achieves outstanding classification accuracies in binary and multi-class tasks, surpassing previous approaches and affirming its efficacy in advancing MI-EEG signal analysis for BCI systems.

This comprehensive exploration delves into the forefront of BCI systems, revolutionizing neural output manipulation and enhancing user interaction with the environment. By focusing on innovative preprocessing and feature extraction techniques, we've significantly advanced the capabilities of BCI systems. Our automated artifact removal method, coupled with a correction-centric approach, ensures robust neural signal processing, preserving vital neurological activity for comprehensive analysis. Furthermore, our feature extraction methods for MI-EEG signals showcase remarkable accuracy and efficiency, leveraging minimal EEG channels while capturing complex temporal and spectral dynamics. These advancements underscore the potential for real-time BCI applications, paving the way for more feasible and effective BCI system designs with profound implications for neuroscientific research and clinical practice.

List of Publications

- Dovedi, T., Upadhyay, R., & Kumar, V. (2022). Hybrid time-reassigned multisynchrosqueezing transform -PICARD -based automated electroencephalography artifact correction methodology for brain–computer interface applications. *International Journal of Imaging Systems and Technology*, *32*(4), 1338–1356. https://doi.org/10.1002/ima.22680 **(IF= 3.3)**
- Dovedi, T., Upadhyay, R., & Kumar, V. (2023). Multivariate variational mode decomposition & phase space reconstruction based motor imagery EEG classification. *Computers and Electrical Engineering*, *108*, 108737. https://doi.org/10.1016/j.compeleceng.2023.108737 **(IF= 4.3)**
- Dovedi, T., Upadhyay, R., & Kumar, V. Enhancing Motor Imagery Task Recognition through Local Maximum Synchro-squeezing Transform and multi-domain features. *Biomedical Signal Processing and Control*. [under review]

Contents

List of Figures

List of Tables

Nomenclature

BCI	Brain Computer Interface
EEG	Electroencephalogram
MI	Motor Imagery
CA	Classification Accuracy
FE	Feature Extraction
NIRS	Near-Infrared Spectroscopy
fMRI	Functional Magnetic Resonance Imaging
MEG	Magnetoencephalography
CAR	Common Average Reference
ICA	Independent Component Analysis
EMG	Electromyogram
EOG	Electrooculogram
ECG	Electrocardiogram
ALS	Amyotrophic Lateral Sclerosis
MS	Multiple Sclerosis
LiS	Locked-in Syndrome
SE	Sparse Entropy
IC	Independent Component
Picard	Preconditional ICA for Real Data
TMSST	Time-Reassigned Multisynchrosqueezing Transform
std	Standard Deviation
MVMD	Multivariate Variational Mode Decomposition
PSR	Phase Space Reconstruction
LMSST	Local Maximum Synchro-Squeezing Transform
NMF	Non-Negative Matrix Factorization
wICA	Wavelet enhanced ICA method
ECOG	Electrocorticography
fNIRS	Functional Near-Infrared Spectroscopy
WT	Wavelet Transform
PCA	Principal Component Analysis

TD	Time domain
FD	Frequency domain
TFD	Time-frequency domain
CSP	Common Spatial Patterns
TFA	time-frequency analysis
STFT	Short-Time Fourier Transform
WPT	Wavelet Packet Transform
CWT	Continuous Wavelet Transform
CNN	Convolutional Neural Networks
RNN	Recurrent Neural Networks
LDA	Linear Discriminant Analysis
SVM	Support Vector Machines
ANN	Artificial Neural Networks
AI	Artificial Intelligence
PWC-ICA	Pairwise Complex ICA
EFICA	Efficient Fast-ICA
WASOBI	Weights-Adjusted Second-Order Blind Identification
MSE	Mean Square Error
PE	Permutation Entropy
HFD	Higuchi’s Fractal Dimension
BSS	Blind Source Separation
mvMDE	Multivariate Multiscale Dispersion Entropy
mvMFE	Multivariate Multiscale Fuzzy Entropy
mvMSE	Multivariate Multiscale Entropy
SST	Synchro-squeezing Transform
TSST	Time Re-assigned Synchro-squeezing Transform
GLCT	General Linear Chirplet Transform
GD	Group Delay
TFR	Time-Frequency Representation
GWF	Gaussian Window Function
PSD	Power Spectral Density
SNR	signal-to-noise ratio
FT	Fourier Transform

R-CSP	regularized-CSP
SRCSP	spatially-regulated-CSP
R-CSP-A	regularized CSP-aggression
ZLDA	CSP-Z-linear discriminant classifier
SGRM	sparse group representation model
TSGSP	temporarily limited spatial group structure method
EMD	Empirical Mode Decomposition
SWT	Synchrosqueezing Wavelet Transform
EWT	Empirical Wavelet Transform
E-SVM	Ensemble Support Vector Machine
VMD	Variational Mode Decomposition
RMS	root mean square
LE	Lyapunov exponent
K-Score	Kappa Score
MLP	Multilayer Perceptron
KNN	K-Nearest Neighbour
XGB	Extreme Gradient Boosting
GB	Gradient Boosting
CB	Cat Boosting
FV	Feature vector
NN	Neural Networks
KFD	Katz Fractal Dimension
LEE	Log Energy Entropy
NE	Norm Entropy
RE	renyi entropy
TE	tsallis entropy
C2CM	Convolution with Channel Mixing
LLR	Low-Rank Representations
B2DDLPP	Bilinear 2D Discriminant Locality Preserving Projection

Chapter 1

Introduction

This chapter offers an insightful overview of Brain Computer Interface (BCI) Systems, focusing on key modules detailed in Section 1.1. A thorough examination is conducted on two critical components: artifact removal and feature extraction. Section 1.2 explores the motivation behind the design of BCI systems, while Section 1.3 delves into real-world applications of the BCI systems. A thorough analysis of challenges faced by researchers in previous BCI system design is presented in Section 1.4. Section 1.5 outlines the objectives of this thesis, followed by an elucidation of the major contributions of the present work to the field of BCI systems in Section 1.6. Finally, Section 1.7 provides a detailed breakdown of the organization of the thesis.

1.1 Overview

Brain computer interface (BCI) technology signifies a paradigm shift in human-machine interaction, offering an alternative channel for individuals to convey cognitive intentions and control external devices. By circumventing conventional neuromuscular pathways, BCIs enable users to interface directly with technology through cerebral signals, thus transcending the constraints posed by severe motor impairments such as Amyotrophic Lateral Sclerosis (ALS), spinal cord injury, and stroke [1]. This technological advancement holds particular significance for individuals experiencing Locked-in Syndrome (LiS), where cognitive abilities remain intact despite the absence of functional muscle control [2]. The essence of BCI lies in its establishment of a direct communication pathway between the brain and external devices, achieved through the analysis of cerebral electrical activity. This process facilitates the translation of cognitive intent into actionable commands, enabling users to interact with assistive devices ranging from speech synthesizers to robotic wheelchairs [3]. The main objective of BCI research is to empower individuals with limited or no motor function, facilitating their active engagement with the surrounding environment.

BCI systems operate by discerning patterns in brain activity indicative of user intentions, thereby bridging the gap between neural signals and device control. This approach not only enhances user autonomy and independence but also fosters social inclusion by enabling meaningful interaction with others and the environment. In essence, BCI technology represents a transformative tool in augmenting human capabilities, promising a future where individuals can seamlessly interface with technology solely through the power of thought. The BCI system design (Figure 1.1) can be explained with four major modules described as:

- Signal Acquisition: BCI acquires neural signals through either invasive or non-invasive methods. Invasive methods involve implanting electrodes inside the human skull, while non-invasive methods entail placing the electrodes on the scalp. Non-invasive methods such as Electroencephalogram (EEG), and Near-Infrared Spectroscopy (NIRS), are less risky, cost-effective, and are widely used in BCI research, primarily due to their portability and high temporal resolution [4].
- Signal Pre-processing: Different techniques are used to enhance and prepare the raw EEG signals acquired from the brain for further analysis and interpretation. Signal preprocessing is a major step in ensuring the accuracy and reliability of BCI systems. Raw EEG signals

often contain noise, artifacts, and interferences from several sources, such as electrical noise, muscle activity, or eye blinks [5]. Common techniques include bandpass filtering, notch filtering, and Common Average Reference (CAR) subtraction. For artifact removal techniques such as Independent Component Analysis (ICA), or regression-based methods can be used to separate and remove the artifacts present in the raw signals.

- Feature Extraction: After pre-processing of EEG signals, relevant features are extracted to capture the information of interest. Feature Extraction (FE) involves various Time Domain (TD) and Frequency Domain (FD) analysis based techniques such as spectral analysis, wavelet analysis, or statistical measures to capture specific patterns related to the user's intentions or cognitive tasks [5].
- Classification: In the classification module, machine learning or deep learning algorithms are employed to interpret the extracted features and categorize these features into different classes or labels [6]. During the training phase, the BCI system is exposed to labelled data, allowing it to learn the relationship between extracted features and corresponding mental states or actions. For example, in Motor Imagery (MI) based BCIs, the goal is to classify whether the user imagines left-hand or right-hand movement.

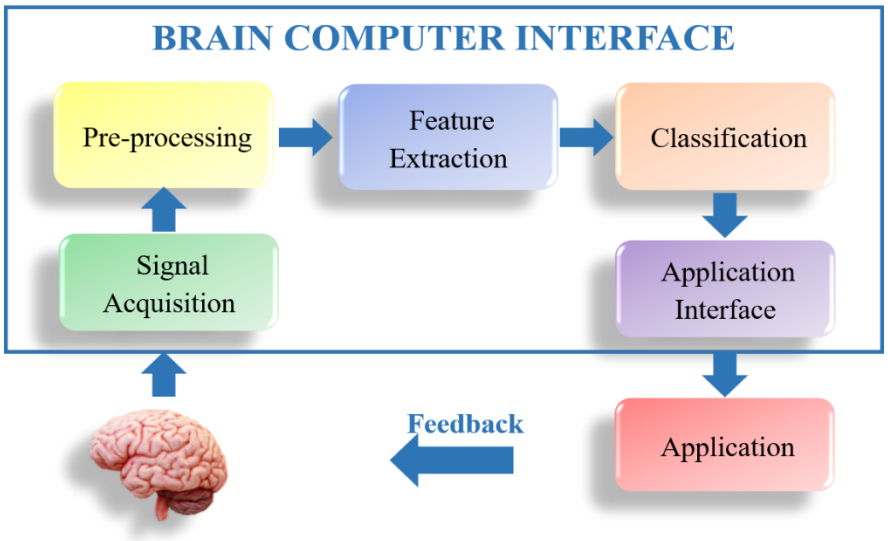

Figure 1.1 BCI system design

The current work delves into the intricacies of the BCI system, with a specific emphasis on two pivotal modules: signal pre-processing and FE. These modules represent critical components that play a foundational role in the functionality and efficacy of BCI systems, shaping the interface's ability to interpret and utilize neural signals for various applications.

1.1.1 EEG signal pre-processing

EEG signals are often contaminated by artifacts, including muscle activity, eye blinks, and electrical noise disturbances. The types of artifacts present in EEG signals are:

- Muscle Artifacts: Muscle contractions, including jaw clenching and facial movements, can introduce high-frequency noise into EEG recordings. This is often referred to as an Electromyographic (EMG) artifact. EMG artifacts introduce high-frequency noise and sharp spikes in the EEG recordings. They can be particularly problematic because they overlap with the frequency range associated with brain signals, making it challenging to distinguish [7].
- Ocular Artifacts: Eye ball movements, blinks, and even small eye twitches can create distinctive EEG patterns that interfere with the brain signals. These are known as Electrooculographic (EOG) artifacts. These artifacts can be mistaken for brain signals, leading to misinterpretation and errors in BCI systems outcomes [8].
- Electrical Noise: External sources, such as power lines, electronic devices, and even other participants' EEG systems in a shared environment, can introduce electrical noise into the recordings. These noises can corrupt EEG signals, causing distortions and baseline fluctuations [8].
- Environmental Artifacts: Environmental factors like electromagnetic interference, temperature changes, or electrode drift can introduce irregularities in the EEG recordings. This makes it challenging to extract relevant brain signals [7].

The existence of various artifacts in EEG signals can yield various detrimental effects on BCI systems efficacy. One significant repercussion is a diminished Classification Accuracy (CA) as artifacts have the potential to distort EEG signals, consequently causing a misinterpretation of the user's intentions or mental states [8]. This misinterpretation, in turn, results in a decreased level of accuracy in BCI control. Furthermore, the presence of artifacts may lead to an increased incidence of false positives, where these extraneous signals are mistakenly classified as brain activity. Moreover, the improper handling of artifact-contaminated data may necessitate discarding such trials, resulting in a loss of information and a subsequent reduction in the signal-to-noise ratio (SNR) in EEG recordings [8].

1.1.2 EEG Feature Extraction for multiclass BCI

Feature Extraction (FE) stands as another pivotal phase in the development of a BCI system, involving the transformation of raw brain signal data into a set of pertinent features [9]. The extracted features play a fundamental role by encapsulating essential information from the signals, serving as input for machine learning algorithms, and enabling BCIs to accurately interpret user intentions [10]. This step is indispensable as it accomplishes multiple objectives: Firstly, it reduces the dimensionality of the data, addressing the computational intensity associated with handling extensive EEG signal datasets and mitigating the risk of overfitting [9]. Secondly, the extracted features offer a more focused representation of brain activity, facilitating the recognition of patterns associated with specific mental tasks or user commands by machine learning algorithms [11]. Lastly, FE streamlines computational requirements for real-time BCI applications, enabling quicker decision-making and responsiveness in processing brain signals [11]. The manifold advantages of FE collectively contribute to the efficacy and efficiency of BCI systems.

FE encompasses several distinct stages, each playing a key role in transforming raw EEG signals into relevant features for BCI systems. The initial phase involves signal preprocessing, wherein EEG signals undergo essential steps to eliminate noise and artifacts [9]. Common techniques employed in this stage include filtering, incorporating methods such as bandpass or notch filtering, along with artifact removal and baseline correction [10]. Subsequently, the process moves on to segmentation, wherein the continuous EEG data is partitioned into smaller segments, often aligned with specific tasks. These segments are then individually analyzed to capture task-specific patterns. The final stage, feature computation, is where a set of features is computed for each EEG segment [11]. These features can span various categories, including TD, FD, or Time-Frequency Domain (TFD) [9]. This meticulous progression through signal preprocessing, segmentation, and feature computation collectively lays the foundation for extracting relevant information from EEG signals and facilitates the subsequent accurate interpretation of user intentions by BCI systems.

1.2 Motivation

The impetus driving the development of BCI systems lies in their potential to significantly enhance the lives of individuals with disabilities. This encompasses not only the prospect of restoring communication and control for those with motor impairments but also to advancing

comprehension of the intricate workings of the human brain. Moreover, BCI systems hold the promise of augmenting human capabilities and opening up innovative channels for communication and interaction [1].

Specifically, BCI systems emerge as a beacon of hope for individuals grappling with neurological disorders such as Amyotrophic Lateral Sclerosis (ALS), Multiple Sclerosis (MS), and brainstem stroke [2]. These conditions compromise the neural connections responsible for muscle control, leading to a loss of voluntary muscle function. Consequently, individuals affected by these ailments often find themselves reliant on others for even the most basic daily activities. This state is clinically recognized as Locked-in Syndrome (LiS), characterized by either total or partial body paralysis [4].

In the case of partial LiS, patients may retain limited control over specific muscles, commonly manifested through eye movements. On the other hand, complete LiS renders individuals entirely immobile, even incapacitating their eye movements [4]. The advent of BCI heralds a transformative era, offering newfound independence and an enhanced quality of life for individuals afflicted with LiS. Through the integration of BCI technology, there exists the potential to restore communication and control for those who have lost these fundamental abilities due to neurological disorders, thereby alleviating the challenges associated with Locked-in Syndrome.

1.3 Applications

Designing BCI systems is motivated by a variety of potential applications and benefits that can significantly impact various fields. The various applications of BCI systems, as depicted in Figure 1.2, are:

- Assistive Technology: One of the primary motivations for BCI development is to create assistive devices that can improve the quality of life for individuals with severe motor disabilities. BCIs can allow these individuals to communicate, control devices, and interact with their environment directly using their brain signals, bypassing the need for traditional motor pathways [12].

- Neurological Rehabilitation: BCIs have the potential to aid in the rehabilitation of individuals who suffer from neurological injuries or disorders, such as stroke or spinal cord injuries. BCIs can be integrated into neurorehabilitation programs for stroke patients or

those with motor impairments. By engaging the brain's plasticity and facilitating neurofeedback, BCIs can promote functional recovery [13].

- Communication Augmentation: BCIs can provide a means of communication for individuals who are unable to communicate with traditional methods due to conditions such as LiS or ALS [12]. These individuals can spell out words or control a communication device by their brain activity using the BCI system.
- Neuroscientific Research: Developing BCIs requires a deep understanding of the brain function and the underlying neural mechanisms. The research and technology development involved in BCIs contribute to advancing our knowledge of the brain, which could have implications for treating neurological and psychiatric disorders [4].
- Mind-controlled Prosthetics: BCIs can enable individuals with limb loss to control prosthetic limbs directly with their thoughts. This can provide a more intuitive and natural control experience compared to traditional prosthetic controls [12-13].

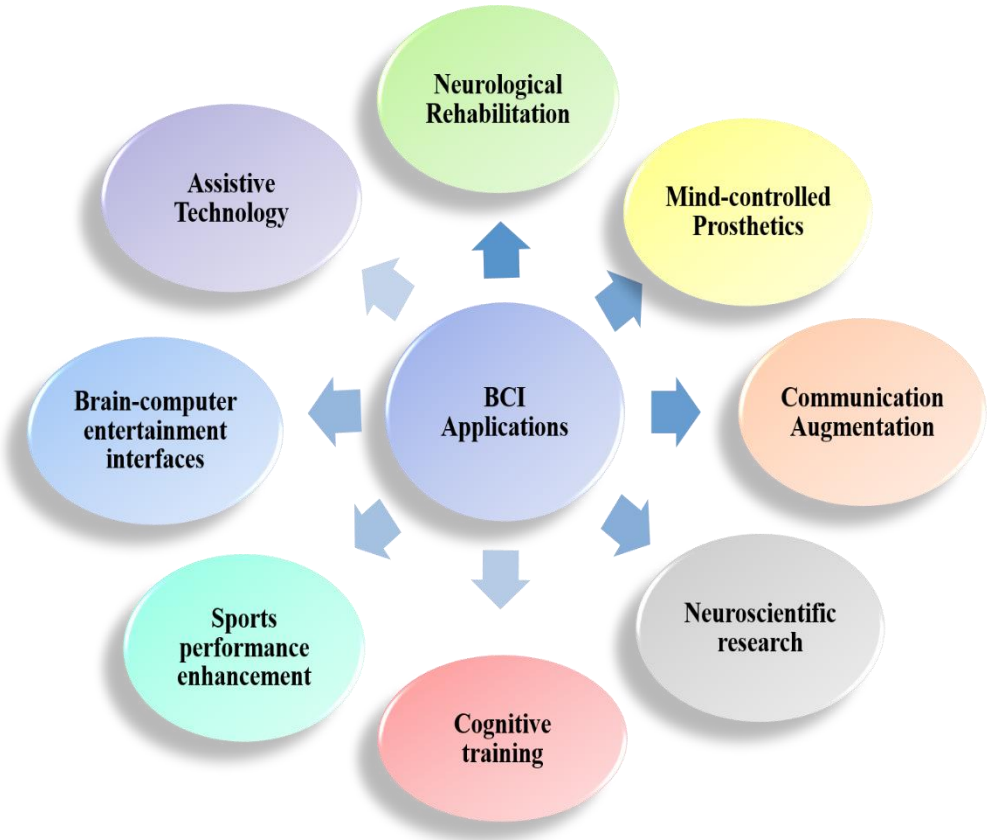

Figure 1.2 Applications of BCI

Apart from these applications BCIs can be used as cognitive training tools to enhance motor learning and skill acquisition. BCIs have the potential to extend human capabilities by allowing

direct brain control of external devices. This could lead to applications in various fields, including aviation, gaming, education, and more, where enhanced cognitive abilities could lead to improved performance [14]. BCIs can revolutionize the gaming and entertainment industry by allowing players to control characters and actions within virtual environments using their thoughts and emotions, creating immersive experiences [15]. BCIs can enable immersive gaming experiences and virtual reality interactions. Players can control avatars and characters using their mental imagery, enhancing the sense of presence and interactivity. Additionally, athletes can use BCIs to visualize and practice complex movements, improving their motor skills and performance. BCIs provide a unique opportunity for mental rehearsal in sports training [14]. The ongoing research and development continue to expand the possibilities and potential applications of BCIs.

1.4 Challenges

Removing artifacts and extracting meaningful feature from EEG signals in the context of a BCI system design is a critical step in ensuring the CA and reliability of the system. There are several challenges in effectively removing the artifacts and extracting relevant features from EEG signals, such as:

- Signal Variability and Non-stationarity: EEG signals are inherently noisy and can vary significantly between individuals and even for the same individual in different sessions [16]. This variability makes it difficult to develop universal artifact removal and FE methods that are robust to these variations. Additionally, EEG signals are non-stationary, making it difficult to develop algorithms that are robust over long recording periods.
- Multiple Artifact Sources: EEG signals can be contaminated by numerous artifacts, such as eye blinks, muscle activity (electromyographic artifacts), electrocardiographic artifacts, and environmental noise [2]. Each source requires specific methods for detection and removal. For instance, artifacts such as muscle tension may vary during the course of a BCI session, requiring adaptive algorithms to continuously adjust for changing artifact characteristics. Additionally, artifacts can overlap neural frequencies of interest in EEG signals, making it challenging to separate the two [4]. For instance, eye blink artifacts often overlap with alpha rhythms.
- Dimensionality and Overfitting: EEG recordings typically involve multiple electrodes placed on the scalp, resulting in a high dimensional signal. Handling this high-dimensional

data can be computationally intensive and may lead to overfitting when extracting features, especially in cases with limited training data [9-10]. It is essential to ensure that the chosen features generalize well to new data and do not merely capture noise from the training dataset [10].

- Temporal Dynamics: MI-EEG signals exhibit complex temporal dynamics that represent the sequence of mental events leading to the indented action. Extracting features that capture these dynamics while avoiding information loss due to down-sampling or feature averaging is challenging. There is a need to strike a balance between reducing dimensionality and retaining essential temporal information [5].
- Feature Selection: Choosing the most relevant features from the EEG data is a crucial task. A wide variety of FE methods exist, including time domain, frequency domain, and TFD approaches [9]. Determining which features to extract and how to combine them effectively is not straightforward and requires careful consideration. It is must determine which combination of features is most effective at capturing the user's intentions [4].

Apart from the mentioned challenges, BCIs often suffer from the data sparsity and computational complexity problems. EEG data for MI tasks are often sparse; FE methods need to be robust to data scarcity and capable of making accurate predictions with fewer training samples [2]. Additionally, many FE techniques, especially those that rely on advanced signal processing or machine learning methods, can be computationally intensive. Real-time BCI applications demand efficient FE algorithms to ensure a low latency in the system [4]. Addressing these challenges requires a multidisciplinary approach, combining expertise in neuroscience, signal processing, machine learning, and data analysis. There is a need to develop innovative solutions aiming to make BCI systems more robust, accurate, and practical.

1.5 Objectives of dissertation

This work was undertaken with a primary emphasis on achieving the following objectives:

- Detailed study for identification of state-of-the-art methods in BCI system design.
- Designing, development and validation of EEG signal pre-processing methodology for artifact removal.
- Designing, development and validation of EEG FE methodology for multi-class BCI system.

1.6 Contributions

The major contributions of the present work in the realm of BCI are listed here as:

1.6.1 EEG artifact removal

- In contrast to traditional ICA-based methods that typically require time-consuming visual inspection for EEG artifact removal, this work proposes an automated approach. A novel ICA based criterion that utilizes Sparse Entropy (SE) for automatic identification of artifactual Independent Components (ICs) is designed. This method streamlines the process by eliminating the need for manual intervention, making the EEG artifact removal process accurate and time-efficient.
- This work introduces an inventive hybrid methodology that integrates the Preconditional ICA for Real Data (Picard) [17] algorithm with Time-Reassigned Multisynchrosqueezing Transform (TMSST) [18] technique. This combination enhances the CA and reliability of EEG artifact correction. The Picard algorithm excels in robust source estimation, while the TMSST technique effectively addresses the spatial and temporal characteristics of EEG artifacts. This novel fusion results in a comprehensive and highly effective approach for artifact correction.
- A key feature of the proposed method is its emphasis on correction rather than outright rejection. By adopting this approach, it is ensured that any valuable neurological activity inadvertently mixed with the artifactual ICs is retained. The strategy enhances the overall quality and comprehensiveness of EEG data analysis. It becomes an asset for both neuroscientific research and clinical applications, as it maintains the integrity of the data, ensuring a more accurate and reliable basis for future studies and diagnosis.

1.6.2 Feature Extraction and classification of multi-class MI-EEG signals

- A method for FE and classification of MI-EEG signals within the BCI context is proposed. The method combines Multivariate Variational Mode Decomposition (MVMD) [19] with Phase Space Reconstruction (PSR) [20] to effectively address the intricate multivariate oscillatory patterns inherent in MI-EEG signals. By doing so, the CA and reliability of the BCI system are enhanced. In order to reduce computational complexity and eliminate redundant information, MI-EEG signals collected from five channels are utilized. The reduction in the methodological complexity enhances the feasibility of the proposed method for practical BCI system design.

- To gain deeper insights into the dynamic behavior of the MI-EEG signals, the approach involves the reconstruction of the modes obtained through MVMD into a 2D phase space. This provides a more intuitive and comprehensive understanding of how MI-EEG signals evolve over time, which is crucial for the success of BCI systems. A wide range of features are derived from the reconstructed MI-EEG signals. These features encompass both statistical metrics and non-linear characteristics, which capture the intricacies of the underlying neural activity.
- The proposed method yields notable results in terms of CA. In binary and multi-class classification tasks, average accuracies of 96.76% and 82.22%, respectively, are achieved. These high CA rates are not only indicative of the efficiency of the proposed method but also highlight its practicality for real-time BCI applications. Moreover, the reduction in the methodological complexity further enhances its feasibility for practical BCI system design.
- In another work, an innovative method for BCI systems that involves a new approach for FE and classification of MI-EEG signals is proposed. The method utilizes Local Maximum Synchro-Squeezing Transform (LMSST) [21] in conjunction with Non-Negative Matrix Factorization (NMF) [22], showcasing significant advancements in the field of BCI technology. In order to reduce computational complexity and eliminate redundant information originating from neighboring channels, a channel selection technique is implemented in the proposed method. The technique selects the most relevant subject-specific channels, ensuring accurate classification of the MI-EEG signals. Consequently, the suggested method becomes suitable for real-time BCI systems.
- The LMSST is employed to extract temporal and spectral information from the MI-EEG signals obtained from the selected channels. By applying the LMSST, the nonlinear MI-EEG signals are transformed into TF representations with high energy concentration and enhanced resolution, thereby facilitating more effective FE.
- The TF coefficients obtained using LMSST are further processed through NMF for capturing meaningful patterns and dimension reduction in order to enable accurate classification of MI-EEG signals. The processed MI-EEG signals are subjected to FE, incorporating statistical and nonlinear measures. A detailed analysis is carried out to pinpoint the most pertinent features that play a crucial role in classifying the MI tasks.
- Seven different classifiers are employed to assess the efficacy of the designed FE method. The classification results validate the proposed method's efficacy for classifying binary and

multi-class EEG signals. The results validate the effective performance of the method in accurately categorizing the MI-EEG signals. Average accuracies of 98.44% and 90.00% are achieved in binary and multi-class classification, respectively. Furthermore, a comprehensive comparison is conducted with previously proposed FE and classification methods, thereby validating the efficacy of the proposed approach.

1.7 Organization of the thesis

Chapter 1, "Introduction," serves as the gateway to this thesis work. It commences with a comprehensive overview of the BCI systems. The motivation behind this research is carefully examined, shedding light on the driving forces that initiated this work. It further delves into real-world applications, underlining their practical importance, and confronts the challenges that the research aims to address. The chapter then concisely outlines specific research objectives and discusses the unique contributions it offers to the field of BCI systems. Lastly, it provides a preview of the thesis structure, providing a roadmap for navigating the chapters ahead.

Chapter 2, "Basics of Brain Computer Interface Systems," is designed to establish a foundational understanding of the BCI systems. The chapter is organized into several sections. It begins with a look at the biological background encompassing the human brain intricacies and brain activity patterns. Subsequently, it delves into the world of BCI systems, offering insights into the various types of BCIs and the techniques for recording brain activity. A special emphasis is placed on EEG, offering its significance in the context of BCI systems.

Chapter 3, "Literature Review," provides a comprehensive review of the literature, focusing on the crucial aspects of preprocessing, FE, and classification in the context of EEG-based BCI systems. First, it explores the various preprocessing techniques proposed in the past for cleaning and enhancing EEG data. Secondly, it delves into FE, explaining how relevant information is derived from the EEG signals using the numerous techniques proposed by the researchers in previous years. Lastly, the chapter discusses the classification methods for interpreting EEG data and decoding the user intentions.

Chapter 4, "Hybrid TMSST-Picard based EEG artifact correction method," presents a novel method for correcting artifacts in EEG recordings, with a focus on its relevance to applications like BCI. The method combines the Picard algorithm and TMSST in a four-step process. An innovative automatic criterion, based on SE, is introduced for the identification of artifactual

components, eliminating the need for manual inspection. This chapter contributes to more efficient artifact correction and the preservation of valuable neurological data. It provides the implementation and the comparative analysis of the proposed framework against the state-of-the-art method, wICA.

Chapter 5 introduces an innovative framework, titled "Multivariate Variational Mode Decomposition & Phase Space Reconstruction based Motor Imagery EEG classification," designed for FE and classification of binary and multi-class MI-EEG signals. This framework leverages MVMD and PSR techniques to extract essential features, subsequently utilizing an Ensemble Support Vector Machine (E-SVM) model for classification. The method's performance is assessed using diverse metrics, and its results are benchmarked against recent approaches, demonstrating its effectiveness in MI-EEG classification for real-time BCI systems. Furthermore, to optimize computational efficiency, only five EEG channels are utilized.

Chapter 6 introduces "LMSST-NMF: A novel Motor Imagery EEG FE and classification method for BCI." This innovative approach is tailored to extract distinctive features from both binary and multi-class MI-EEG signals, enhancing the precision of classification. By combining LMSST and NMF, it effectively captures meaningful features. Additionally, a channel selection technique is integrated to streamline computational complexity. The method's performance is assessed using various metrics and is benchmarked against recent approaches, underscoring its potential for practical real-time BCI application, characterized by its efficiency and low computational requirements.

Chapter 7 serves as the culminating chapter of this thesis, providing a comprehensive conclusion to the findings and contributions of the work within the domain of BCI. The work has provided valuable insights into the development of BCI technology. Furthermore, this chapter looks ahead to future research and exploration in the field of BCI.

Chapter 2

Basics of Brain Computer Interface

This chapter serves as the basis for comprehending BCIs. We first highlight the vital importance of understanding the complexities of the human brain in enabling effective BCI systems. The chapter navigates the biological background, specifically dissecting the structure of the human brain, which is critical for precise BCI applications, whether for aiding those with motor disabilities or addressing neurological conditions. Additionally, it delves into the electrical and chemical dynamics of brain activity, clarifying the fundamental neural communication processes and the role of neurotransmitters. Subsequently, the chapter turns its focus toward BCIs, categorizing them into invasive and non-invasive methods, laying emphasis on the significance of recording brain electrical activity as the foundation for BCI operations. The chapter also focuses on EEG as a preferred choice in BCI systems, outlining its various merits and its capacity to measure brain wave frequencies and discern their cognitive correlations.

2.1 Biological Background

Understanding the intricates of the human brain is paramount in the quest of developing an effective BCI system. The human brain is an incredibly complex and sophisticated organ, with billions of neurons interconnected in intricate networks. These neurons communicate through electrical impulses and chemical signals, forming the basis of our thoughts, emotions, and actions [23]. To unlock the potential of BCIs, it is essential to grasp how these neural processes work. Therefore, understanding the structure of the brain is crucial. The brain is divided into various regions, each responsible for specific functions. For instance, the frontal cortex plays role in decision-making and motor control, while the temporal lobe is involved in processing auditory information and memory [24]. Knowledge of these regions helps in targeting specific areas for BCI applications, such as assisting individuals with motor disabilities or those suffering from neurological conditions like epilepsy.

Furthermore, understanding the brain's electrical activity is essential for developing an efficient BCI system. Neurons communicate through electrical impulses known as action potentials [23]. Techniques like EEG are used to record these electrical signals. Researchers must decipher the patterns and frequencies of these signals to interpret a user's intentions accurately. This understanding enables BCIs to decode brain activity and translate it into commands for external usage. In addition to electrical activity, BCIs can also tap into the brain's chemical signals. Neurotransmitters play a vital role in modulating mood, attention, and overall brain function [24]. For instance, BCI systems designed to assist individuals with mood disorders may need to monitor neurotransmitter levels and respond accordingly. Understanding the brain's chemical processes help in the development of BCIs that can provide targeted interventions for mental health and neurological conditions. Therefore, comprehending how the human brain works at the structural, electrical, chemical, and adaptive levels is fundamental to advancing BCI technology. This knowledge enables scientists and engineers to develop BCIs that can accurately decode neural activity, restore lost functions, and enhance human-computer interaction. As our understanding of the brain continues to grow, so does the potential for innovative and transformative BCI systems that can improve the lives of countless individuals.

2.1.1 Structure of the Human Brain

The human brain is a highly intricate organ that can be divided into several major regions, as shown in Fig. 2.1 including:

- Cerebrum: This is the largest and the most developed part of the brain, which is responsible for higher-order functions such as thinking, feeling, and learning [25]. It is partitioned into two hemispheres (left and right), which are further subdivided into four lobes: the frontal lobe, the parietal lobe, the temporal lobe, and the occipital lobe. The frontal lobe is involved in decision-making, planning, and personality [26]. The parietal lobe is responsible for sensory perception and spatial awareness. The temporal lobe is associated with memory and auditory processing, and the occipital lobe is responsible for visual processing [25].

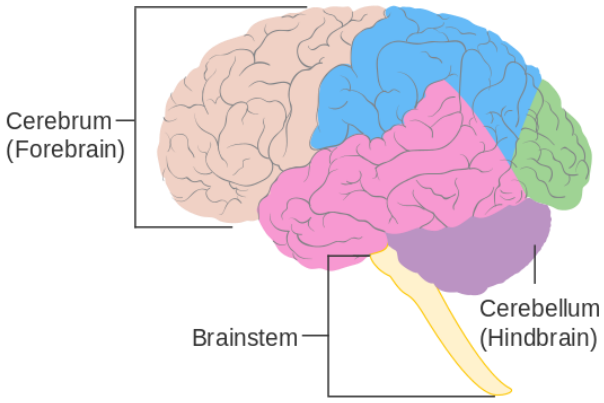

Figure 2.1 Structure of Human Brain [27]

- Cerebellum: The cerebellum is situated at the base of the brain and is accountable for coordinating voluntary movements, balance, and posture. It also plays a role in motor learning and fine-tuning movements [25].
- Brainstem: The brainstem connects the brain to the spinal cord and is vital for basic life functions such as breathing, heart rate regulation, digestion, and consciousness . It comprises the medulla oblongata, pons, and midbrain [28].
- Limbic system: This set of interconnected structures is involved in emotions, motivation, memory, and learning. The limbic system comprises the hippocampus (responsible for forming and storing memories), the amygdala (linked to emotions, particularly fear and aggression), and the hypothalamus (responsible for regulating functions like thirst, hunger, and body temperature) [25].

2.1.2 Brain Activity Patterns

Brain activity and communication are closely linked. The brain is constantly sending and receiving signals, which allows us to think, feel, and move. These signals are transmitted through neurons or nerve cells, which are the fundamental building blocks of the brain.

Neurons communicate with each other by sending electrical signals and releasing chemicals called neurotransmitters [29]. Neurons play a crucial role in facilitating communication within the brain and transmitting signals to the several parts of the body. Neurons exhibit a distinctive structure comprising three primary components. Firstly, the cell body, or soma, plays a crucial role in processing incoming signals and generating outgoing signals [29]. Housed within the cell body are the nucleus and the majority of the neuron's organelles. Secondly, dendrites, short and branching extensions emanating from the cell body, receive incoming signals from other neurons or sensory receptors and convey them towards the cell body. Lastly, the axon, a long and slender extension, carries electrical impulses from the cell body to other neurons, muscles, or glands [29].

The communication between neurons involves a combination of electrical and chemical signals, unfolding through a series of distinct steps. The process begins with the maintenance of a voltage difference across the cell membrane known as the resting membrane potential, arising from disparate ion concentrations inside and outside the cell [30]. Upon receiving a sufficient stimulus, typically from dendrites, the neuron depolarizes, resulting in a negative electrical charge within the neuron. If depolarization reaches a critical threshold, an action potential, a rapid voltage change, is initiated and travels down the axon [30].

Subsequently, at the termination of the axon, the action potential reaches a specialized structure called the synapse [29]. In this synaptic junction, neurotransmitters are released [30]. These neurotransmitters bind to receptors on the receiving neuron's dendrites, facilitating the transmission of the signal. The binding of neurotransmitters can either excite or inhibit the receiving neuron, generating a postsynaptic potential. If the signal strength surpasses a threshold, it can lead to the initiation of a new action potential in the receiving neuron [29].

Neurons engage in the processing and integration of information through an intricate network of connections. They receive input from various sources, amalgamate these signals, and subsequently generate output signals that can be transmitted to other neurons. This information processing mechanism is fundamental to brain function, forming the basis of all cognitive processes and behaviors [30].

2.2 Brain Computer Interfaces (BCIs)

The foremost step in designing a BCI system is the recording of the brain's electrical activity. Various methods for recording brain electrical activity as shown in Fig. 2.2 include:

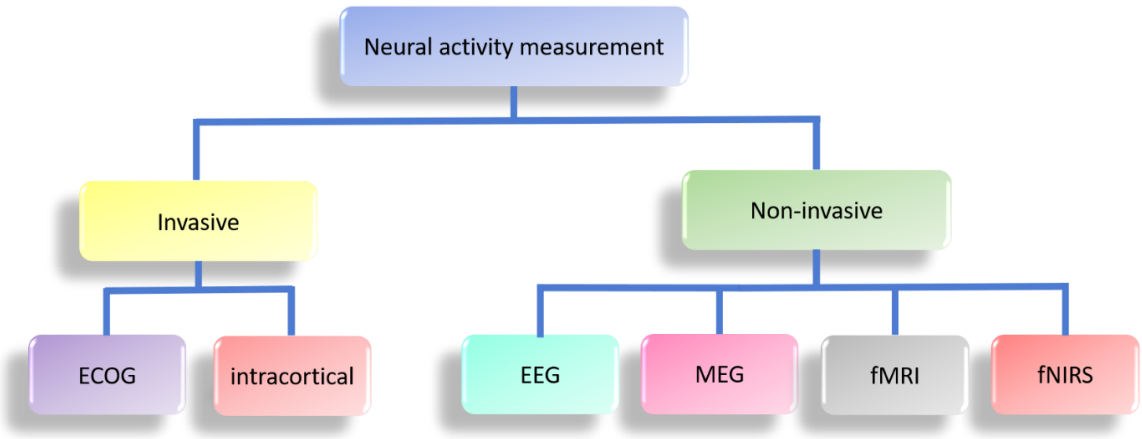

Figure 2.2 Neural activity measurement methods

2.2.1 Invasive methods

Invasive methods of recording require surgical implantation of electrodes or sensors into brain tissue or on the brain's surface. These methods offer high-quality signal data but are typically reserved for medical applications due to their invasiveness [31]. Invasive methods provide exceptionally high-quality and precise neural data, making them suitable for fine-grained control and complex applications. These methods offer an excellent spatial resolution, allowing for precise localization of neural activity [32]. The invasive methods offer long-term stability as once implanted, they can remain in place for extended periods, providing stable neural recordings over time. The invasive methods include:

- Electrocorticography (ECoG): This method involves placing a grid of electrodes directly on the surface of the brain. ECoG provides high spatial and temporal resolution, making it suitable for precise BCI applications [31]. It is often used for individuals with severe motor disabilities.
- Intracortical electrode arrays: These are small arrays of microelectrodes implanted directly into the brain tissue. They offer high spatial resolution and can record neuron activity [33]. Intracortical BCIs are primarily used in research and for individuals with spinal cord injuries.

2.2.2 Non-Invasive Methods:

Non-invasive BCIs do not require surgical procedures and are more widely accessible. The non-invasive methods include:

- Electroencephalography (EEG): EEG is one of the most common non-invasive methods for recording brain activity. It involves placing electrodes on the scalp to measure electrical

potentials generated by the neural activity. EEG is widely used for various BCI applications due to its safety, portability, and relatively low cost [32].

- Magnetoencephalography (MEG): MEG records the magnetic fields generated by neural activity. While it provides good spatial resolution, it is less common and more expensive than EEG due to the need for specialized equipment [34].
- Functional Magnetic Resonance Imaging (fMRI): While primarily used for imaging brain function, fMRI can indirectly capture brain activity patterns. It has excellent spatial resolution but is not suitable for real-time BCI applications due to its low temporal resolution [31].
- Near-Infrared Spectroscopy (NIRS): NIRS measures changes in blood oxygenation levels in the brain, which can be used to infer neural activity. It offers portability and has been explored for various BCI applications [33].
- Functional Near-Infrared Spectroscopy (fNIRS): This is a variation of NIRS that specifically targets brain function. It uses near-infrared light to measure changes in blood oxygenation and is suitable for real-time BCI applications [31].

2.3 Electroencephalography (EEG)

Electroencephalography (EEG) offers several advantages over other recording techniques when used in the BCI systems. These advantages make EEG a popular choice for designing BCI systems. EEG is a non-invasive neurophysiological technique used to record the electrical activity of the brain over time. EEG measures the electrical potential generated by the neurons in the brain and provides relevant information about brain activity [2]. In order to record EEG, small metal discs or sensors are attached to the subject's scalp at various locations [4]. The electrodes are typically placed in a specific pattern according to the international 10-20 system, which helps in standardizing electrode placement. The electrodes are connected to an EEG machine, which amplifies and records the electrical signals produced by the brain [5]. These signals are typically displayed as a series of waveforms on a computer monitor or paper printout. The various advantages that make EEG a popular choice for designing BCI systems are:

- Non-invasive: EEG is entirely non-invasive; it does not necessitate surgery or penetration of the skin or skull [31]. This reduces the risk to the user, making it safe and accessible for a wide range of applications.

- Portability: EEG systems are portable and lightweight making them suitable to be used in various settings, including homes, clinics, and research laboratories. The portability is valuable for applications such as assistive devices, where users need to operate BCIs in their everyday environments [31].
- High temporal resolution: EEG provides excellent temporal resolution, allowing it to capture rapid variations in brain activity with millisecond precision. This is essential for tasks that require real-time feedback and control, such as neurofeedback and cursor control [32].
- Real-time: EEG signals can be processed and interpreted in real-time, allowing users to receive immediate feedback and control devices or applications in real-world scenarios [33].
- Affordability: EEG equipment is relatively affordable compared to other neuroimaging techniques like fMRI or invasive methods like intracranial electrodes [33]. This makes EEG more accessible to a broader population.
- Adaptability: EEG-based BCIs can be designed to detect a wide range of cognitive states and mental commands, making them versatile for different applications. These systems can adapt to the user's brain signals with training, allowing users to improve their control over time [34]. Adaptability is crucial for personalized and long-term use.
- Safety: EEG is considered a safe technique with a low risk of adverse effects or complications, making it suitable for a wide range of users, including those with medical conditions or disabilities [33].
- Wide application range: EEG can capture a broad range of brain activity, including MI, sensory perception, cognitive processes, and emotional states [34]. This versatility makes it suitable for various BCI applications, from motor control to communication and neurofeedback.
- Minimal discomfort: The placement of EEG electrodes on the scalp is minimally uncomfortable and does not cause pain or tissue damage, which is often the case with invasive recordings [31].

EEG records the brain's spontaneous electrical activity, which includes various types of brain waves. These brain waves are categorized into distinct frequency bands, such as alpha, beta, delta, theta, and gamma [32]. Each of these frequency bands has its own characteristic features

and is associated with different cognitive and physiological states. Some common EEG frequency bands and their characteristics are listed in Table 2.1.

Table 2.1 Characteristics of various frequency bands

Frequency Bands	Frequency range (Hz)	Amplitude (μV)	Other characteristics
Delta	0.5-4	<100	Delta waves are the slowest EEG waves. These waves are most prominent during deep sleep and in infants. In adults, the presence of delta waves during wakefulness may indicate brain pathology or drowsiness.
Theta	4-8	<100	These waves are often observed during light sleep, drowsiness, and the transition between wakefulness and sleep. Enhanced theta activity may be associated with memory consolidation, creative thinking, and problem-solving.
Alpha	8-13	20-60	Alpha waves lie in the range of 8-13 Hz and are most prominent when a person is awake but relaxed with closed eyes, such as during meditation or daydreaming. A decrease in alpha activity is associated with increased alertness and cognitive engagement, while an increase in alpha activity might indicate reduced alertness.
Beta	13-30	<20	Beta waves are prominent during wakefulness and active or attentive cognitive states. These waves range from 13-30 Hz and are often associated with tasks that require focused attention. Beta activity is further divided into low-beta (13-17 Hz) and high-beta (17-30 Hz). Low-beta is linked to relaxed wakefulness, while high-beta is associated with increased mental activity.
Gamma	30-100	<2	Gamma waves are the fastest frequency waves ranging from 30-100 Hz. These waves are thought to be associated with cognitive processes, such as perception, learning, and problem-solving. Enhanced gamma activity is observed in states of high cognitive processing, and it is thought to reflect the synchronization of neural networks (NN).

The EEG signals can vary among individuals and even within the same individual, depending on their current metal state, age, and other factors. These frequency bands serve as a valuable tool for understanding brain activity and assessing conditions like epilepsy, sleep disorders, and cognitive functions [33].

Chapter 3
Literature Review

This chapter is dedicated to providing a comprehensive understanding of EEG-based BCIs. The chapter is organized into key sections according to the context of EEG-based BCI systems. It commences with an exploration of preprocessing techniques, highlighting the crucial steps and methodologies involved in cleaning and enhancing EEG data, ensuring the reliability and quality of signals. Subsequently, the chapter transitions into the realm of FE, shedding light on the various techniques and algorithms employed to extract relevant information from the EEG signals. Moving forward, the chapter delves into classification, explaining the methods used to categorize and interpret EEG signals to decipher user intentions. Altogether, Chapter 3 provides a review of the literature, focusing on the critical aspects of preprocessing, FE, and classification in the context of EEG-based BCI systems.

BCI systems possess a crucial capability in translating neural signals into actionable commands for controlling external devices. This intricate process unfolds through essential stages, prominently featuring pre-processing, FE, and classification as pivotal modules. The diverse array of techniques employed by researchers, spanning from early stages to the present, for the development of these modules are detailed below:

3.1 Preprocessing

In the early stages of EEG research, artifact removal was a manual and visually guided procedure. Human experts were relied upon to scrutinize EEG data and identify segments contaminated by artifacts. These artifacts could arise from sources such as eye blinks, muscle activity, and electrical interference. While manual inspection allowed for the removal of artifacts, it was subjective and required expert intervention [9]. Additionally, researchers also introduced averaging techniques, which play a significant role in reducing the effects of artifacts. However, the averaging techniques are less effective when dealing with non-stationary signals, as these techniques assume that the underlying brain activity is consistent across trials [9]. To further enhance data quality, basic signal processing filters such as band-pass and notch filters were introduced to eliminate unwanted frequency components. These filters help attenuate artifacts originating from sources like power line interference and other high-frequency artifacts. However, they had limitations in effectively eliminating complex and non-stationary artifacts [11].

In the 1990s, the emergence of ICA brought significant advancement in EEG artifact removal. ICA is a powerful method for source separation that allows for the decomposition of EEG signals into independent components [35]. A part of these components corresponds to the underlying neural activity, while others may represent artifactual sources. Researchers could then remove or reject artifactual components, providing a data-driven approach to artifact correction [35].

The Wavelet Transform (WT) emerged as another notable development in the field of EEG artifact removal. Wavelet analysis provided a multi-resolution approach to EEG artifact removal, making it suitable for non-stationary and time-varying artifacts [36]. By representing EEG data in different frequency bands and time scales, researchers could better isolate and remove unwanted components. On the other hand, adaptive filtering techniques also gained prominence, offering dynamic artifact removal capabilities [37-38]. Techniques like adaptive

noise cancellation and adaptive regression could flexibly adapt to the changing nature of artifacts in EEG data [39]. This flexibility was particularly useful when dealing with physiological artifacts like muscle noise. Further, innovations included the introduction of Principal Component Analysis (PCA) [40] and artifact subspace reconstruction [41], aiming to identify and separate artifact sources from EEG data. These methods focused on reducing the impact of artifacts on the EEG signals by isolating and minimizing their existence.

Table 3.1 EEG artifact removal methods with respective advantages and challenges

Method	Description	Advantages	Challenges
Manual Inspection-based Methods	Visual inspection by experts to identify and manually remove artifacts.	Direct identification of specific artifacts.	Time-consuming, and requires expertise.
Filtering Techniques [37-38]	Use of digital filters to remove unwanted frequency components, e.g., bandpass, notch filters.	Simple implementation, real-time processing.	May distort EEG signals, not effective for all artifacts.
Independent Component Analysis (ICA) [35]	Decomposes EEG signals into independent components, allowing the removal of artifacts.	Effective for various artifacts, non-invasive.	Relies on assumptions of statistical independence.
Regression-based Methods [39]	Regression models to estimate and remove artifacts based on external reference signals.	Flexible, can be applied to various artifacts.	Dependence on accurate reference signals.
Wavelet Transform [36]	Decomposes EEG signals into different frequency components, making it easier to identify and remove artifacts.	Good time-frequency localization.	Parameter selection can be challenging.
PCA (Principal Component Analysis) [40]	Decomposes EEG signals into principal components, useful for dimensionality reduction and artifact removal.	Efficient dimensionality reduction.	Assumes linear relationships, may not capture all artifacts.
Artifact Subspace Reconstruction (ASR) [41]	Identifies and removes artifacts by reconstructing the signal subspace without artifacts.	Effective for various artifacts.	Sensitive to assumptions about the signal subspace.
Hybrid Methods [42-43]	Combining multiple techniques (e.g., ICA with filtering) to improve artifact removal.	Synergistic effects of different methods.	Increased complexity, potential for method interactions.

Recent years have witnessed a transformative shift in EEG artifact removal techniques, marked by the integration of machine learning and deep learning approaches. These methods aim to automate the detection and removal of artifacts, reducing the need for manual intervention.

Hybrid methods, which combine multiple artifact removal techniques, have become popular [42-43]. For instance, researchers use ICA to separate sources and then use a machine learning algorithm for further artifact rejection [43]. The approach enhances the overall quality of EEG data. Real-time artifact removal techniques have also been developed to enable online EEG data processing [44-45]. This is especially useful in BCI applications, where real-time feedback and control are essential. Table 3.1 presents a compilation of various EEG artifact removal methods, highlighting their respective merits and associated challenges. As technology and research continue advancing, the field of EEG artifact removal is expected to evolve further, offering more innovative and effective techniques for improving the quality of EEG data and advancing our understanding of the human brain.

3.2 Feature Extraction

Various methods have been developed and employed to effectively extract and classify appropriate features from the EEG signals, encompassing the Time Domain (TD), Frequency domain (FD), Time-Frequency domain (TFD), and other advanced innovative approaches. Table 3.2 compiles a range of FE methods, delineating their respective advantages and challenges. In the early stages of MI-based BCIs, TD methods were predominantly used for FE. TD analysis techniques provide valuable insights about the temporal characteristics of EEG signals, enabling effective FE and classification. The advantages of TD analysis methods lie in their simplicity, computational efficiency, and interpretability [46]. However, TD analysis methods may not fully capture the complex dynamics and nonlinear interactions present in EEG signals as these methods rely primarily on the amplitude and temporal properties of the signal, neglecting frequency domain characteristics. Furthermore, TD features are not robust to artifacts and noise present in EEG recordings, potentially affecting CA [47].

As research progressed, frequency domain methods emerged as an important tool for FE. The most commonly used frequency domain analysis technique is the Fourier Transform (FT), which decomposes the signal into its constituent sinusoidal components [46]. Frequency domain analysis methods can capture the oscillatory patterns specific to MI tasks, providing discriminative features for accurate classification. These methods are computationally efficient and are often robust to noise and artifact contamination. However, MI tasks often involve time-varying patterns, and frequency domain analysis methods are not capable of capturing these temporal characteristics [47]. Additionally, the choice of specific frequency bands for FE can

vary across individuals or tasks, making it challenging to find a universal frequency band that suits all subjects.

The advent of Common Spatial Patterns (CSP) encouraged researchers to emphasize on spatial information. CSP utilized spatial filters to enhance the discriminative power of EEG features related to MI [48]. This approach aimed to identify spatial patterns that maximally differentiate between different MI tasks. While it excels at extracting discriminative spatial patterns, it may not fully capture the temporal dynamics or inter-channel dependencies of the data. Another limitation of CSP is the requirement for a sufficient amount of labelled training data [46]. CSP estimates spatial filters based on the differences in the variance of the two classes of MI signals. Insufficient training samples can lead to suboptimal filter estimation, thereby affecting classification performance. Obtaining adequate high-quality labelled data can be challenging in some scenarios, particularly when working with individuals with limited motor control or during lengthy experimental sessions. Furthermore, selecting the frequency band of interest is critical for successful FE using CSP [49].

Recognizing the importance of capturing both temporal and spectral information simultaneously, researchers explored hybrid approaches combining TD and frequency domain features. These Time-Frequency Analysis (TFA) approaches aim to capture both temporal and spectral characteristics of MI-EEG signals, enhancing the accuracy of classification algorithms. These methods allow the analysis of transient changes in spectral content over time, capturing the dynamic nature of brain activity during MI tasks [50]. The TFA methods primarily encompass two main approaches: the Short-Time Fourier Transform (STFT) and WT. The STFT provides a TF representation of a signal by dividing it into short, overlapping segments and then applying the FT to each segment. The STFT, while widely used, suffers from resolution problems and struggles to capture time-varying patterns adequately [51]. The trade-off between low and high-frequency resolution further complicates its suitability for brain signal analysis. Another popular TFA approach is the WT, which decomposes signals into different frequency sub-bands using wavelet basis functions [51]. Unlike the STFT, the WT allows for variable time-frequency resolution, making it appropriate for analyzing non-stationary signals such as EEG. The wavelet-based methods have been useful in various studies to extract time-frequency features from MI-EEG signals, including Wavelet Packet Transform (WPT) and variations of Continuous Wavelet Transform (CWT) [52]. However, the wavelet-

based methods have certain limitations, such as the dependence on the choice of mother wavelet and the trade-off between time and frequency resolution.

Table 3.2 Various FE methods with respective advantages and challenges

FE Method	Description	Advantages	Challenges
Time Domain Methods [46]	Extracts statistical features directly from the temporal domain of EEG signals, such as mean, variance, and skewness.	Computationally efficient and provides basic statistical characteristics.	May not capture intricate temporal patterns in the signal.
Frequency Domain Methods [47]	Focuses on specific frequency components of EEG signals, extracting features like power in alpha, beta, and gamma bands.	Provides insights into frequency-specific brain activity patterns.	May overlook information present in other frequency bands.
Common Spatial Patterns (CSP) [48-49]	Identifies spatial filters through eigenvalue decomposition to maximize the variance between motor imagery classes in EEG signals.	Effective for enhancing class separability in multi-class scenarios.	Sensitive to noise and requires sufficient labeled data.
Time-Frequency Representations (TFR) [51]	Analyzes changes in frequency content over time, providing a dynamic view of motor imagery-related activity in the time-frequency domain.	Captures temporal variations in spectral features for dynamic analysis.	Computational complexity.
Deep Learning Approaches [53-57]	Utilizes neural networks, such as convolutional neural networks (CNNs) or recurrent neural networks (RNNs), for automatic hierarchical feature extraction.	Automatically learns complex hierarchical features from raw EEG data.	Requires large amounts of labeled data, computationally intensive.
Transfer Learning [57-60]	Adapts knowledge from a source domain (e.g., a related BCI task) to improve FE for the target domain (motor imagery) with pre-trained models.	Utilizes pre-existing knowledge to enhance performance with limited labeled data.	Challenges in domain adaptation and source-target task alignment.
Hybrid Methods [54]	Integrates multiple FE techniques (e.g., time domain with frequency domain) to synergistically enhance overall feature representation.	Exploits complementary strengths of different methods for improved robustness.	Increased computational complexity, potential for method interactions.

In recent years, deep learning made a significant impact on the FE of EEG signals, particularly with the rise of Convolutional Neural Networks (CNNs) and Recurrent Neural Networks (RNNs) [53-57]. These networks demonstrated an ability to automatically learn hierarchical features from raw EEG data. Transfer learning became a prevalent strategy, leveraging pre-

trained deep learning models on large datasets for FE tasks [57-60]. Recent years have seen an increasing emphasis on extracting features that capture temporal dynamics and relationships within EEG data. Attention mechanisms within deep learning architectures have been explored to focus on relevant portions of the EEG signals [61]. The integration of multimodal data, combining EEG with other neuroimaging modalities, has led to the extraction of hybrid features, providing a more holistic view of brain activity. The field of EEG FE continues to evolve, with a focus on capturing intricate patterns in the temporal and spatial domains of the EEG signals, driven by advancements in both technology and analytical methodologies.

3.3 Classification

Numerous classifiers have been utilized over the years for the classification of MI-EEG signals, each with its unique principles of operation. Table 3.3 details different types of MI-EEG classification methods. In the early years, linear classifiers such as Support Vector Machines (SVMs) and Linear Discriminant Analysis (LDA) [62-64] were popularly used in classification problems. The LDA aimed to find the optimal linear combination of features that could effectively separate different classes, while SVMs sought to determine a hyperplane that best segregated the data into distinct categories, employing various kernel functions to transform the input data into higher dimensional spaces [65].

With advancement in the computational capabilities in the early 2000s, there came a major shift towards non-linear classifiers. Artificial Neural Networks (ANNs) became prominent, consisting of interconnected nodes organized into layers that process input data through hidden layers to perform classification. The mid-2000s saw a rise in ensemble classifiers, such as Bagging and Boosting [66-67]. Bagging involved training multiple instances of the same classifier on different subsets of the training data, effectively reducing overfitting and improving generalization. Boosting, on the other hand, focused on sequentially training weak classifiers, with subsequent classifiers giving more weight to misclassified instances, thus enhancing the overall CA.

Hybrid classifiers emerged in the late 2000s, combining the strengths of different classifiers or integrating information from various modalities. Hybrid approaches often incorporate spatial filters like CSP with linear or non-linear classifiers, optimizing both FE and classification simultaneously. Additionally, hybrid classifiers explored the fusion of EEG data with other modalities, such as fNIRS or EMG, to improve overall classification performance. The 2010s

marked a significant shift towards deep learning models, including CNNs and RNNs [53-56]. CNNs, adept at capturing spatial patterns, automatically learned hierarchical features from raw EEG signals. RNNs, designed for sequential data, captured the temporal dynamics of MI tasks, remembering past information for improved classification [55-56]. Transfer learning also gained prominence in the same decade, leveraging knowledge from pre-trained models on relevant tasks. Models trained on larger datasets or different EEG-related tasks were fine-tuned for MI classification, addressing challenges associated with limited labelled data [57-61].

Table 3.3 MI-EEG classification methods with respective advantages and challenges

Classification Method	Description	Advantages	Challenges
Linear Discriminant Analysis (LDA) [62]	Projects EEG features into a lower-dimensional space that maximizes class separability using linear transformations.	Simple implementation, computationally efficient.	Assumes linear separability, may not capture complex decision boundaries.
Support Vector Machine (SVM) [63-64]	Constructs hyperplanes to maximize the margin between classes in a high-dimensional feature space.	Effective for high-dimensional data, versatile with various kernels.	Choice of kernel parameters, may struggle with noisy or imbalanced data.
Neural Networks (NN) [66]	Utilizes artificial neural networks, such as feedforward or recurrent networks, for non-linear classification.	Can learn complex non-linear relationships in EEG data.	Requires large amounts of labeled data, computationally intensive.
Convolutional Neural Networks (CNN) [53-56]	Specialized neural networks for grid-structured data, such as EEG spectrogram images, to capture spatial hierarchies.	Effective for extracting hierarchical spatial features.	Requires substantial labeled data, computationally intensive.
Ensemble Methods [67]	Combines multiple classifiers to improve overall performance, e.g., Bagging or Boosting.	Increases robustness and generalization of the classification model.	Increased computational complexity, potential model interactions.
Transfer Learning Approaches [57-61]	Adapts knowledge from pre-trained models or domains to enhance classification performance for motor imagery.	Utilizes prior knowledge to improve performance with limited labeled data.	Challenges in domain adaptation and source-target task alignment.
Hybrid Methods [60]	Combines multiple classification techniques (e.g., SVM with NN) to leverage the strengths of each approach.	Synergistic effects of different methods for improved robustness.	Increased complexity, potential for method interactions.

In recent years, explainable Artificial Intelligence (AI) techniques have been integrated with classifiers. Attention mechanisms in deep learning models highlight relevant portions of input data, providing insights into which electrodes or time stamped points are crucial for decision-

making [61]. Feature importance analysis for traditional classifiers aids in understanding the neurophysiological correlates of MI, enhancing interpretability. As the field progresses, there is a growing emphasis on the development of classifiers that can operate in practical scenarios. Ongoing research endeavours continue to explore novel approaches, aiming to enhance the CA, generalization ability, and real-world applicability of classifiers for MI-EEG signals.

3.4 Conclusion:

The development of effective and robust BCI systems relies on the seamless integration of pre-processing, FE, and classification modules. Ongoing research in these areas continues to push the boundaries of BCI technology, making it more accessible, reliable, and adaptable for various applications. As the field progresses, interdisciplinary collaboration between neuroscience, signal processing, and machine learning communities will play a crucial role in shaping the future of BCI systems.

Chapter 4

Hybrid TMSST-Picard based EEG artifact correction

This chapter introduces an innovative approach for automated correction of EEG artifacts. The methodology employs Pre-Conditional ICA to separate EEG activity into its original components. A thresholding criterion based on Sparse Entropy (SE) is developed to automatically identify artifact components, and the TMSST coefficients are then estimated. Processing of these coefficients retains cerebral activity leaked into artifactual components. The process concludes with inverse transformation and inverse ICA to achieve artifact-free EEG activity. The effectiveness of this methodology is substantiated through validation on both simulated and real EEG data. Results demonstrate the efficiency of the approach in preserving valuable cerebral information, rejecting artifacts, and showcasing its potential for diverse applications in BCI systems.

4.1 Introduction

In order to design an efficient BCI system, the first step is the removal of non-cerebral activities that interfere with cerebral activity in the EEG recordings. These non-cerebral activities act as artifacts in the EEG recordings. Usually, several artifact sources such as Electromyogram (EMG), Electrocardiogram (ECG), eyeblink, and ocular artifacts are present with the recorded EEG signals [68]. The EMG artifacts are introduced by the contraction of various muscles at the time of brain activity recording and are usually mixed with EEG signals [68]. Eyeblink and other ocular artifacts, usually high in magnitude, are major sources of contamination in the EEG activity. Instrumentational noise, electrical disturbances, and external electromagnetic activities could also be the sources of artifacts in EEG signals [7]. These sources of artifacts adversely corrupt the on-going EEG activity, making it difficult to extract useful information from EEG recordings and leading to erroneous classification in the BCI system [8].

Therefore, artifact removal from EEG activity is very important and has become a vital area of research in the past few years. Few researchers chose to exclude the contaminated EEG trails via identification using an appropriate thresholding criterion. However, this approach faces the drawback of losing valuable neurological information, thus making it unsuitable for the BCI system [7]. Methods utilizing Electrooculogram (EOG) referencing have demonstrated effectiveness in successfully eliminating EOG artifacts from EEG signals. In these methods, portions contaminated by ocular activity are estimated and subtracted from ongoing EEG recording. Despite being quite successful, these methods require an additional electrode for recording ocular activity, which turned out to be a drawback for their use in BCI systems [8].

Since the inception of ICA, it has emerged as a widely adopted approach for EEG denoising [71-74]. The ICA based approaches for EEG artifact removal typically entail three key steps. First, the recorded EEG activity $x(t)$, is de-mixed into Independent Components (ICs), $\hat{S}_{IC}$ (t). Subsequently, a visual identification process is employed to recognize and discard artifactual ICs (ICs contaminated with non-cerebral/artifactual activity) resulting in denoised ICs $\hat{S}_{IC\_denoised}$ (t). Finally, the artifact-free EEG signals, $\hat{x}_{clean}(t)$, are reconstructed by applying inverse ICA [35].

These approaches rely on expert visual inspection for identification of artifactual ICs [75], rendering them impractical for real-time BCI applications. Also, the rejection of entire ICs leads to the loss of valuable neurological information leaked to those ICs, eventually affecting

the information extraction from EEG activity [75]. Researchers have proposed TFA-based techniques, including WT, for the suppression or elimination of artifacts from EEG signals [76]. These methods involve thresholding and zeroing of the decomposed TF coefficients associated with the artifacts. The careful selection of an appropriate thresholding criterion is a pivotal step in implementing such methods [77-78]. TFA methods struggle to achieve an appropriate threshold value, leading to the loss of neurological activity. Moreover, the threshold value selected in these methods is fixed and does not adapt to input EEG activities.

To overcome the limitations of ICA rejection and TFA based denoising methods, Castellanos and Makarov suggested Wavelet enhanced ICA method (wICA) for artifact suppression [35]. This hybrid method combines ICA and WT to automatically remove EEG artifacts. Still, its application is restricted in real-time systems due to its sensitivity to pre-defined basis functions and a need for adaptive threshold value selection.

Considering the limitations of previous methods, in the present work, a novel automated TMSST-Picard based EEG artifact correction methodology is proposed for real-time BCI applications. The proposed fully automatic methodology is hybrid in nature and combines the Picard algorithm and TMSST. The proposed methodology unfolds in four steps. In the initial step, the contaminated EEG activity, comprising both artifactual and cerebral sources, undergoes de-mixing into ICs (EEG sources) using the Picard algorithm.

The Picard algorithm ensures a fast and efficient decomposition of EEG activity. A novel criterion based on SE is suggested and utilized for efficient and automatic identification of artifactual ICs in the second step. In the third step, the TFA of identified artifactual ICs is carried out using TMSST. Further, the TMSST coefficients, corresponding to the artifactual origins, are corrected using the spike zone thresholding criterion. Finally, inverse TFA and inverse ICA are performed, which results in noise and artifact-free clean EEG activity in the fourth step.

The contributions of the present work in EEG artifact suppression are:

- A novel criterion based on SE is proposed for automatic identification of artifactual ICs, unlike the conventional ICA based methods, which need visual inspection for EEG artifact removal.
- A novel hybrid methodology based on the Picard algorithm and TMSST is proposed for EEG artifact correction.

- The methodology corrects the artifactual ICs rather than rejecting them, which will help in retaining useful neurological activity leaked to the artifactual ICs.

The effectiveness of the proposed automatic artifact correction methodology is verified using both simulated and real contaminated EEG data. The experiments show that the proposed methodology is beneficial for correcting the artifactual EEG activity. The methodology's performance and reliability were assessed through a comparison with the state-of-the-art wICA EEG artifact suppression method.

4.2 Materials and Methods

A detailed description of datasets utilized for developing the proposed EEG artifact correction methodology is provided in this section. The methodology is developed using the simulated EEG activity and further validated on the real EEG activity. The wICA method [35], used for comparison with the proposed methodology, is also elaborated further in this section.

4.2.1 Simulated EEG data

The simulated EEG like activity is generated for assessing the outcomes and enhancing the procedural understanding of the proposed TMSST-Picard based EEG artifact correction methodology. The EEG-like activity has been simulated by following the work of Akthar et al. [79]. A sampling rate (f_s) of 256 Hz is preferred to maintain consistency with the experimentally recorded EEG activity.

In order to assess the effectiveness of the proposed methodology, 40 realizations of 6-channel EEG-like activity are simulated. A set of typical realization of six simulated EEG sources is presented in Figure 4.1(a). In Figure 4.1(a), Source-1 signifies random brain electrical activity contaminated with ocular artifacts, Source-2 to Source-4 signifies random artifact-free brain electrical activity, and Source-5 and Source-6 signify rhythmic brain activity of 12 Hz and 25 Hz, respectively. Finally, contaminated scalp EEG data is generated by multiplying source signals with a random mixing matrix (A) of size 6×6 [79]. Figure 4.1(b) represents the contaminated EEG activity produced after the random mixing of sources presented in Figure 4.1(a).

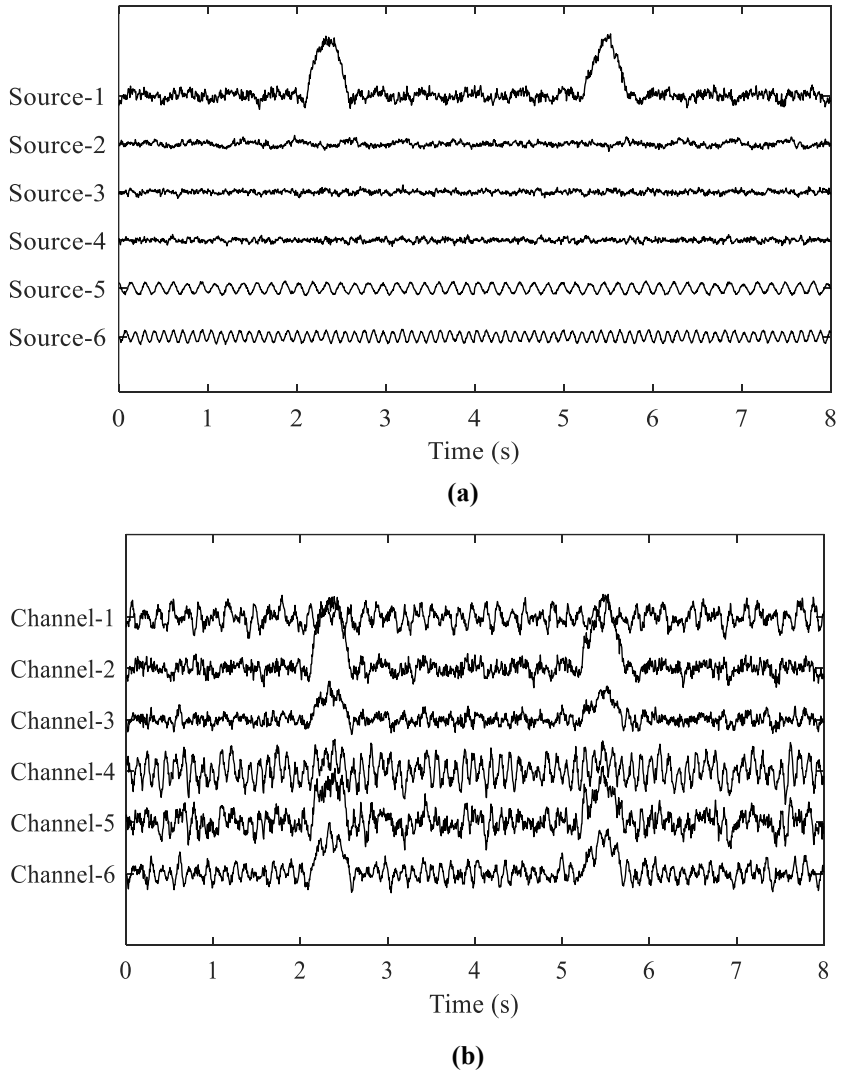

Figure 4.1 (a) Simulated EEG sources **(b)** 6-channel simulated EEG activity obtained by multiplying sources with a random mixing matrix.

4.2.2 Experimental EEG data

The efficacy of the methodology is evaluated on 19-channel and 128-channel experimentally recorded EEG activities. The 19-channel EEG activity is available online [35]. The recording of EEG signals is carried out by following the international 10-20 system of electrode placement, using a 19-channel ECI Electro-cap system. The recordings are carried out on healthy subjects at a sampling rate of 256 Hz, with their eyes open. The signals are subsequently filtered using a 50 Hz notch filter and 4 Hz high pass filter for removing 50 Hz line noise and low frequency artifacts and noises.

The recordings of the 128-channel EEG dataset are carried out in a dark testing room with BioSemi (BioSemi, Amsterdam, The Netherlands) recording system. The C17 electrode is

placed 10% of the distance measured between the nasion and inion above the nasion. Cz channel is laid over the top and center of the scalp. The electrode offset of ± 25µV is maintained during the EEG recording. The recordings are carried at a sampling rate of 2048 Hz using BioSemi acquisition software. Later, the signals are filtered by applying a 50 Hz notch filter and a 0.16-100 Hz band-pass filter.

4.2.3 Wavelet enhanced ICA (wICA) based EEG artifact suppression

For comparison purposes, the wICA artifact suppression method is performed on the same experimental EEG datasets. This section provides a description of the wICA EEG artifact suppression method. Wavelet enhanced ICA based EEG artifact suppression method was proposed by Castellanos and Makarov [35]. A significant aspect of the wICA method includes its ability to correct artifactual ICs instead of simply rejecting them. This reduces the risk of losing neurological activity along with artifactual origins. Moreover, wICA does not require an additional EOG reference channel for ocular artifact removal.

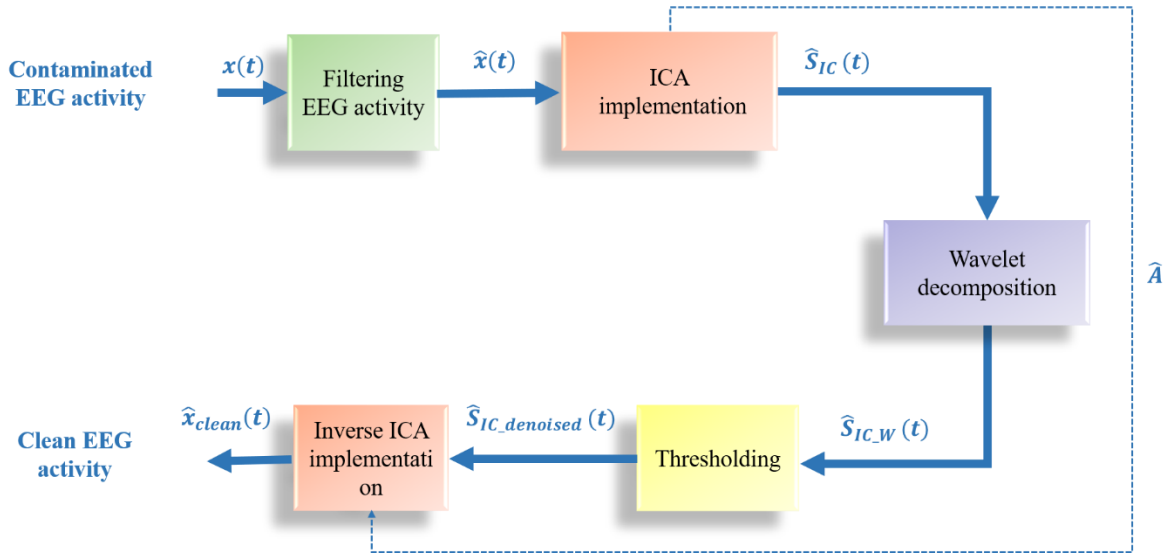

Figure 4.2 Schematic diagram of Wavelet enhanced ICA based EEG artifact suppression method

Figure 4.2 represents the schematic diagram of the wICA EEG artifact suppression method. The wICA method is implemented in three steps. Firstly, the contaminated EEG activity $\hat{x}(t)$ is de-mixed into fundamental ICs, i.e. $\hat{S}_{IC}$ (t). Secondly, the WT is applied to the de-mixed EEG activity, and a threshold is selected to suppress the wavelet coefficients corresponding to the artifactual origins. In order to obtain the denoised ICs, $\hat{S}_{IC\_denoised}$ (t), all wavelet coefficients higher than the estimated threshold are set to zero, and inverse WT is performed.

The wavelet coefficients lower than the threshold, are directly being used for inverse WT process. Thirdly, the clean EEG activity, $\hat{x}_{clean}(t)$, is attained by performing inverse ICA.

Choosing the appropriate threshold value is a critical step in the wICA method, since an inaccurate selection can result in loss of neurological activity. The wICA method works on the fixed threshold value given in Eq. (4.1).

$$\tau = 2\ log\ L\sigma \tag{4.1}$$

where L represents the length of the data segment; $\sigma = median\ (|W\ (d, b)\ |)/0.6745$, which estimates the magnitude of the neural wide band signal, where d and b define the scale and time localization, respectively.

The wICA EEG artifact suppression method is capable of retaining useful neurological information. However, this method lacks in the identification of artifactual ICs for wavelet-based correction and thus processes all ICs instead. Also, this method is not very suitable for real-time BCI systems due to its sensitivity to pre-defined basis functions and a fixed threshold. To tackle the challenge of selecting the optimal threshold value, various criteria have been proposed by researchers in the past [80-81]. However, determining the ideal threshold and base wavelet selection remains a complex and application-specific task.

4.3 Proposed Method

In the present work, a hybrid TMSST-Picard based methodology is proposed in order to correct artifacts from EEG activity. The schematic diagram of the methodology of EEG artifact correction is presented in Figure 4.3. Initially, the recorded EEG activity is filtered using a notch filter and a high pass filter. The filtered EEG activity is then de-mixed into ICs by implementing an appropriate ICA algorithm. Further, the artifactual ICs are automatically identified using SE based criterion. The identified artifactual ICs are then processed through the TMSST in order to obtain TF coefficients.

The TF coefficients, associated with artifactual origins exhibit higher values as compared to the coefficients of neurological activity. An adaptive thresholding criterion is applied to suppress the TF coefficients corresponding to the artifactual origins. Henceforth, inverse TMSST and inverse ICA are implemented in order to obtain artifact-free clean EEG activity.

The pseudo-code of the proposed TMSST-Picard based EEG artifact correction methodology is presented in Algorithm 4.1.

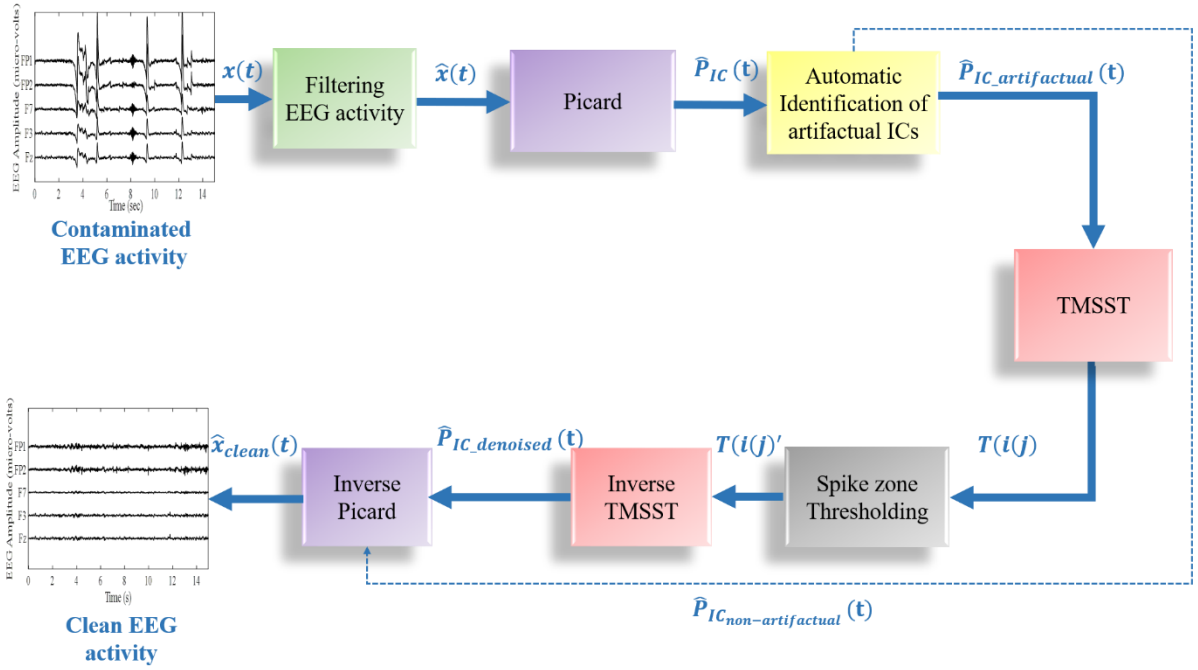

Figure 4.3 Schematic diagram of proposed TMSST-Picard based EEG artifact correction methodology

Algorithm 4.1. TMSST-Picard based EEG artifact correction methodology

Input: n-channel contaminated EEG activity $x(t)$
Output: n-channel artifact-free EEG activity $\hat{x}_{clean}(t)$
Parameter choice: Threshold selection parameters: $A = 0.01$; $B = 0.5$; $G = 1$;
TMSST parameters: $Window\ length = 130$; $Iteration\ number = 10$;
Procedure:
1 Filter the input signal $x(t)$ with 50 Hz notch filter and band pass filter: $\hat{x}(t) \leftarrow x(t)$
2 Implement Picard algorithm to de-mix $\hat{x}(t)$ into ICs: $\hat{P}_{IC}$ (t) $\leftarrow \hat{x}(t)$
3 Calculate SE of $\hat{P}_{IC}$ (t)
4 **for** $i \leftarrow 1$ to n **do**
5 **if** $SE(i)$ > Threshold **then**
6 $SE(i)$ is artifactual: $\hat{P}_{IC_{artifactual}}$ (t);
7 Go to step 11;
8 **else**
9 $SE(i)$ is non- artifactual: $\hat{P}_{IC_{non-artifactual}}$ (t);
10 Go to step 14;
11 Implement TMSST on identified artifactual ICs to obtain TF coefficients: $T(i,j) \leftarrow \hat{P}_{IC\_artifactual}$ (t)
12 Apply spike zone thresholding criterion on TF coefficients: $T(i,j)' \leftarrow T(i,j)$
13 Perform inverse TMSST on thresholded TMSST coefficients: $\hat{P}_{IC_{denoised}}$ (t) $\leftarrow T(i,j)'$
14 Combine $\hat{P}_{IC_{denoised}}$ (t) and $\hat{P}_{IC_{non-artifactual}}$ (t)
15 Perform inverse ICA (Picard): $\hat{x}_{clean}(t) \leftarrow \hat{P}_{IC_{denoised}}$ (t) + $\hat{P}_{IC_{non-artifactual}}$ (t)
16 End

The succeeding sections provide a detailed description of the processing steps involved in designing the proposed methodology.

4.3.1 EEG de-mixing using ICA

In order to efficiently de-mix EEG activity, the selection of an appropriate ICA algorithm is important. For the selection of an appropriate ICA algorithm, Fast-ICA [82], Multicombi-ICA [83], Pairwise Complex ICA (PWC-ICA) [84], and Picard [17] are implemented on 40 realizations of 6-channel simulated EEG activity. The Fast-ICA algorithm is an advancement of the conventional ICA algorithm, suggested by Hyvarinen [82]. It has extensive applications, including EEG and MEG artifact removal. In another work, Tichavsky et al. [83] proposed the Multicombi-ICA algorithm. The multicombi-ICA algorithm is designed by combining two popular algorithms, i.e., EFICA (Efficient Fast-ICA) [85] and WASOBI (Weights-Adjusted Second-Order Blind Identification) [86]. The authors demonstrated that the Multicombi-ICA algorithm performs well in analyzing EEG data. Recently, another algorithm, PWC-ICA, was introduced by Ball et al. [84] for analyzing EEG data. The authors demonstrated that the PWC-ICA algorithm performs well on simulated as well as real EEG dataset. The Picard algorithm, which is another variation of the conventional ICA algorithm, was proposed by Ablin et al. [17]. The authors successfully verified the efficiency of the Picard algorithm on several EEG signals.

In the present work, a comparative analysis of these four ICA algorithms is carried out on the simulated EEG activity to find the most suitable algorithm for EEG data analysis. Figure 4.4(a) shows 6-channel simulated EEG sources, which are mixed with a random mixing matrix in order to obtain the simulated EEG activity. This simulated EEG activity is de-mixed into fundamental ICs, i.e., simulated EEG sources, by implementing the four ICA algorithms. Figure 4.4(b), Figure 4.4(c), Figure 4.4(d), and Figure 4.4(e) depict the sets of ICs extracted after applying Fast-ICA, Multicombi-ICA, PWC-ICA, and Picard, respectively. On comparing the ICs extracted using Multicombi-ICA (shown in Figure 4.4(c)) and PWC-ICA (shown in Figure 4.4(d)) algorithms with the original EEG sources (shown in Figure 4.4(a)), it can be deduced that the two ICA algorithms failed to recover the rhythmic EEG sources. However, Fast-ICA (shown in Figure 4.4(b)) and Picard algorithms (shown in Figure 4.4(e)) successfully separated the original EEG source activity. Both of these algorithms have successfully estimated the eye-movement and eye-blink artifactual sources. The rhythmic EEG sources are also well separated by both of these algorithms. To further analyze the effectiveness of the ICA algorithms, the reconstruction Mean Square Error (MSE) is calculated with reference to the simulated EEG sources. The reconstruction MSE is estimated using four measures, including

Kurtosis, Skewness, Permutation Entropy (PE) [87], and Higuchi's Fractal Dimension (HFD) [88], and the results are shown in Table 4.1. It is analyzed that the Picard algorithm outperforms the other three algorithms and reproduced the least reconstruction MSE. Therefore, Picard is used in the present work for EEG source separation. A description of the Picard algorithm is provided in the succeeding section.

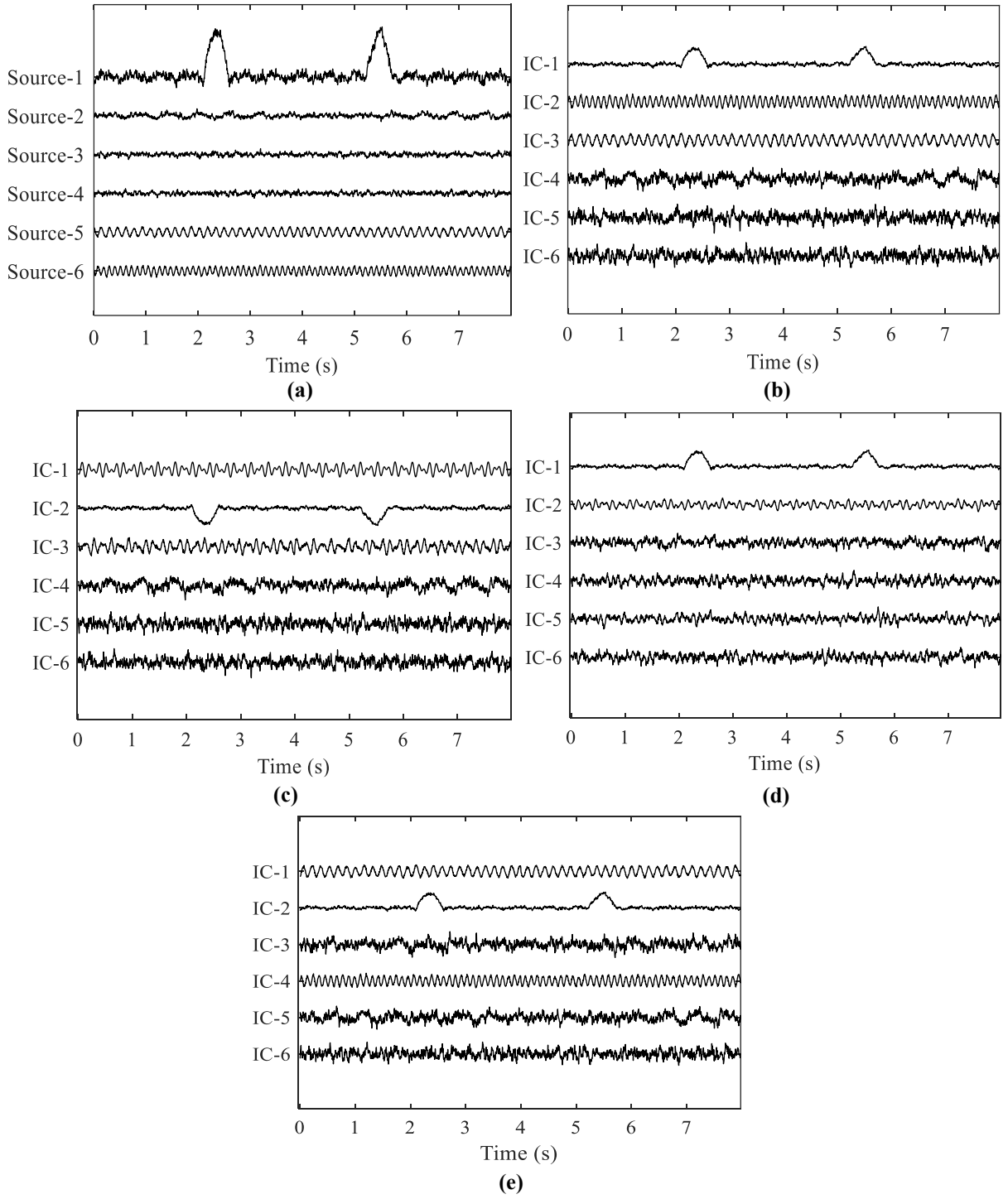

Figure 4.4(a) Simulated EEG sources **(b)** Simulated EEG activity de-mixed using Fast-ICA algorithm **(c)** Simulated EEG activity de-mixed using Multicombi-ICA algorithm **(d)** Simulated EEG activity de-mixed using PWC-ICA algorithm **(e)** Simulated EEG activity de-mixed using Picard algorithm.

Table 4.1 Reconstruction Mean Square Error (MSE) of de-mixed EEG activity

MSE	**ICA Algorithms**			
	Picard	*Multicombi*	*PWC*	*Fast*
Kurtosis	**8.83E-02**	7.18E-01	3.35E+00	1.07E-01
Skewness	**5.56E-02**	2.67E+01	1.38E-01	1.22E-01
Permutation Entropy	**3.20E-03**	2.88E+00	5.36E-01	1.61E-02
Higuchi's FD	**3.00E-04**	5.10E-02	1.96E-01	4.00E-04

4.3.2 EEG de-mixing using Picard

The Picard algorithm is a variation of the conventional ICA method. ICA is a Blind Source Separation (BSS) method that recovers the statistically ICs from a multidimensional random vector without any prior knowledge of the mixing process. ICA starts with an assumption that K number of concurrently recorded and filtered EEG signals; $\hat{x}(t) = \{\hat{x}_1(t), \hat{x}_2(t) \dots\dots\dots\dots, \hat{x}_K(t)\}$ are a linear mixture of N $(where\ N \leq K)$ unknown artifactual and neurological sources; $s(t) = \{s_1(t), s_2(t) \dots\dots\dots\dots\dots, s_N(t)\}$, i.e., $\hat{x}(t) = A.s(t)$, where A signifies the unknown mixing matrix. The ICA algorithm estimates the mixing matrix A from $\hat{x}(t)$, which in turn will help to recover the original sources (ICs). Once the matrix A is acquired, the de-mixing matrix W can be evaluated as $W = A^{-1}$. Therefore, the ICs can be estimated using Eq. (4.2).

$$\hat{S}_{IC}\,(\mathrm{t}) = W.\hat{x}(t) \tag{4.2}$$

The idea of the development of the Picard algorithm is built on the popular Infomax ICA algorithm [89], which utilizes a likelihood function based on the super-Gaussian component model. In the past, a number of methods have been proposed for faster maximization of infomax likelihood [17]. This is done by exploiting the second-order derivatives (the Hessians) of the likelihood function. However, these Hessian approximations are not accurate enough on real data. The Picard algorithm overcomes this problem by utilizing the L-BFGS optimization algorithm that uses a BFGS matrix to estimate the Hessians. The Picard algorithm uses sparse approximate Hessians as a preconditioner to the L-BFGS algorithm. It refines the Hessian approximation utilizing past iterations memory. Ablin et al. [17] have demonstrated the effectiveness of the Picard by performing numerical comparisons on a number of algorithms of the same class. According to the results of these numerical comparisons, the Picard algorithm performs very well, specifically on real data. Authors have also demonstrated the ability of the

Picard algorithm to extract meaningful sources from real EEG activity by implementing it on 13 real EEG datasets. In the present work, Picard proved to be highly efficient in de-mixing the EEG activity.

4.3.3 Automatic identification of artifactual ICs

The identification of artifactual ICs is a vital step in the proposed TMSST-Picard based EEG artifact correction methodology. For efficient correction of artifacts, it is important to identify all the artifactual ICs appropriately. In the present work, a novel SE based criterion for automatic identification of artifactual ICs is proposed. The SE based criterion is developed by considering the common characteristics possessed by artifactual components. As evident from the previous studies [90], the cerebral and non-cerebral (artifactual) activities significantly differ in statistical as well as morphological features, such as temporal dependency, spiking activity, Standard Deviation (std), kurtosis, and topographical distribution of amplitude [90]. The proposed criterion is developed on the basis of these features possessed by the artifactual components. Multivariate Multiscale Dispersion Entropy (mvMDE) [91] based sparsity method is proposed for calculating SE of the ICs, $\hat{P}_{IC}$ (t).

mvMDE is a popular non-linear parameter specially designed to measure the irregularity of multivariate time series. It is demonstrated to be efficient in discriminating the physiological states of the biomedical signals [91]. Furthermore, mvMDE is more stable and faster than the recently developed popular non-linear parameters, including Multivariate Multiscale Fuzzy Entropy (mvMFE) and Multivariate Multiscale Entropy (mvMSE) [92]. The SE based criterion is an extension of the sparsity-based criterion suggested by Zima et al. in 2012 [90]. The basis of this sparsity-based criterion is that the artifactual components have a short duration as compared to the chosen frame length. These artifactual components have higher maximum absolute value, and the median of absolute value is close to zero in comparison to the std. The SE of the de-mixed ICs can be calculated by Eq. (4.3), where std denotes the standard deviation of $\hat{P}_{IC}$.

$$SE = \frac{\max\left[|\hat{P}_{IC}(t)|\right]}{std[\hat{P}_{IC}(t)]} \times \left(\log\left\{\frac{std[\hat{P}_{IC}(t)]}{median[|\hat{P}_{IC}(t)|]}\right\}\right) \times mvMDE\{\hat{P}_{IC}(t)\} \tag{4.3}$$

The SE values of de-mixed simulated EEG activity are 0.25, 13.51, 4.85, 0.28, 3.58, 4.11 for ICs 1-6 respectively. It is evident from Figure 4.5(e) that IC-2 is contaminated by ocular artifacts. Henceforth, it is observed that the SE value of IC-2 is much higher compared to other

ICs. For the automatic identification of the artifactual ICs, an optimal threshold value needs to be estimated. A thresholding criterion based on the mean and std of calculated SE values of de-mixed ICs is proposed. The proposed thresholding criterion is given by Eq. (4.4).

$$\underline{T} = B \times (\mu(SE) + \sigma(SE)) \tag{4.4}$$

where $\mu(SE)$ and $\sigma(SE)$ are the mean and std of the calculated SE values of de-mixed ICs, and B is the weight assigned for identifying the artifactual ICs.

Table 4.2. SE values of de-mixed 19-channel EEG activity

IC	SE Value	IC	SE Value
1	**62.01433**	11	**41.75081**
2	24.44813	12	24.58352
3	**37.06547**	13	14.42586
4	16.77196	14	**40.1408**
5	29.31904	15	10.13045
6	**137.0724**	16	14.13779
7	**50.5378**	17	23.76656
8	**49.87293**	18	13.54382
9	16.46225	19	12.27183
10	18.14941		
$\boldsymbol{\mu(SE) = 33.4982}$		$\boldsymbol{\sigma(SE) = 29.2847}$	
$\underline{T} = \mathbf{31.3914}$			

As a result of experiments performed with numerous sets of real EEG activity, the value of B is fixed at 0.5. The SE values of de-mixed 19-channel real EEG activity are given in Table 4.2. The mean and std of the 19-channel de-mixed EEG activity are given by $\mu(SE)$ and $\sigma(SE)$, respectively, and the calculated threshold value is given by $\underline{T}$. The ICs having SE values above the estimated threshold ($\underline{T}$) are considered to be artifactual ($\hat{P}_{IC\_artifactual}(t)$). These identified artifactual ICs ($\hat{P}_{IC\_artifactual}(t)$) are further processed through TMSST coefficients thresholding for removing the artifactual origins. The succeeding section provides a brief description of the TMSST method.

4.3.4 Time Re-assigned Multisynchrosqueezing Transform (TMSST)

TFA methods find extensive application in examining the non-stationary characteristics of EEG signals. In the present work, a new TFA-based method, i.e., TMSST [18], is used for analyzing the behaviour of EEG activity. TMSST produces high TF resolution and energy concentration for non-stationary signals compared to the other popular transforms, such as Synchro-squeezing Transform (SST) [93], Time Re-assigned Synchro-squeezing Transform (TSST)

[94], General Linear Chirplet Transform (GLCT) [95] and STFT-based SST [96]. Time Re-assigned Multisynchrosqueezing Transform is a high energy concentrated TSST based method that utilizes a fixed-point iteration algorithm [18]. The energy concentration of TSST is further enhanced in TMSST for better analysis of non-stationary signals. The TMSST method is briefly explained in the rest of this section.

A frequency-varying mono-component signal can be expressed as [18]:

$$\hat{s}(\omega) = A(\omega)e^{i\varphi(\omega)} \tag{4.5}$$

here, $A(\omega)$ specifies the amplitude of the signal in FD, $\varphi(\omega)$ specifies the phase of the signal, and Group Delay (GD) of the signal is expressed as $-\varphi'(\omega)$.

When representing in TFD, the ideal Time-Frequency Representation (TFR) of the mono-component signal is given by Eq. (4.6), where $\delta(t)$ is the Dirac delta function.

$$I(t,\omega) = A(\omega)e^{i\varphi(\omega)}\delta(t+\varphi'(\omega)) \tag{4.6}$$

According to Eq. (4.6), the TF feature of the mono-component signal should ideally be in the GD trajectory [18]. The STFT of Eq. (4.5) in FD is given by:

$$G(t,\omega) = (2\pi)^{-1}\int_{-\infty}^{+\infty}\hat{s}(\xi)\,\hat{g}(\xi-\omega)e^{i(\xi-\omega)t}d\xi \tag{4.7}$$

where $\hat{g}(\xi)$ is the moving Gaussian Window Function (GWF) [18].

The STFT result of the signal given by Eq. (4.5) is further explored by assuming that it has weak frequency variations, i.e., $\exists\varepsilon$ is sufficiently small, $|A'(\omega)| \leq \varepsilon$ and $\varphi''(\omega) \leq \varepsilon$ for $\forall\omega$. The first-order expansion of the signal is given by:

$$\hat{s}(\xi) = A(\omega)e^{i(\varphi(\omega)+\varphi'(\omega)(\xi-\omega)} \tag{4.8}$$

For signals with strong frequency variations, i.e., $\exists\varepsilon$ is sufficiently small, $|A'(\omega)| \leq \varepsilon$ and $\varphi'''(\omega) \leq \varepsilon$ for $\forall\omega$. Eq. (4.5) can be expanded as [18]:

$$\hat{s}(\xi) = A(\omega)e^{i(\varphi(\omega)+\varphi'(\omega)(\xi-\omega)+0.5\varphi''(\omega)(\xi-\omega)^2} \tag{4.9}$$

and the FT of the GWF is given as:

$$\hat{g}(\omega) = \sqrt{2\sigma\pi}e^{-0.5\sigma\omega^2} \tag{4.10}$$

From Eq. (4.8), (4.9) & (4.10), we get,

$$G(t,\omega) = \sqrt{2\sigma\pi}\, A(\omega) e^{i\varphi(\omega)} (2\pi)^{-1} \int_{-\infty}^{+\infty} e^{0.5(i\varphi''(\omega)-\sigma)(\xi-\omega)^2}\, e^{i(t+\varphi'(\omega))(\xi-\omega)} d\xi \tag{4.11}$$

The 2D GD estimate of $G(t,\omega)$ is given by [18]:

$$\hat{t}(t,\omega) = -\varphi'(\omega) + \frac{\varphi''(\omega)^2}{\sigma^2+\varphi''(\omega)^2}(t+\varphi'(\omega)) \tag{4.12}$$

Substituting $t = -\varphi'(\omega)$ in Eq. (4.12) [18], we have

$$\hat{t}(-\varphi'(\omega),\omega) = -\varphi'(\omega) \tag{4.13}$$

This indicates that GD, $-\varphi'(\omega)$ is a fixed point of $\hat{t}(t,\omega)$ [18]. For reducing the error between $\hat{t}(t,\omega)$ and $-\varphi'(\omega)$, TMSST utilizes a fixed-point iteration algorithm with the first iteration given as:

$$\hat{t}(\hat{t}(t,\omega),\omega) = -\varphi'(\omega) + \left(\frac{\varphi''(\omega)^2}{\sigma^2+\varphi''(\omega)^2}\right)^2 (t-\varphi'(\omega)) \tag{4.14}$$

The new 2D GD estimate:

$$\hat{t}(\hat{t}(t,\omega),\omega)+\varphi'(\omega) < \hat{t}(t,\omega)+\varphi'(\omega) \tag{4.15}$$

This implies that the new 2D GD estimate is closer to $-\varphi'(\omega)$, as compared to the previous one. Further, by executing the second iteration, we get

$$\hat{t}(\hat{t}(\hat{t}(t,\omega),\omega),\omega) = -\varphi'(\omega) + \left(\frac{\varphi''(\omega)^2}{\sigma^2+\varphi''(\omega)^2}\right)^3 (t-\varphi'(\omega)) \tag{4.16}$$

the GD estimate is given by Eq. (4.16):

$$\hat{t}(\hat{t}(\hat{t}(t,\omega),\omega),\omega)+\varphi'(\omega) < \hat{t}(\hat{t}(t,\omega),\omega)+\varphi'(\omega) \tag{4.17}$$

It is seen from Eq. (4.17) that for each additional iteration, the new GD estimate approaches towards $-\varphi'(\omega)$ [18]. Therefore, after N iterations, the new GD estimate is given by:

$$\hat{t}^{[N]}(t,\omega) = -\varphi'(\omega) + \left(\frac{\varphi''(\omega)^2}{\sigma^2+\varphi''(\omega)^2}\right)^N (t+\varphi'(\omega)) \tag{4.18}$$

With a large number of iterations, the $\hat{t}^{[N]}(t,\omega)$ approaches $-\varphi'(\omega)$ [18], which shows that high TF energy can be achieved for a strong frequency-varying signal. The evaluation results of the TMSST algorithm illustrate its effectiveness in producing high-energy concentration

TFR for each component of the signal. In addition, the TMSST is highly efficient in reconstructing the transformed signals. In the present work, the artifact-free ICs are reconstructed by inverse transformation of the thresholded TMSST coefficients. Therefore, the signal reconstruction property of TMSST is essential for the development of the proposed methodology.

4.3.5 TMSST coefficients thresholding

After identification of the artifactual ICs, the TMSST coefficients thresholding is performed with the aim of correcting artifacts present in the ICs. In this process, the artifactual ICs are transformed to TFD by performing TMSST. The thresholding is performed only on the identified artifactual ICs, $\hat{P}_{IC\_artifactual}$ (t). A number of identified artifactual ICs from real EEG activity and their corresponding TMSST coefficients are depicted in Figure 4.5(a-b). Figure 4.5(a-b) demonstrates that the artifactual activity accounts for higher amplitude values of TMSST coefficients. Thus, spike zone thresholding of the TMSST coefficients $T(i,j)$ is performed to suppress the coefficients of artifactual activity.

Daly et al. [97] suggested the criterion of spike zone thresholding for EEG artifact removal. In spike zone thresholding, all the coefficients with an amplitude higher than a fixed threshold value are identified as coefficients of spiking (artifactual) activity. In the present work, the TMSST coefficients with an amplitude greater than $G \times (\mu(T) + \sigma(T))$ are identified as artifactual. Here, $\mu(T)$ and $\sigma(T)$ signifies the mean and std of the amplitude of TMSST coefficients, respectively, and G refers to the gain applied for adjusting the amplitude of spikes. The thresholding applied to the TMSST coefficients $(T(i,j))$ for suppressing the artifactual activity is given by Eq. (4.19),

$$T(i,j)' = \begin{cases} w' \times T(i,j) & if\ T(i,j) > G \times (\mu(T) + \sigma(T)) \\ T(i,j) & else \end{cases} \tag{4.19}$$

where, w' signifies the weight given to $T(i,j)$ while thresholding. Analyzing the results of numerous experiments conducted on simulated as well as real EEG activity, gain G and weight w' values are set to 1 and 0.01, respectively. Further, the thresholded TMSST coefficients, $T(i,j)'$ are processed using inverse TMSST algorithm for obtaining artifact-free ICs, $\hat{P}_{IC\_denoised}$ (t). Lastly, inverse ICA (Picard) is performed on both $\hat{P}_{IC\_denoised}$ (t) and $\hat{P}_{IC_{non-artifactual}}$ (t) to obtain artifact-free EEG activity, $\hat{x}_{clean}(t)$.

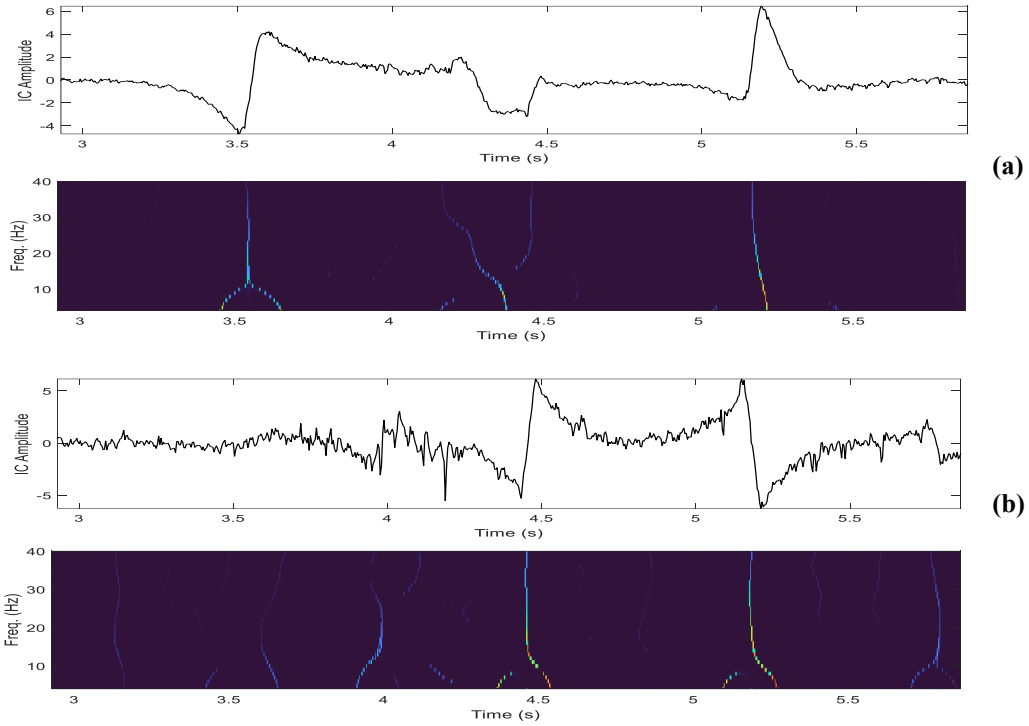

Figure 4.5 Automatically detected artifactual ICs and corresponding TMSST coefficients **(a)** IC-1 and **(b)** IC-7

4.4 Results and Discussion

The outcomes of the proposed methodology of artifact correction are evaluated using visual inspection and statistical features (Power Spectral Density (PSD), std, and kurtosis) are also compared with the state-of-the-art wICA EEG artifact suppression method. The parameter tuning of the proposed methodology is conducted using simulated EEG activity. Subsequently, the tuned parameters are applied to test and validate real EEG activity captured using 19-channel and 128-channel EEG devices.

4.4.1 Visual inspection

In order to demonstrate the efficacy of the proposed EEG artifact correction methodology, the outcomes of simulated and real EEG activity are visually inspected. Figure 4.6 showcases the efficacy of the proposed methodology when applied to simulated EEG activity. The 6-channel contaminated EEG activity obtained from simulated source signals is shown in Figure 4.6(a). After implementing the methodology on simulated EEG activity, the obtained clean EEG activity is depicted in Figure 4.6(b). It is evident from the results that the methodology has effectively corrected the simulated EEG activity. Also, it can be seen that the cerebral activity is effectively retained without any loss of information. The effectiveness of the proposed

methodology is further evaluated on 19-channel contaminated EEG activity. Figure 4.7(a) depicts the experimentally recorded 19-channel contaminated EEG activity. It can be observed that the recorded EEG activity is contaminated by multiple ocular and high-frequency artifacts. The eye blink artifacts, high-frequency artifacts, and other disturbances present in the EEG activity are depicted in Figure 4.7(a).

Picard algorithm is applied to the contaminated real EEG activity to de-mix the contaminated trails into ICs. Figure 4.7(b) shows the 19 ICs of the de-mixed 19-channel EEG activity. After visual inspection, it is observed that ICs 1, 6, 7, 8, 11, and 14 are sources of artifactual activity. For automatic identification of the artifactual ICs, SE based criterion is applied to the19 ICs. The estimated values of SE parameters are depicted through the bar chart in Figure 4.7(c). Based on the proposed SE based criterion of artifactual ICs identification, the ICs with SE parameter values above the threshold (T) are identified to be artifactual. Therefore, ICs 1, 3, 6, 7, 8, 11, and 14 are marked as artifactual ICs. Thereafter, the identified artifactual ICs are processed through the TMSST coefficient thresholding criterion.

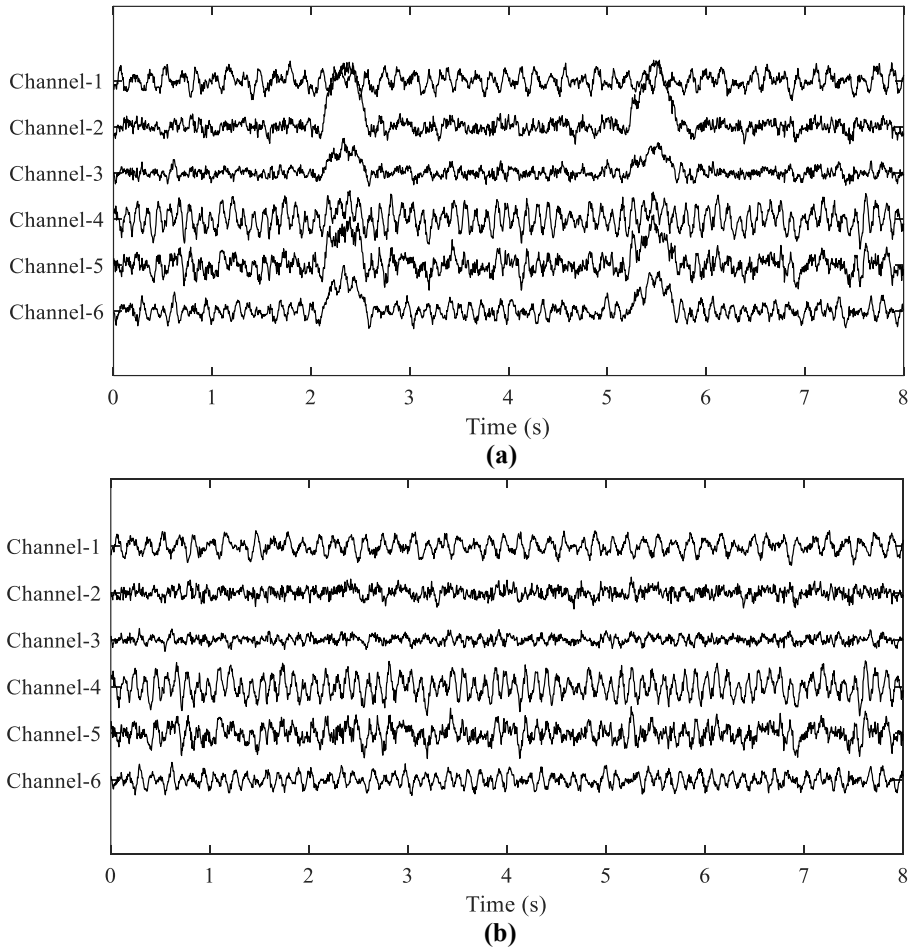

Figure 4.6(a) 6-channel simulated EEG activity **(b)** Artifact-free simulated EEG activity.

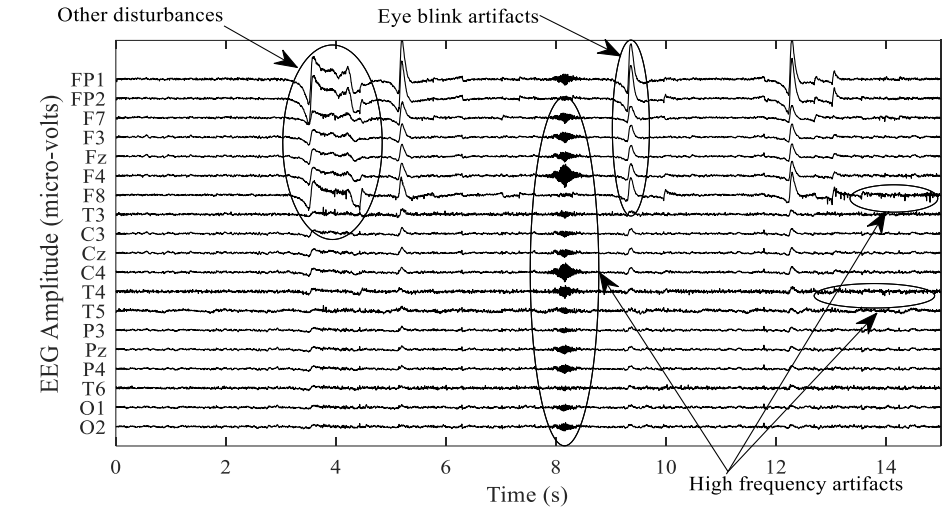

(a)

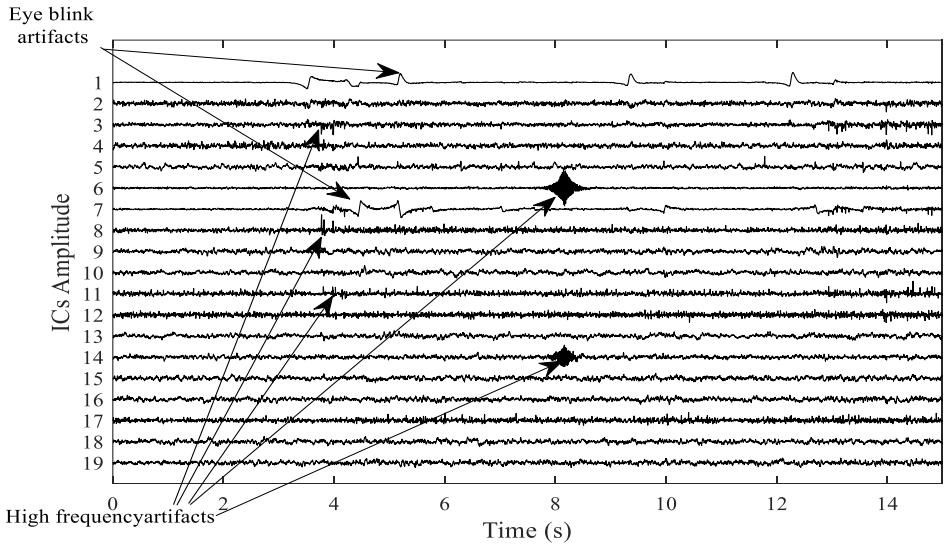

(b)

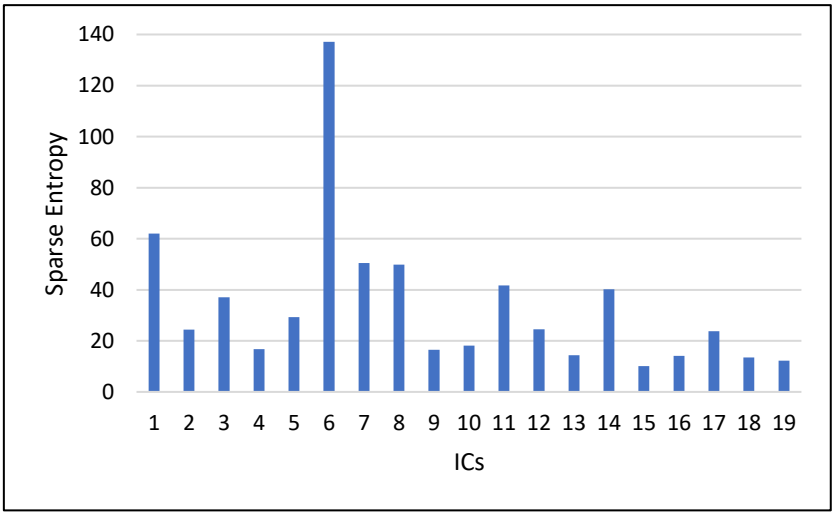

(c)

Figure 4.7 (a)19-channel contaminated real EEG activity **(b)** EEG activity de-mixed into ICs using Picard algorithm **(c)** Estimated SE parameter values of de-mixed ICs

A comparison of the identified artifactual ICs and corresponding artifact-corrected ICs is depicted in Figure 4.8(a) and Figure 4.8(b). It is observed that the proposed TMSST coefficients thresholding criterion successfully corrected the artifactual ICs. It is also evident that the non-artifactual activity is successfully retained, and there is no loss of cerebral information. Thereafter, inverse ICA (Picard) is performed on the artifact-free/artifact-corrected ICs and the non-artifactual ICs to attain artifact-free clean EEG activity. Figure 4.9 shows the 19-channel clean EEG activity obtained after treatment of contaminated EEG activity. For further evaluation, the results of the proposed TMSST-Picard based artifact correction methodology are compared with the wICA method of EEG artifact suppression. For this purpose, the wICA EEG artifact suppression method is performed on the same 19-channel contaminated EEG activity. The outcomes of the wICA approach are compared with those of the proposed methodology. The comparison of single-channel contaminated EEG activity and corresponding artifact-corrected/cleaned EEG activity, obtained by wICA and proposed TMSST-Picard based EEG artifact correction methodology, can be seen in Figure 4.10(a), Figure 4.10(b), and Figure 4.10(c). The segments where the artifacts are evidently visible are chosen for comparison purposes. It is evident that the proposed TMSST-Picard based methodology strictly follows the original non-artifactual EEG activity and corrects the artifactual activity without introducing additional noise. It can be observed that the non-artifactual EEG activity is preserved, and there is no loss of cerebral information.

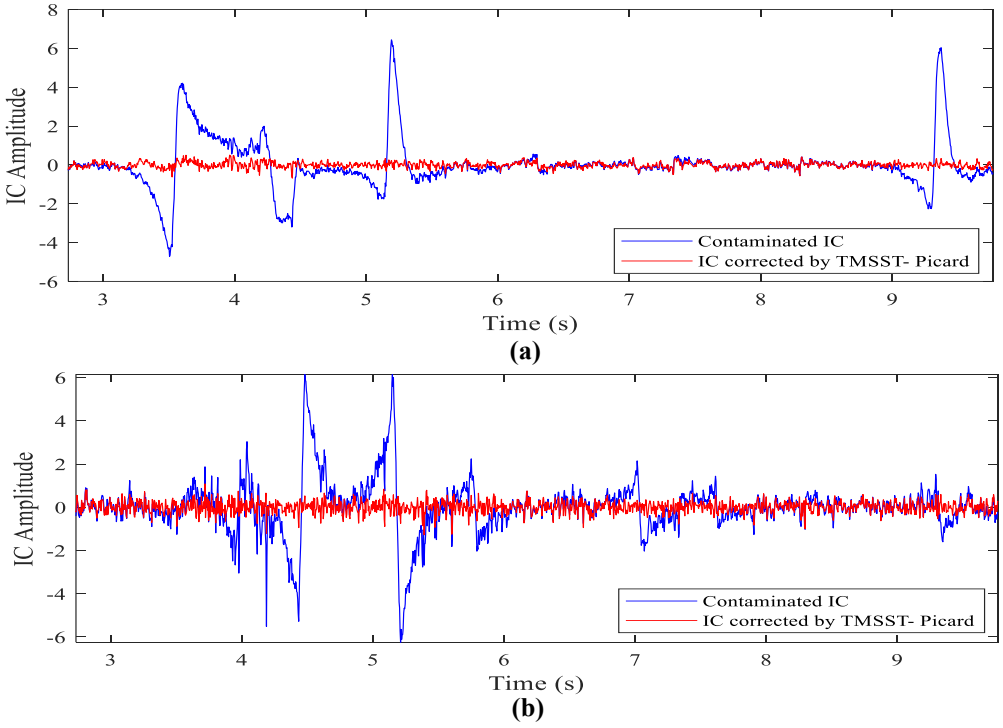

Figure 4.8 Comparison of contaminated ICs with artifact corrected ICs **(a)** IC-1 **(b)** IC-7

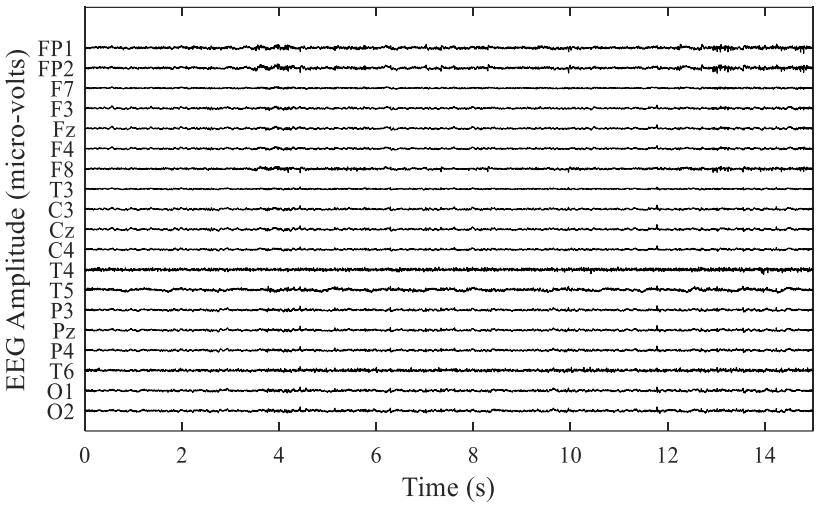

Figure 4.9 Artifact free 19-channel EEG activity

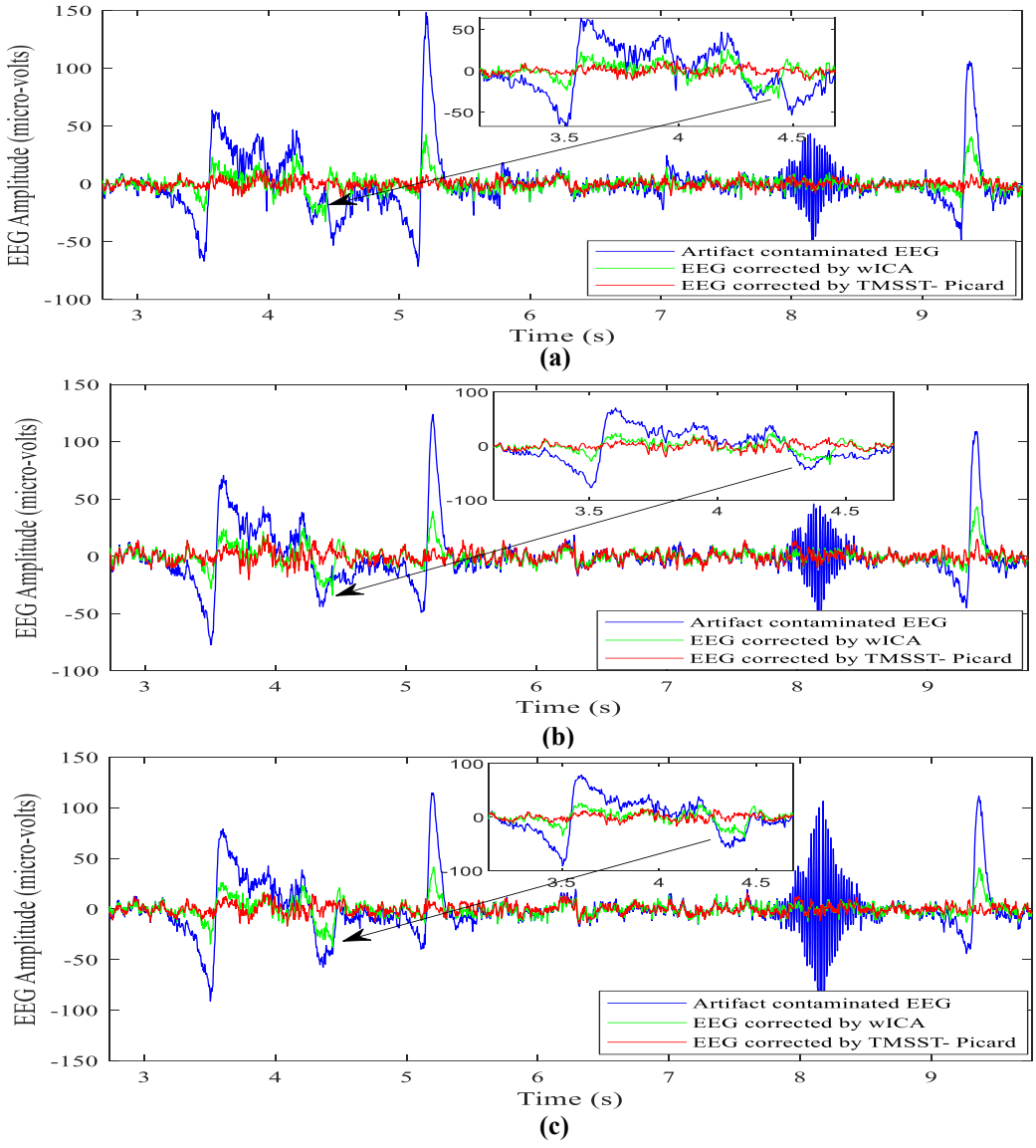

Figure 4.10 Comparison of the EEG activity cleaned using wICA and proposed TMSST-Picard based method with contaminated EEG activity **(a)** CH-3 **(b)** CH-4 **(c)** CH-6

On the other hand, it is evident from Figure 4.10 that a significant amount of residual artifactual activity is present in the output of the wICA EEG artifact suppression method. Also, it can be observed that few additional sources of noise and artifacts are introduced by the wICA method. It is observed from Figure 4.10 that the wICA method successfully removed the high-frequency artifacts; however, residual eyeblink artifacts are still present in the treated EEG activity. It is evident that the proposed TMSST-Picard based artifact correction methodology outperformed the wICA method.

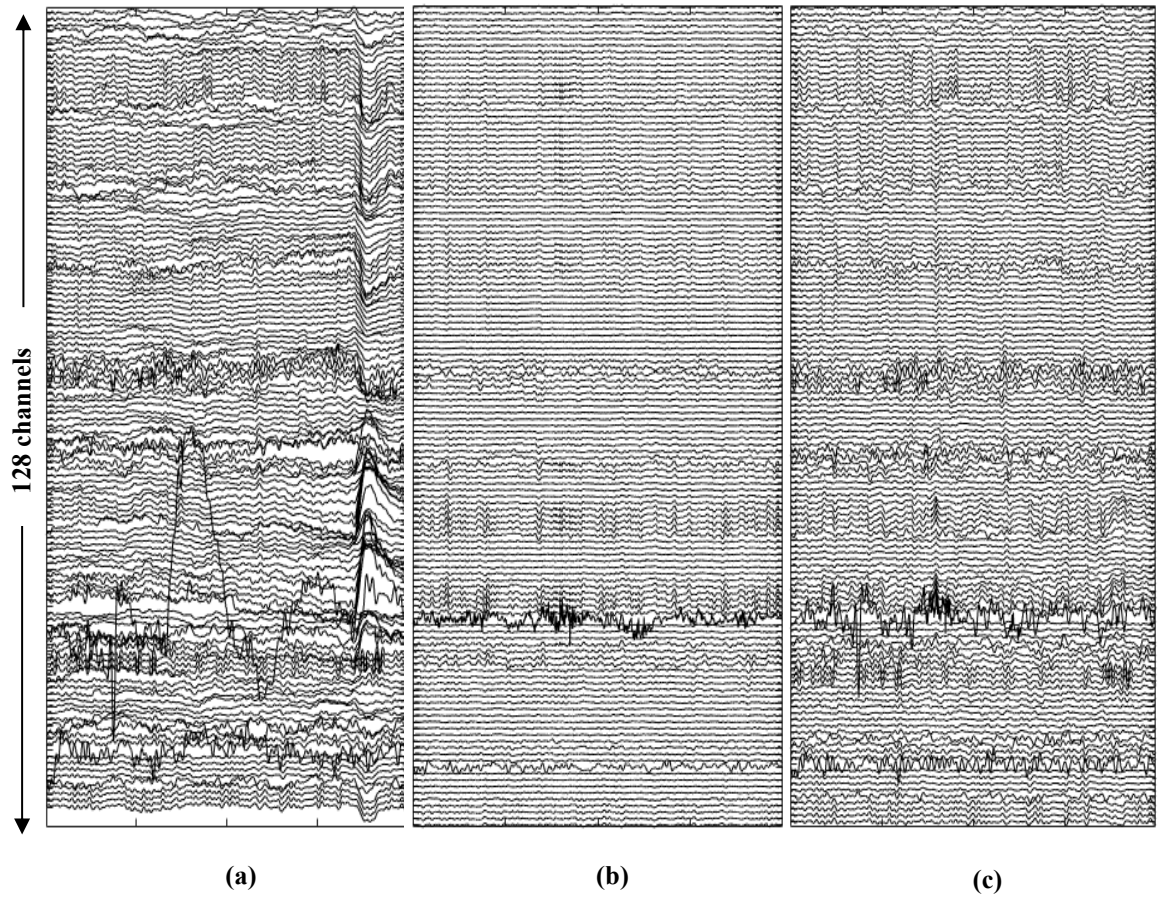

Figure 4.11(a) 128-channel contaminated EEG activity **(b)** EEG cleaned using the proposed methodology **(c)** EEG cleaned using the wICA method.

For further evaluation, the proposed TMSST-Picard based methodology is also tested on 128-channel EEG activity. A comparison is made by also performing the wICA method on the 128-channel EEG activity. Figure 4.11(a) represents a segment of the contaminated 128-channel EEG activity. This activity is cleaned using the proposed TMSST-Picard based methodology (shown in Figure 4.11(b)) and the wICA method (shown in Figure 4.11(c)).

The proposed TMSST-Picard based methodology successfully corrects the contaminated EEG activity. Also, the non-artifactual activity is retained, and there is no loss of cerebral information. It is observed that artifactual regions are suppressed, whereas the cerebral regions

are not affected by the suppression. In Figure 4.11(c), it can be observed that the wICA method is not completely able to clean the contaminated EEG activity. It is observed that the artifactual regions are not suppressed adequately. The comparative study validates that the proposed TMSST-Picard based artifact correction methodology performs better than the wICA EEG suppression methodology on 128-channel EEG activity as well.

Table 4.3. Performance analysis on 19-channel and 128-channel EEG activity

Parameters	19-Channel EEG	128-Channel EEG
P	6	116
N	13	12
TP	6	116
TN	12	9
Sensitivity	100%	100%
Specificity	92.30%	75%
Classification Accuracy	94.73%	97.65%

To further examine the effectiveness of the proposed methodology, various parameters are calculated for 19-channel and 128-channel real EEG activity, as shown in Table 4.3. The real number of artifactual ICs (P) and non-artifactual ICs (N) are identified by visual inspection Further, the True Positive (TP) and True Negative (TN) parameters are calculated, where TP represents the number of artifactual ICs identified by the proposed methodology which are actually artifactual, and TN represents the number of identified non-artifactual ICs that are actually non-artifactual. Sensitivity, Specificity, and CA of 19-channel and 128-channel real EEG activity are analyzed. It is observed that the proposed methodology obtained a CA of 94.73% and 97.65% for 19-channel and 128-channel EEG activity, respectively.

4.4.2 Standard deviation (std), kurtosis, and PSD based evaluation

For further verification, the spectral properties of the contaminated and clean EEG are also evaluated. A comparison is made between the spectral properties of EEG activity cleaned using the wICA method and the proposed TMSST-Picard based method. The PSD of both the contaminated and cleaned EEG activity is plotted in Figure 4.12(a), Figure 4.12(b), and Figure 4.12(c), which are the spectral responses of the EEG activity depicted in Figure 4.12(a), Figure 4.12(b), and Figure 4.12(c) respectively. On comparing these spectral responses with the contaminated EEG activity, it is observed that both methodologies have slightly changed the spectral properties of the EEG activity.

However, this modification is more evident at the lower frequencies. The majority of the artifacts are present in the low frequency, and correcting such artifacts leads to the change in PSD at the low frequencies. However, at higher frequencies, the spectral response of the cleaned EEG activity is almost similar to the original EEG activity. The artifacts in EEG signals introduce outliners in the signal and also lead to high variance [39]. std and kurtosis are good indicators of peaky distribution and variability [39]. Therefore, for further evaluation of the proposed methodology, the distribution of the contaminated and corrected 19-channel EEG activity is analyzed by computing std and kurtosis.

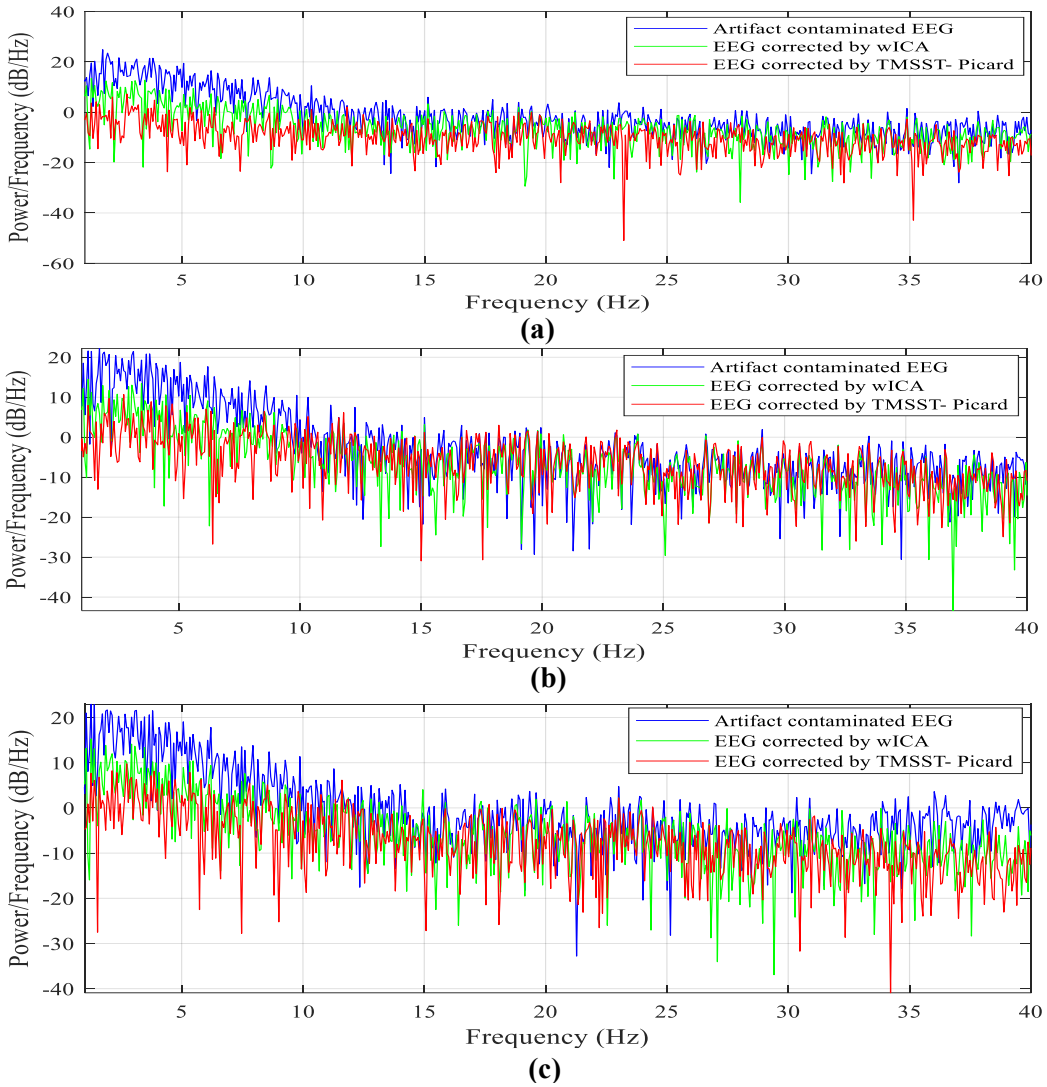

Figure 4.12 Comparison of the PSD of EEG activity cleaned using wICA and proposed TMSST-Picard based method with PSD of contaminated EEG activity **(a)** CH-3 **(b)** CH-4 **(c)** CH-6

Figure 4.13(a) graphically represents the std of 19-channel contaminated and corrected EEG activity. It is observed that the distribution of contaminated EEG is peaky and has a high std attributed to the occurrence of artifacts. It can be observed that the std of the wICA-corrected

EEG is reduced, validating the removal of artifacts. However, the distribution is still peaky and unstable, signifying that wICA does not fully eliminate the artifacts.

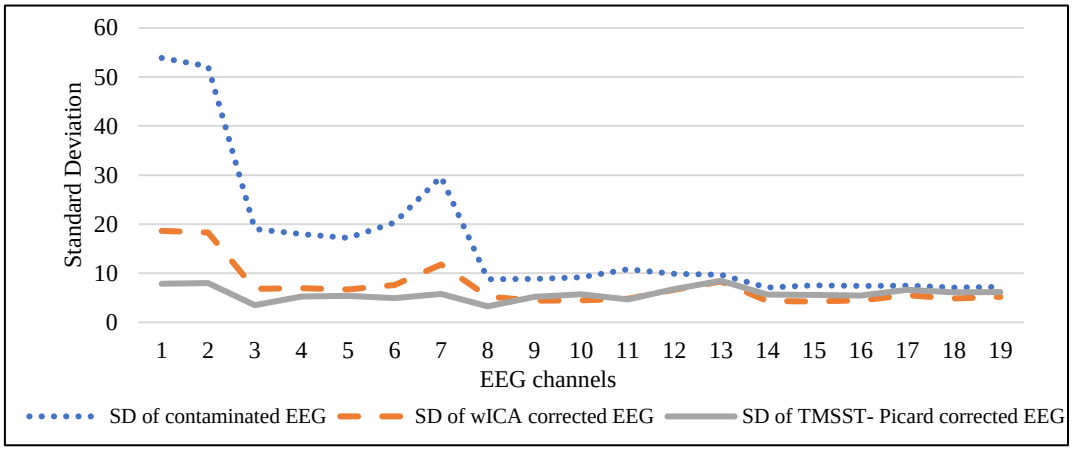

(a)

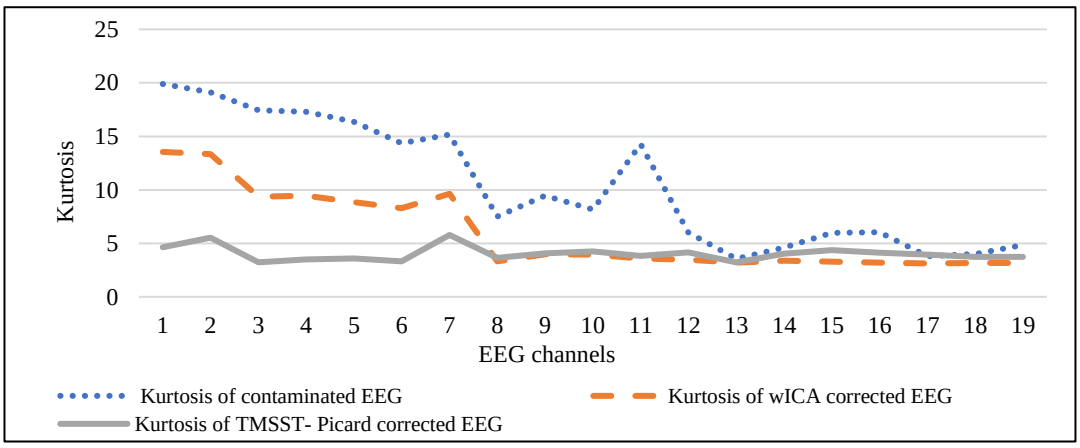

(b)

Figure 4.13 (a) Standard deviation (std) of 19-channel contaminated EEG, wICA corrected EEG, and TMSST-Picard corrected EEG **(b)** Kurtosis of 19-channel contaminated EEG, wICA corrected EEG and TMSST-Picard corrected EEG.

The std of the TMSST-Picard corrected EEG is markedly reduced and exhibits stability with no observable peaks. This validates that TMSST-Picard performs better than the wICA method in cleaning the EEG activity. Also, it is noticed that in the case of wICA-corrected EEG, the std of channels 14-19 is overly reduced, while there are negligible artifacts in these channels. This demonstrates that the wICA method is not able to suppress the artifactual activity completely and also suppresses the cerebral activity in a few channels. Figure 4.13(b) graphically represents the kurtosis values computed from contaminated and corrected 19-channel EEG activity. The contaminated EEG distribution displays a high kurtosis value, indicative of artifacts. The kurtosis of the wICA-corrected EEG has diminished to some extent in channels 1-7 and significantly decreased in channels 8-19. However, the distribution

remains unstable, indicating that wICA does not entirely eliminate the artifacts. The kurtosis of the TMSST-Picard corrected EEG undergoes a substantial reduction, demonstrating stability and affirming its effective in cleaning the EEG activity. Also, it is observed that in the case of wICA-corrected EEG, the kurtosis of channels 13-19 has been overly reduced; however, there are negligible artifacts in these channels. This shows that the wICA method suppresses the cerebral regions also.

4.4.3 Discussion

The proposed methodology is developed on 6-channel simulated EEG activity. The parameter tuning of the methodology is performed on simulated EEG activity, and later, the tuned parameters are used to test and validate real EEG activity captured using 19-channel and 128-channel EEG devices. After testing 40- realizations of simulated EEG activity and analyzing the reconstruction MSE, the Picard algorithm is found to be the most suitable for separating the EEG sources from the contaminated EEG activity in this work. For the automatic identification of the artifactual ICs, an optimal thresholding criterion based on the mean and std of calculated SE values of de-mixed ICs is proposed. The ICs having SE values above the estimated threshold ($\underline{T}$) are considered to be artifactual. The proposed SE based criterion identifies the artifactual ICs automatically, and the identified artifactual ICs are then processed through the TMSST coefficients based thresholding criterion. An adaptive thresholding criterion is applied to suppress the TF coefficients corresponding to the artifactual origins.

o demonstrate the efficacy of the EEG artifact correction methodology, the outcomes of simulated and real (19-channel and 128-channel) EEG activities are visually inspected. The results demonstrate that the SE based criterion correctly identifies the artifactual ICs. It is evident that the methodology has effectively corrected the simulated and real EEG activity without any loss of cerebral information. For further evaluation, the results of the proposed TMSST-Picard based artifact correction method are compared with the state-of-the-art wICA method of EEG artifact suppression. The comparison results demonstrate that the proposed TMSST-Picard based methodology strictly follows the original non-artifactual EEG activity and corrects the artifactual activity without introducing any additional artifacts. On the other hand, it is seen that a significant amount of residual artifactual activity is present in the output of the wICA EEG artifact suppression method. Also, it can be observed that few additional sources of noise and artifacts are introduced by the wICA method. Although the wICA method successfully removed the high-frequency artifacts, however, residual eyeblink artifacts are still

present in the treated EEG activity. It is evident that the TMSST-Picard based artifact correction methodology outperformed the wICA method.

For further evaluation, the Sensitivity, Specificity, and CA of 19-channel and 128-channel real EEG activity are analyzed. It is observed that the proposed methodology obtained CA of 94.73% and 97.65% for 19-channel and 128-channel EEG activity, respectively. The sensitivity of 100% and the specificity of 92.30% and 75% are obtained in the case of both 19-channel and 128-channel real EEG activity, respectively. The outcomes of the proposed methodology of artifact correction are also evaluated using various statistical features such as PSD, std, and kurtosis. From the std and kurtosis distribution, it can be observed that the wICA is not entirely able to correct the artifacts. In contrast, the proposed TMSST-Picard based methodology shows highly stable results, demonstrating its effectiveness in correcting the artifacts. The efficiency of the developed methodology is validated by comparing the time and FD features of the clean and the contaminated EEG activity. The results illustrate that the methodology of automatic EEG artifact correction is able to correct the artifacts present in both simulated and real EEG activities.

4.5 Conclusion

In this work, an efficient methodology is proposed for both the identification and correction of EEG artifacts. The methodology is fully automated and does not require visual inspection for artifact identification and correction. An automatic criterion based on SE is proposed for the identification of artifactual ICs. Later, the identified artifactual ICs are corrected using the TMSST coefficients based thresholding criterion. The results are analyzed on the basis of visual inspection and various statistical features (PSD, std, and kurtosis). For further evaluation, sensitivity, specificity, and CA of both 19-channel and 128-channel real EEG activity is calculated. The proposed methodology achieves a CA of 94.73% and 97.65% for 19-channel and 128-channel EEG activity, respectively. A comparison is made with a state-of-the-art method based on wICA. The time and FD analysis of the contaminated and cleaned EEG activity illustrates that the methodology performs better than the wICA method. The outcomes demonstrate that the methodology is proficient of retaining useful neurological/cerebral information and corrects artifact sources significantly from the contaminated EEG activity. Notably, the proposed methodology of automatic EEG artifact correction has the potential to be used in real-time BCI/disease diagnosis applications by reducing the false classification rate due to the artifacts present in the EEG activity.

Chapter 5

MVMD &PSR based MI- EEG task recognition

This chapter proposes a novel methodology for FE and the classification of MI-EEG signals. The proposed methodology is based on MVMD and PSR. A number of statistical and non-linear features are extracted and classified using the E-SVM model. The efficiency of the methodology is assessed on the BCI competition-IV(2a) dataset. The performance evaluation metrics include average CA, precision, F1-Score, recall, and Kappa Score (K-Score).

5.1 Introduction

One prevalent approach in BCI system design is MI, where the system records the EEG activity when the subject is engaged in the imagination of body parts movements such as hands, feet, and tongue. By analyzing these MI-EEG signals, the BCI system can discriminate between various imagined tasks and provide meaningful commands for controlling assistive devices and applications [98]. However, extraction of features from the MI-EEG signals by examining the brain dynamics is a challenging task in order to develop a successful BCI system due to the inadequate spatial resolution and low SNR of the MI-EEG signals [98]. Therefore, the FE and classification of MI-EEG signals are crucial for designing an efficient BCI system. Various methods of FE, such as CSP, FT, Autoregressive models, and Sparse representation, have been employed by researchers in the past. The FT-based approaches consider the FD information and are unable to get the TD information [19]. On the other side, the Autoregressive based methods are affected by the noise variations and hence are not very successful in extracting features [19]. The researchers have used CSP and sparse representation-based approaches, including regularized-CSP (R-CSP), spatially-regulated-CSP (SRCSP) [99], regularized CSP-aggression (R-CSP-A), CSP-Z-linear discriminant classifier (ZLDA) [100], sparse group representation model (SGRM) [101], and temporarily limited spatial group structure method (TSGSP) [102] in the past. These methods struggle with overfitting issues and are unsuitable for subjects with different training samples [19]. Researchers have also used CSP-based methods for subject-independent experiments; however, the CA achieved with such methods is not satisfactory [103]. Also, a large amount of training data is required in these approaches. In addition, such methods do not consider the multivariate nature of the signals, making them unsuitable for EEG signals as EEG rhythms may drift into diverse frequency bands [19].

To overcome these problems, multivariate extensions of Empirical Mode Decomposition (EMD) [104], Synchrosqueezing Wavelet Transform (SWT) [105], and Empirical Wavelet Transform (EWT) [106] have been proposed by researchers in recent years. These approaches are sensitive to noise and are not appropriate for long-duration signals [107]. The multivariate extension of EMD lacks mathematical formulation and suffers from the mode mixing problem. The Multivariate EMD is dependent on empirical and algorithmic characteristics and is sensitive to sampling rate and noises [107]. The EWT-based methods need predefined adaptive wavelet filter bank boundaries, which may be difficult in real-life situations due to their

complexity. Hence, the previously proposed multivariate methods need improvement to be used in MI-EEG FE for real-time BCI systems.

In recent years, researchers have suggested deep learning based FE and classification methods. The proposed methods viz. EEGNet [108], EEGNet with NSL [109], and CWT filter bank [110] are based on CNN. In these studies, the FE and classification of MI tasks are carried out using CNN. Although these methodologies produced good results with a high average CA, the training of networks is a time-consuming process. Also, the methods suffer from overfitting problems as a small number of samples per class are used to train the network. Moreover, these methods use data from a large number of channels, which increases the computational load. Hence, there is a scope for improvement in the deep learning-based methods for real-time BCI applications.

The present work aim at developing an automatic and efficient FE and classification methodology for BCI systems with a minimum number of EEG channels. In this work, a novel methodology based on MVMD and PSR is developed for FE of MI-EEG signals. The MI-EEG signals are decomposed with the help of MVMD into a number of oscillatory modes to extract meaningful information. The modes obtained are reconstructed into 2D phase space using PSR in order to better understand and analyze the MI-EEG signals. PSR is utilized for extracting the non-linear dynamics from the MI-EEG signals. The evolution of the dynamic behavior of the decomposed MI-EEG signals over time is clearly illustrated with the help of the PSR. A number of significant statistical and non-linear features are extracted from decomposed and reconstructed MI-EEG signals. A detailed analysis is conducted, and the best suitable features are selected for classifying the MI-EEG signals in various MI tasks. The E-SVM model is designed and used to classify MI-EEG signals accurately. MVMD is utilized to deal with the multivariate oscillatory nature of the MI-EEG signals. The MVMD overcomes the limitations of the previously proposed multivariate techniques, including multivariate EMD [104], multivariate SWT [105], and multivariate EWT [106]. The MVMD provides mode separability and does not require any predefined wavelet filter bank boundaries. The proposed methodology is compared to the recent methods based on CSP and deep-learning. It is analyzed that the methodology produces improved results and also uses the data from only five channels, which reduces the computational load. Also, the overfitting issues in the CSP and deep learning-based methods are overcome by carrying out 10-fold cross-validation while calculating the results.

The main contributions of the present work are:

- A novel MVMD-PSR based methodology for FE of MI-EEG signals for the BCI system is proposed. The MVMD is utilized to deal with the multivariate oscillatory nature of MI-EEG signals.
- Reconstruction of the modes decomposed using MVMD into 2D phase space is suggested for better understanding the dynamic behavior of the MI-EEG signals.
- Multiple features, including statistical as well as non-linear features, are extracted from the reconstructed MI-EEG signals.
- An average CA of 96.76% and 84.22% is obtained in binary and multi-class classification with only five EEG channels. It reduces the methodological load and makes the methodology feasible for designing a real-time BCI system.

5.2 Materials and Methods

5.2.1 Dataset

The efficacy of the proposed method is tested on a widely used multi-class MI-EEG dataset, BCI Competition IV(2a) [111]. The dataset comprises MI-EEG recordings collected from 9 healthy subjects. In the experiment, the subjects were prompted to imagine four distinct MI tasks, each associated with a specific class in the cue-based BCI paradigm. The four tasks are left-hand movement, right-hand movement, movement of both feet and tongue movement. The data is recorded in 2 sessions, with each session consisting of 6 runs with short breaks in between [111]. Each run comprises 48 trials, making a total of 288 trials per session. While recording, the subjects sat in front of a computer screen with a fixation cross displayed at the beginning of the recording trial at t=0s, accompanied by a short warning tone. At t=2s, a cue in the form of an arrow appeared on the screen, pointing in the left (class 1), right (class 2), up (class 4), or down (class 3) direction. The cue continued on screen for 1.25s, prompting the subject to perform the desired MI task. The subject continued the MI task until the fixation cross disappeared at t=6s, followed by a break with a blank screen [111].

In order to record the EEG activity, 22 Ag/AgCl electrodes were used with a 3.5 cm distance between them. The EEG signals were carefully captured at a sampling rate of 250 Hz and underwent filtering using a band pass filter with a passband frequency spanning from 0.5 Hz to 100 Hz [111]. A notch filter was used to suppress the 50 Hz line noise. Figure 5.1 depicts the

timing scheme employed for recording the MI paradigm. The EEG activity of 2s after the onset of the cue, i.e., from 2.5s to 4.5s, is utilized for testing the method proposed in present work. The placement of EEG recording channels adheres to the internationally recognized 10-20 system, which is visually represented in Figure 5.2.

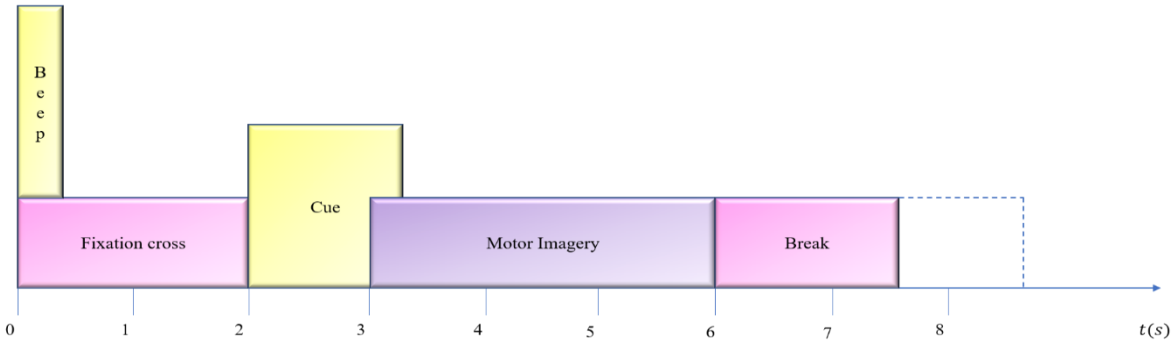

Figure 5.1 Timing scheme for recording the MI paradigm

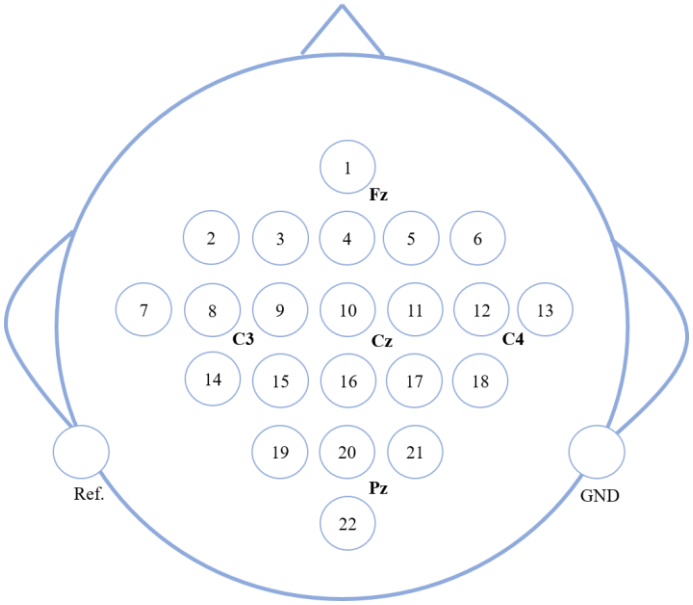

Figure 5.2 Electrode placement for recording EEG according to 10-20 international system

5.2.2 MVMD

In the present work, the MI-EEG signals are decomposed into various joint modes obtained empirically in an adaptive frequency scale using MVMD. It is an extension of the popular Variational Mode Decomposition (VMD) algorithm, which processes multivariate signals containing any number of channels [107]. The MVMD inherits the desirable properties of the standard VMD method without requiring any extra user inputs. It extracts multivariate modulated oscillations from the input signals, whereas VMD needs to be applied to each channel separately, obtaining univariate oscillations from each channel [107]. Therefore, VMD is not successful in covering multivariate oscillations, and hence, any joint information from

multiple channels could not be obtained. The MVMD also possesses the mode alignment property, leading to an alignment of modes having similar frequency across multiple channels, which is not guaranteed in the case of VMD. Hence, MVMD is appropriate for decomposing non-stationary multivariate signals such as EEG. In MVMD, the multivariate MI-EEG time series with C number of channels can be denoted as $x(t) = [x_1(t), x_2(t), \dots\dots\dots\ x_C(t)\ ]$ [107]. The MVMD extracts M number of multivariate modulated oscillations or modes $O_m(t) = \hat{x}_1(t), \hat{x}_2(t), \dots\dots\dots \hat{x}_C(t)$ from the multivariate MI-EEG signals, $x(t)$. MVMD intends to extract a collection of common multivariate modulated oscillations from the input signals. The extracted multivariate modulated oscillations or modes $O_m(t)$ can be represented as [107]:

$$O_+^m(t) = O^m(t) + jHO^m(t) = \begin{bmatrix} O_+^{m,1}(t) \\ O_+^{m,2}(t) \\ \vdots \\ \vdots \\ O_+^{m,C}(t) \end{bmatrix} \tag{5.1}$$

The bandwidth of $O_m(t)$ is calculated by utilizing the L_2 norm of gradient function of the harmonically shifted $O_+^m(t)$. The cost function F can be calculated as [107]:

$$CF = \sum_m \sum_C \left\| \partial_t [O_+^{m,C}(t) e^{-j\Omega_m t} \right\|_2^2 \tag{5.2}$$

where the frequency element Ω_m is employed for the harmonic mixing of the $O_+(t)$ vector. The bandwidth of the modulated multivariate oscillations is calculated by adjusting the unilateral spectrum range of input channels using the frequency element Ω_m and applying the Frobenius standard of the subsequent matrix. Thus, the cost function can be calculated as [107]:

$$CF = \sum_m \sum_C \left\| \partial_t [O_+^{m,C}(t) e^{-j\Omega_m t} \right\|_2^2 \tag{5.3}$$

where the analytic modulated signal is represented by $O_+^{m,C}$ with the channel number denoted as C and the mode number denoted as m. The constrained variational problem can be inscribed as [107]:

$$\text{minimize } \{O_{m,c}\},\ \{\Omega_m\} \left\{ \sum_m \sum_C \left\| \partial_t [O_+^{m,C}(t) e^{-j\Omega_m t} \right\|_2^2 \right\} \text{ subject to } \sum O_{m,c} = x_C(t), c = 1,2, \dots, C \tag{5.4}$$

For changing the constrained problem to an unconstrained variational problem, the quadratic penalty denoted as β along with Lagrangian multipliers was introduced [107]. The ADMM was employed to resolve the variational problem of producing different modes and calculating the

center frequency. The obtained mode and center frequency can be represented in the spectral-domain as [19]:

$$\tilde{O}_{m,C}^{n+1}(\Omega) = \frac{\tilde{x}_C(\Omega) - \sum_{i \neq m} \tilde{O}_{i,C}(\Omega) + \tilde{\lambda}_C(\Omega)/2}{1 + 2\beta(\Omega - \Omega_m)^2} \tag{5.5}$$

$$\Omega_k^{n+1} = \frac{\sum_C \int_0^\infty \Omega \left|\tilde{O}_{m,C}(\Omega)\right|^2 d\Omega}{\sum_C \int_0^\infty \left|\tilde{O}_{m,C}(\Omega)\right|^2 d\Omega} \tag{5.6}$$

5.2.3 Phase Space Reconstruction (PSR)

PSR is considered as an efficient tool for the extraction of the non-linear characteristics of a signal [20]. The change in dynamic behavior of a signal over the changing time can be clearly illustrated with the help of the PSR of the signal. The PSR is advantageous for searching patterns in high-dimensional or low-dimensional dynamic systems. The phase space of a d-dimensional signal $X\ (m) = \{x(1), x(2), x(3), \ldots x(M)\}$, can be stated as [20]:

$$Z(m) = (X(m), X(m + l) \ldots, X(m + (d - 1)l)) \tag{5.7}$$

$$Z(m) = \begin{bmatrix} X(1) & X(1+l) & \ldots & \ldots & \ldots & X(1+(d-1)l) \\ X(2) & X(2+l) & \ldots & \ldots & \ldots & X(2+(d-1)l) \\ . & . & \ldots & \ldots & \ldots & . \\ . & . & \ldots & \ldots & \ldots & . \\ . & . & \ldots & \ldots & \ldots & . \\ X(M-(d-1)l) & X((M-(d-1)l)+l) & \ldots & \ldots & \ldots & X(M) \end{bmatrix} \tag{5.8}$$

where $m = 1, 2, \ldots, M - (d - 1)l,$ with M number of data points in the signal, with l time lag and d embedding dimension of the 2D phase space [112]. In the proposed methodology, the value of d is taken as 2 with $l = 1$, and the 2D PSR is utilized for extracting information from the MI-EEG signals. The 2D PSR is the graphical representation of the two time-delayed vectors $X(m)$ and $X(m + 1)$ of the input signal $X\ (m)$ on the x-axis and y-axis, respectively. Various researchers have used 2D PSR to measure the uncertainty of biomedical signals [20]. In the present work, to extract information from the PSR plots, the Euclidean distance is computed from the delayed vector points to the origin point (0, 0), which can be mathematically represented as [20]:

$$E(m) = \sqrt{X^2(m) + X^2(m + 1)} \tag{5.9}$$

Various statistical and non-linear features are extracted in the present work from the calculated Euclidean distances in order to classify the MI-EEG signals. A detailed description of extracted features is provided in the succeeding section.

5.3 Proposed Method

In the present work, the MI-EEG signals from five input channels i.e. Fz, C3, CZ, C4, and Pz, are decomposed using MVMD. The five central EEG channels are considered instead of the 22 channels to lessen the complexity of the methodology. The MVMD successfully deals with the multivariate nature of the MI-EEG signals without incorporating the mode mixing problem faced by the previously discussed multivariate approaches. The MVMD method decomposes the MI-EEG signals into various multivariate modulated oscillations/modes.

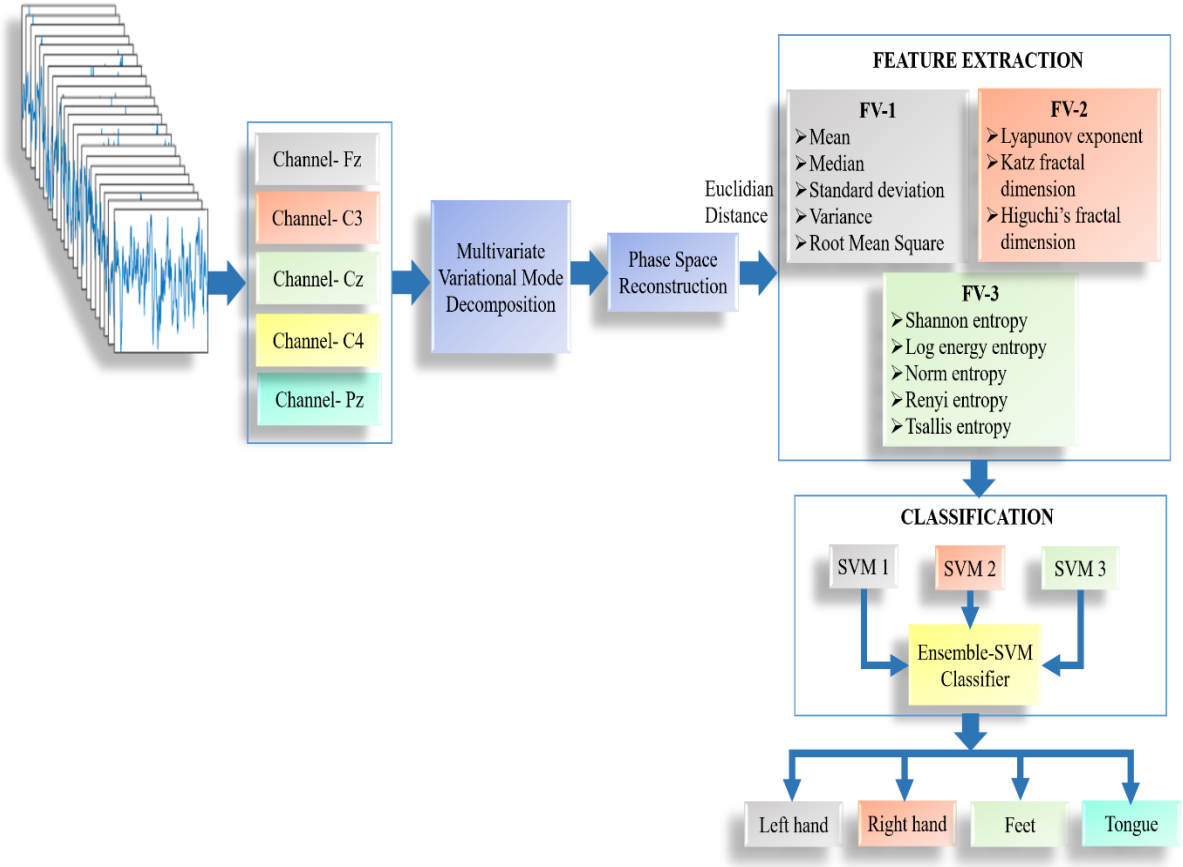

Figure 5.3 Proposed method for FE and classification of MI-EEG signals

Various statistical and non-linear features are extracted from reconstructed signals by calculating the Euclidean distances from the 2D phase space. Three different feature vectors (FVs) are constructed using the extracted features. The formed FVs are further utilized for classifying the 2-class and 4-class MI-EEG signals. For classification purposes, the E-SVM classifier is used, and the MI-EEG signals are classified into four MI tasks. After performing multiple experiments on 2-class (i.e., left hand and right hand) and 4-class (i.e., left hand, right hand, feet, and tongue) MI-EEG signals, the best features and the suitable number of

decomposition modes are selected. Figure 5.3 depicts the proposed MVMD-PSR based methodology for FE and classification of MI-EEG signals. The algorithm and detailed description of the proposed methodology are as follows:

Algorithm 5.1. MVMD-PSR based MI-EEG FE methodology

Input: **5**-channel MI-EEG signals $x(t)$
Output: Classified MI tasks: left hand, right hand, feet, and tongue
Parameter choice: MVMD parameters: $Number\ of\ modes\ (M) = 2\ to\ 5$;
PSR parameters: $Time\ delay = 1;\ Embedding\ dimension = 2;$
Procedure:
1 Decompose the 5-channel MI-EEG signals $x(t)$ into multivariate oscillations/modes $\tilde{O}$ using MVMD.
2 Reconstruct the decomposed signals $\tilde{O}$ into 2D phase space: $Z(m) \leftarrow \tilde{O}$
3 Calculate the Euclidean distance of the reconstructed signals $Z(m)$ from the origin (0,0): $E(m) \leftarrow Z(m)$
4 Extraction of statistical and non-linear features from the calculated Euclidean distance: F $\leftarrow E$(m)
5 Formation of three FVs with different features and variable modes of MVMD
6 Classify the extracted FVs into 2-class and 4-class MI tasks using the E-SVM classifier.
7 End

Figure 5.4(a-d) represents the EEG signals and their modes corresponding to five EEG channels for different MI tasks. Figure 5.4(a) represents the MI-EEG signals decomposed into four modes for class A (left hand), Figure 5.4(b) depicts the decomposed modes for class B (right hand), and Figure 5.4(c) and Figure 5.4(d) epitomizes the decomposed modes for class C (feet) and class D (tongue) respectively. The decomposed EEG signals are then reconstructed in 2D phase space using PSR, as shown in Figure 5.5 (a-d), and the Euclidean distance is calculated to extract features from the reconstructed signals. Figure 5.5(a), Figure 5.5(b), Figure 5.5(c), and Figure 5.5(d) represent the 2D PSR for mode 1, mode 2, mode 3, and mode 4, respectively, corresponding to four classes. Class A (left hand) is depicted in red; class B (right hand) is shown in blue, and class C (feet) and class D (tongue) are depicted in yellow and green color, respectively. Two time-delayed vectors $X(m)$ and $X(m+1)$ of the extracted modes are represented on the x-axis and the y-axis, respectively.

It is analyzed from Figure 5.5(a) that the PSR coefficients for class B are accumulated more around the origin and are uniformly separated into positive and negative regions. For class A (left hand), the PSR coefficients are far from the origin compared to class B. Class C has PSR coefficients far from the origin, whereas, in class D, the PSR coefficients are accumulated near the origin but contain more negative values than other classes. From Figure 4(b), it is analyzed that the PSR coefficients in class B and class D are accumulated near the origin, whereas the PSR coefficients in class A and class C are scattered comparatively. Figure 5.5(c) depicts the PSR plots for mode 3. It is observed from Figure 5.5(c) that the PSR coefficients are closer to the origin as compared to mode 1(Figure 5.5(a)) and mode 2 (Figure 5.5(b)).

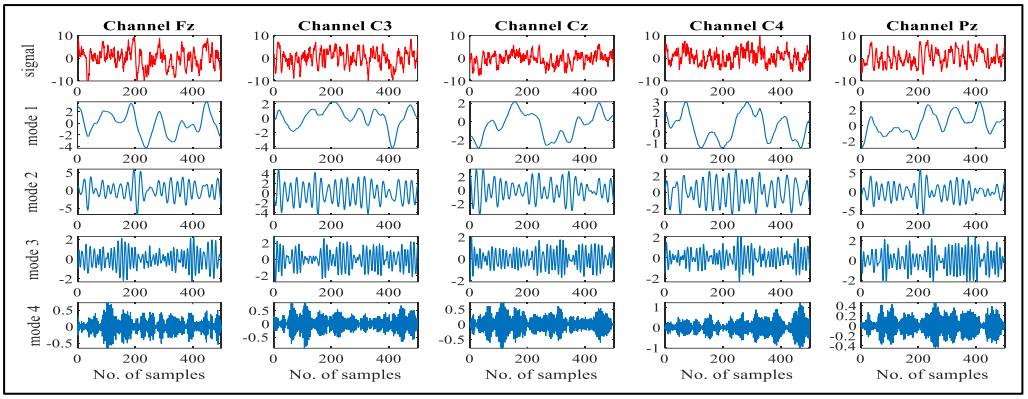

(a)

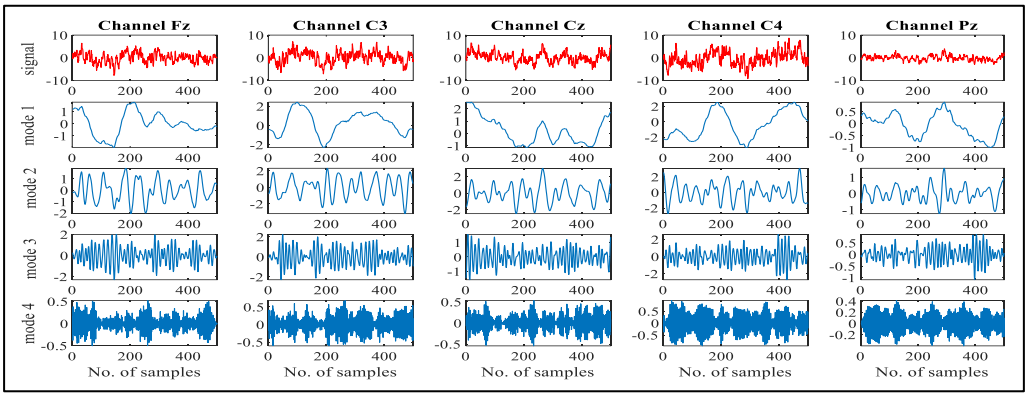

(b)

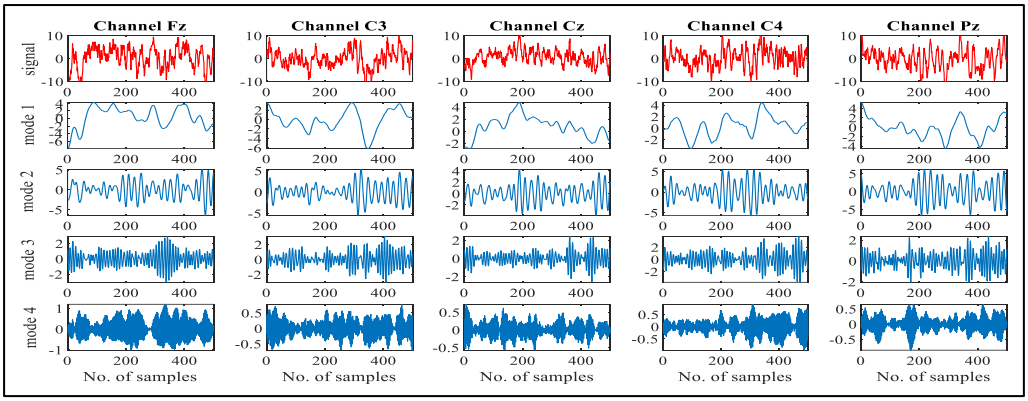

(c)

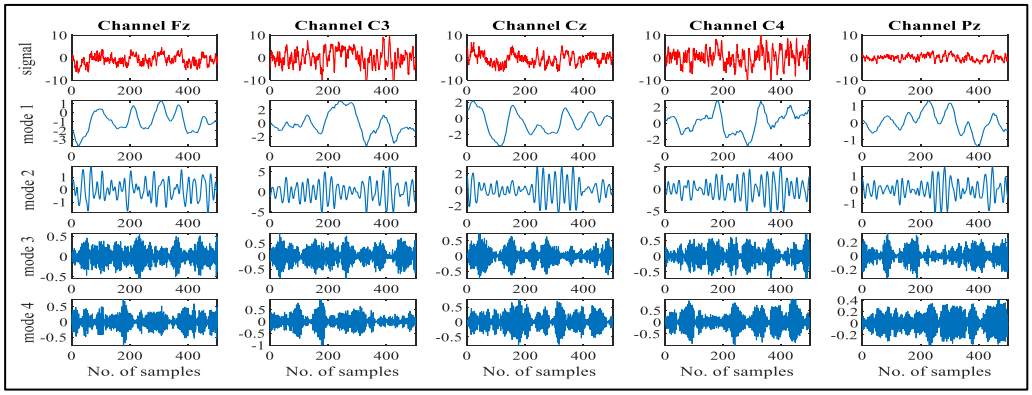

(d)

Figure 5.4 EEG signals and decomposed modes corresponding to channels Fz, C3, Cz, C4, and Pz for **(a)**left hand, **(b)** right hand, **(c)** feet, and **(d)** tongue

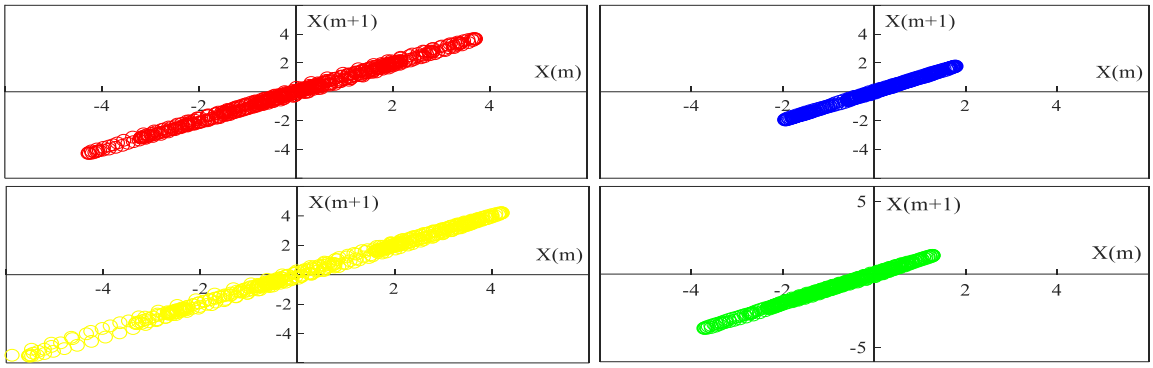

(a)

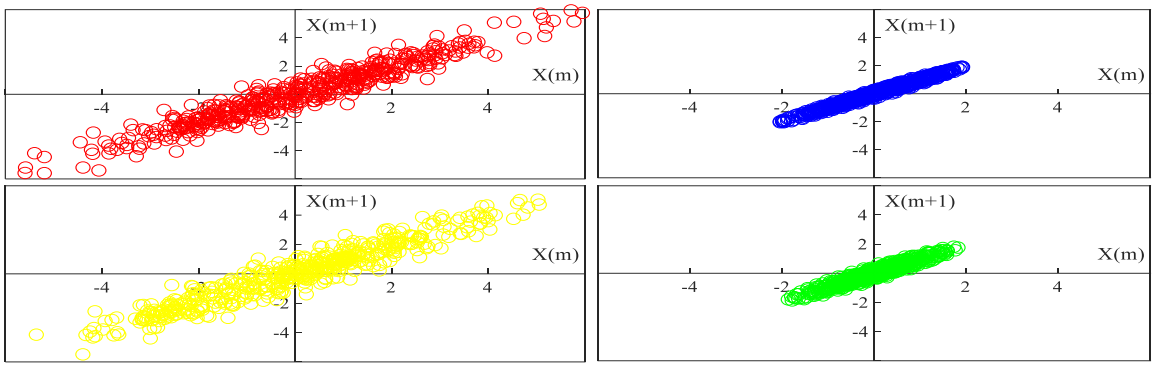

(b)

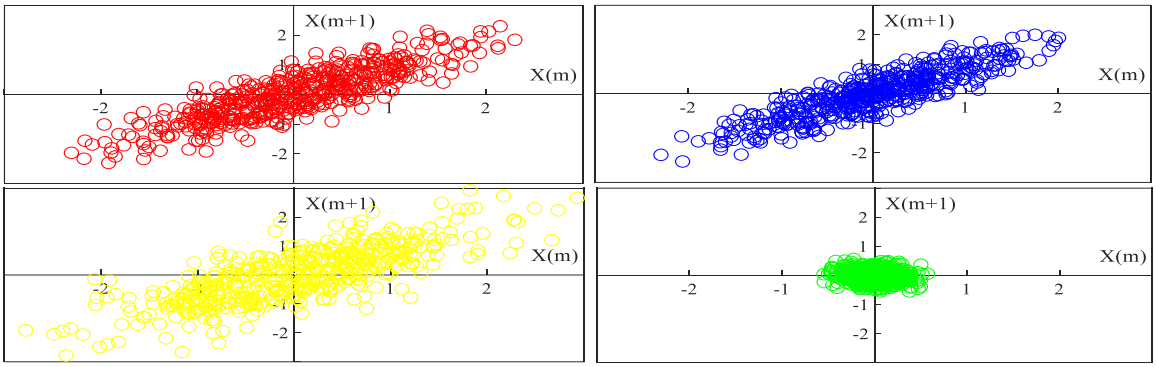

(c)

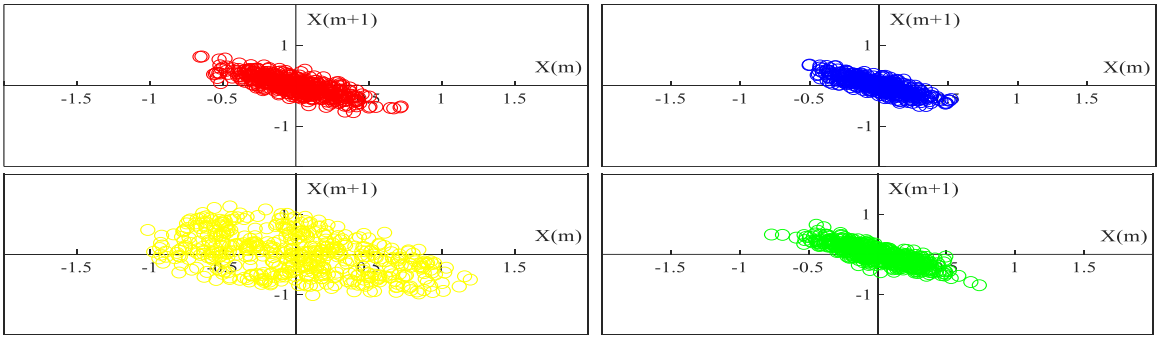

(d)

Figure 5.5 2D PSR for **(a)** mode 1, **(b)** mode 2, **(c)** mode 3, and **(d)** mode 4 corresponding to class A (red), class B (blue), class C (yellow) and class D (green)

Also, the PSR coefficients are most scattered for class C and are least scattered in class D. From Figure 5.5(d), it is observed that the PSR coefficients in the case of mode 4 are nearer to the origin as compared to all other modes and are also least scattered. It is observed that the distribution of PSR coefficients changes with the change in class in all the modes. The reconstruction of the decomposed modes into 2D phase space helps better represent and differentiate the MI-EEG signals. For evaluating further, the Euclidean distance is calculated between the origin points (0,0) and the time-delayed vectors $X(m)$ and $X(m+1)$ for extracting discriminable features to classify the MI-EEG signals.

Table 5.1 Multiple statistical and non-linear features extracted for forming the three FVs

FV-1		FV-2		FV-3	
S. No.	**Feature**	**S. No.**	**Feature**	**S. No.**	**Feature**
1	Mean	1	LE	1	Shannon entropy
2	Median	2	KFD	2	LEE
3	std	3	HFD	3	NE
4	Variance			4	RE
5	RMS			5	TE

Various features are calculated from the decomposed and reconstructed MI-EEG signals to classify the signals accurately. Three different FVs are constructed using statistical and non-linear features to analyze and classify the MI-EEG signals. Mean, median, std, variance and root mean square (RMS) are considered and calculated to construct the first FV. The second FV contains the Higuchi's fractal dimension, Lyapunov exponent (LE), and Katz's fractal dimension-based features. Entropy-based features are calculated to construct the third FV, including Shannon entropy, log energy entropy (LEE), norm entropy (NE), renyi entropy (RE), and tsallis entropy (TE). Table 1 enlists the multiple features considered for forming the three FVs. Multiple experiments were performed on the constructed FVs to classify 2-class and 4-class MI-EEG signals. The classification results were analyzed for the three FVs with a variable number of decomposition modes. The number of decomposition modes are varied from 2-5 in the present work. On the basis of these experiments, FV-1 proved to be the most promising one in the MI-EEG classification. Further, analyzing the classification results, the suitable value for the number of decomposition modes was found to be $M = 4$. The classification results for the three constructed FVs with different number decomposition modes are enlisted and discussed in the results and discussion section.

The MI-EEG signals are trained and tested in the proposed methodology using 10-fold cross-validation to avoid overfitting and statistical biasing. The SVM is a broadly used tool for the

classification of MI-EEG signals due to its versatility. For classifying the MI-EEG signals, an E-SVM classifier is used in the present work. An ensemble classifier utilizes multiple independent models and derives and output based on majority voting. In the present work, an ensemble classifier is used to avoid incorrect predictions due to bias, variance, and noise. The designed E-SVM model for classifying the MI-EEG signals is depicted in Figure 5.6. The classifier is designed using three independent SVM classifiers, viz. SVM 1, SVM 2, and SVM 3 for classifying the MI-EEG signals into 2-class and 4-class MI tasks.

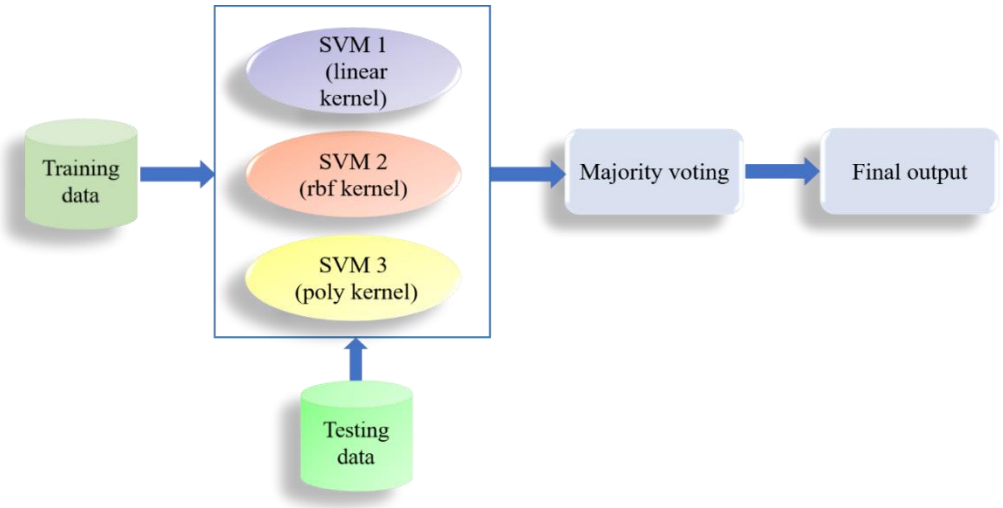

Figure 5.6 Ensemble SVM model for classifying the MI-EEG signals

The three SVM models are designed with different kernels: SVM 1 is designed using the linear kernel, SVM 2 uses the rbf kernel, and SVM 3 is built using the poly kernel. Later, a voting classifier is used to ensemble the results of the three SVM classifiers. Finally, the MI-EEG signals are classified depending on the majority voting results. The classification results of the three SVM classifiers and the E-SVM classifier are calculated and analyzed for the constructed FVs while varying the decomposition mode number from 2-5.

5.4 Results and Discussion

The proposed methodology uses MVMD and PSR to decompose and reconstruct the MI-EEG signals. Figure 5.7(a-d) shows the decomposed MI-EEG signals into four modes and their corresponding 2D PSRs for the four classes. It is analyzed that the obtained 2D PSRs are different for all four modes. Also, a considerable difference can be observed in the 2D PSRs of different classes. Several statistical and non-linear features are extracted from the calculated ED of the 2D PSR, and the EEG signals are classified using the E-SVM classifier. Various quantitative parameters are calculated and analyzed to evaluate the efficacy of the proposed

methodology's performance. The CA is considered the first parameter for measuring the performance of the proposed FE and classification methodology of MI-EEG signals.

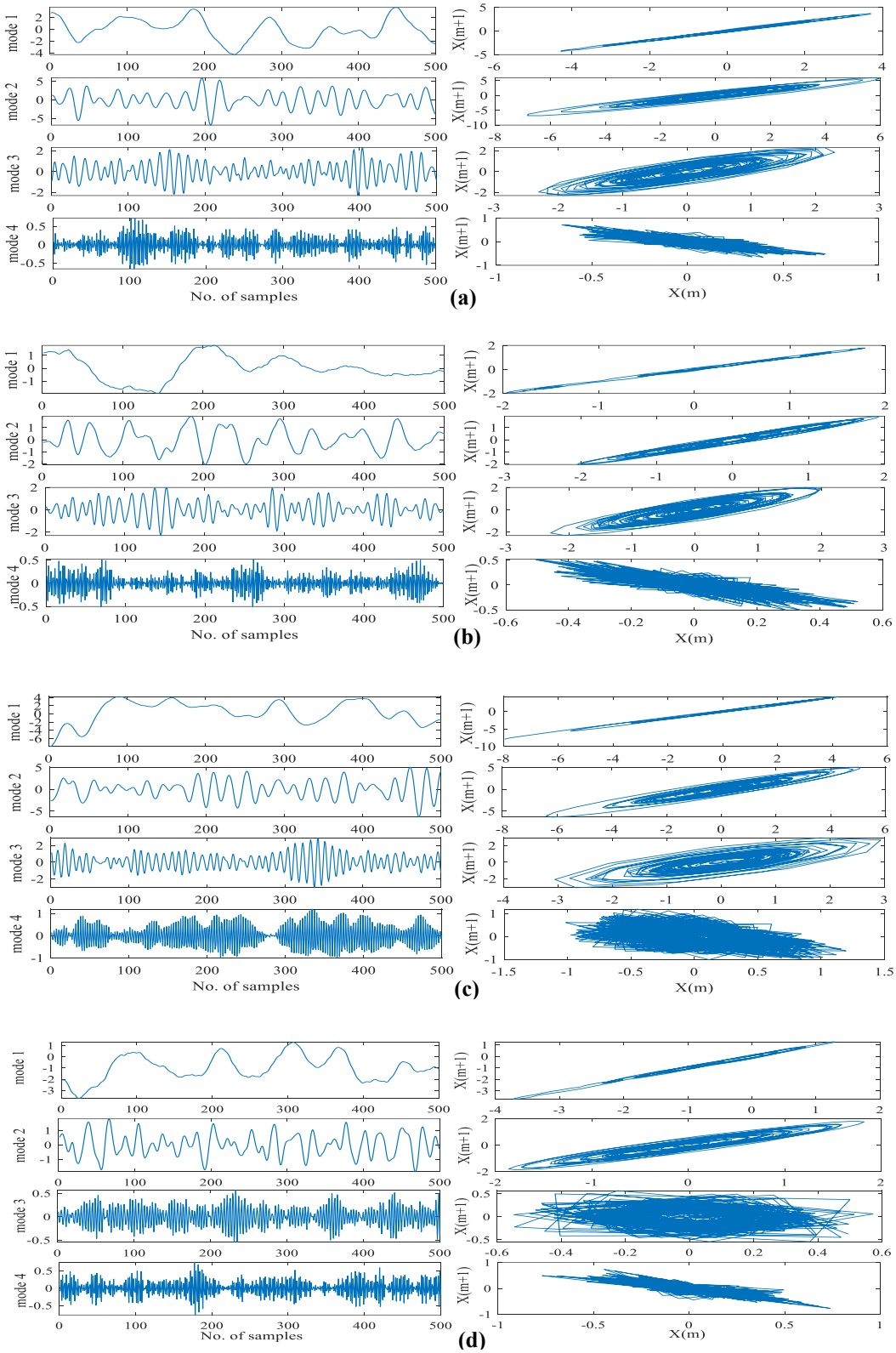

Figure 5.7 Decomposed modes of the MI-EEG signals and their corresponding 2D phase space reconstructed signals for (a)left hand, (b) right hand, (c) feet, and (d) tongue

Table 5.2 2-class and 4-class MI-EEG signals classification performance for three different FVs

2-class					4-class				
		FV-1					FV-1		
No. of modes	**SVM 1 (linear)**	**SVM 2 (rbf)**	**SVM 3 (poly)**	**Ensemble-SVM**	**No. of modes**	**SVM 1 (linear)**	**SVM 2 (rbf)**	**SVM 3 (poly)**	**Ensemble-SVM**
M-2	96.42%	96.47%	**97.85%**	**97.85%**	M-2	**91.35%**	88.22%	87.57%	89.64%
M-3	**98.57%**	97.19%	**98.57%**	**98.57%**	M-3	93.76%	93.75%	93.42%	**93.78%**
M-4	98.57%	99.28%	99.28%	**99.28%**	M-4	94.44%	**95.17%**	92.40%	95.16%
M-5	98.57%	**100.00%**	98.57%	98.57%	M-5	**94.12%**	93.78%	93.43%	93.78%
		FV-2					FV-2		
M-2	91.52%	89.47%	**94.33%**	92.90%	M-2	65.91%	57.21%	**72.15%**	66.95%
M-3	**97.90%**	96.52%	96.57%	**97.90%**	M-3	70.80%	54.13%	**71.84%**	70.11%
M-4	**97.19%**	92.28%	96.47%	**97.19%**	M-4	75.68%	68.42%	**77.06%**	75.00%
M-5	**98.61%**	97.19%	**98.61%**	**98.61%**	M-5	78.83%	66.31%	**79.51%**	79.17%
		FV-3					FV-3		
M-2	**95.04%**	**95.04%**	93.00%	**95.04%**	M-2	81.29%	84.40%	82.30%	**84.75%**
M-3	**98.57%**	95.76%	96.47%	97.19%	M-3	87.83%	91.00%	89.24%	**91.69%**
M-4	**97.85%**	97.14%	97.14%	**97.85%**	M-4	**99.65%**	95.16%	94.40%	97.57%
M-5	**98.57%**	96.42%	97.14%	97.85%	M-5	89.95%	91.00%	89.24%	**92.04%**

Table 5.2 shows the CA results achieved for 2-class (left hand and right hand) and 4-class (left hand, right hand, feet, tongue) MI-EEG signals. The number of decomposition modes is varied from 2-5, and classification accuracies are calculated from three different FVs. The classification results in Table 5.2 show that the best classification performance is achieved with FV-1 for both 2-class and 4-class MI-EEG classification. The highest CA of 99.28% and 95.16% is achieved with the number of decomposition modes M=4 for 2-class and 4-class, respectively. The classification results conclude that the extracted statistical features are useful in classifying both binary and multi-class MI-EEG signals with high CA. The non-linear features extracted to form the FV-2 perform well for 2-class classification but are not successful in classifying 4-class EEG data. The CA of 97.19% is achieved in the case of 2-class classification, whereas in 4-class classification, the maximum CA achieved is only 79.17%. It is analyzed that the extracted non-linear features are not successful in differentiating between the four classes. On the other hand, the FV-3, which consists of entropy-based features, performs well in both binary and multi-class MI-EEG signal classification. CA of 97.85% and 97.57% is achieved for 2-class and 4-class classification, respectively. Figure 5.8 represents the classification results for 2-class classification with the E-SVM classifier. It is observed that FV-1 performs very well with the changing number of decomposition modes, and an average CA of 98.57% is achieved. The average CA obtained with FV-2 and FV-3 is 96.98% and 96.65%, respectively.

Figure 5.9 represents the CA achieved for 4-class MI-EEG signals with a variable number of modes using three FVs. It is observed that the results obtained from FV-1 outperform the results obtained from FV-2 and FV-3. The highest average CA of 93.09% is obtained from FV-1. Also, FV-2 performs very well, with an average CA of 91.50%. However, the results obtained from FV-3 are not satisfying, with an average CA of only 72.81%. From the classification results depicted in Figure 5.8 and Figure 5.9, it is concluded that FV-1 outperforms the other two FVs. Hence, the statistical features calculated for forming the FV-1 are considered for further evaluation.

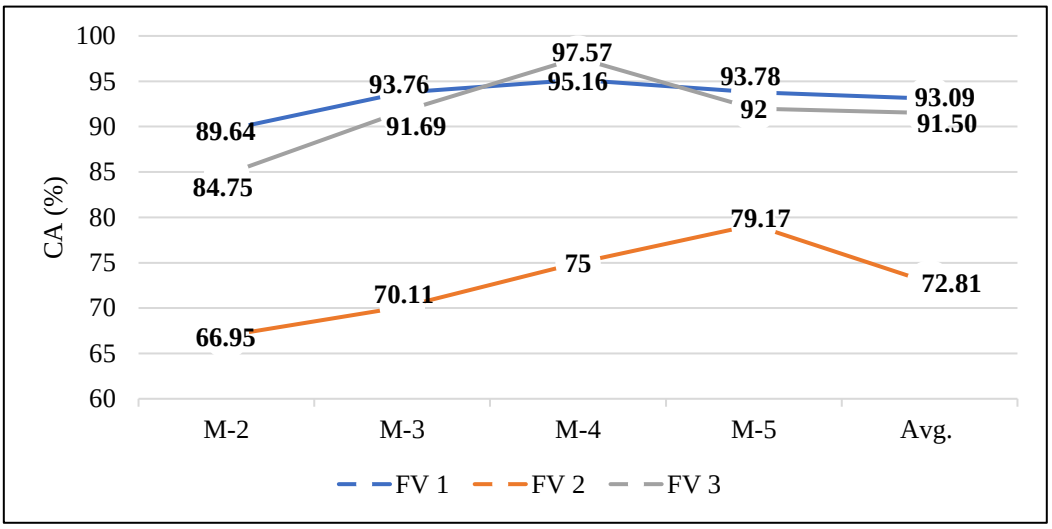

Figure 5.8 CA (%) achieved for 2-class (left hand and right hand) MI-EEG signals, with variable modes using the three FVs

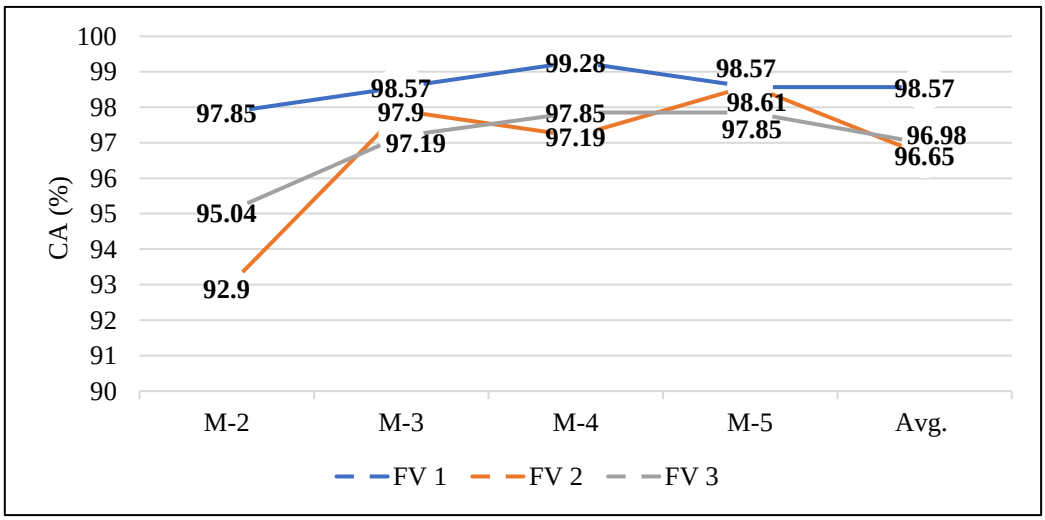

Figure 5.9 CA (%) achieved for 4-class MI-EEG signals, with a variable number of modes using three FVs

In the present work, it is concluded that the suitable value for the number of decomposition modes is $M = 4$; hence, M is fixed to 4 in further calculations. For binary classification, the 4-classes are paired, and their classification results are obtained and analyzed. Table 5.3 shows

the CA obtained for all six pairs of classes of nine subjects: A01-A09. It is analyzed that the highest CA of 100% is achieved at specific occasions. The average CA is calculated subject-wise as well as class-wise. The highest average CA of 97.76% is achieved in the case of subject A08. The lowest average CA of 76.06% is obtained in the case of subject A05. When compared class-wise, class AB (left hand vs. right hand) achieved the highest average classification of 96.76% for all nine subjects. The lowest average CA of 84.37% is obtained in the case of class AC (left hand vs. feet).

Table 5.3 CA (%) for nine different subjects across six pairs of classes

	CA (%)						
Subject	**Class-AB**	**Class-AC**	**Class-AD**	**Class-BC**	**Class-BD**	**Class-CD**	**Average**
A01	99.28	86.28	100	100	97.9	100	97.24
A02	94.61	59.42	85.76	95.85	96.61	82.71	85.82
A03	98.51	81.85	99.33	98.61	91.66	98.61	94.76
A04	100	100	100	100	100	66.76	94.46
A05	82.04	85.52	63	75.09	75.76	75	76.06
A06	99.33	71.47	99.33	99.28	77.57	100	91.16
A07	98.57	90.19	95.8	99.28	100	91.66	95.91
A08	99.28	92.95	100	97.85	97.23	99.28	**97.76**
A09	99.28	91.66	100	97.9	86.23	97.95	95.50
Average	**96.76**	84.37	93.69	95.98	91.44	90.21	92.07

For further validation of the proposed methodology, the K-Score is calculated and analyzed for 2-class and 4-class MI-EEG signal classification. The K-Score, also known as Cohen's kappa coefficient, is a significant performance measure of inter-rater agreement or reliability. It is commonly used for BCI problems, providing a more robust evaluation by considering the possibility of wrong classifications.

In the context of BCI classification, the K-Score is used to assess the agreement between the predicted classes generated by a BCI system and true classes of the intended user's brain activity. It quantifies the degree of agreement beyond what would be expected by chance. The K-Score ranges from -1 to 1, with 1 showing perfect agreement and -1 indicating disagreement between the predicted and true classes. The K-Score greater than 0.8 indicates excellent agreement, between 0.6 and 0.8 indicates good agreement, between 0.4 and 0.6 indicates moderate agreement, and less than 0.4 indicates poor agreement. The K-Score can be computed using the confusion matrix:

$$\mathrm{K-Score} = (P_o - P_e)/(1 - P_e) \tag{5.10}$$

where P_o represents the observed agreement, which is the proportion of the total agreement between the predicted class and true class, and P_e represents the expected agreement, which is an agreement expected by chance. The K-Score provides a more robust evaluation metric beyond simple CA, specifically when dealing with imbalanced datasets or situations where chance agreement is a concern.

Table 5.4 Calculated K-Score for nine different subjects across six pairs of classes

	K-Score						
Subject	**Class-AB**	**Class-AC**	**Class-AD**	**Class-BC**	**Class-BD**	**Class-CD**	**Average**
A01	0.99	0.72	1.00	1.00	0.96	1.00	0.94
A02	0.89	0.19	0.71	0.92	0.93	0.65	0.71
A03	0.97	0.63	0.99	0.97	0.83	0.97	0.89
A04	1.00	1.00	1.00	1.00	1.00	0.33	0.88
A05	0.64	0.71	0.26	0.50	0.51	0.50	0.52
A06	0.99	0.43	0.99	0.99	0.55	1.00	0.82
A07	0.97	0.80	0.92	0.99	1.00	0.83	0.91
A08	0.99	0.86	1.00	0.96	0.94	0.99	**0.95**
A09	0.99	0.83	1.00	0.96	0.72	0.96	0.91
Average	**0.93**	0.68	0.87	0.92	0.82	0.80	0.84

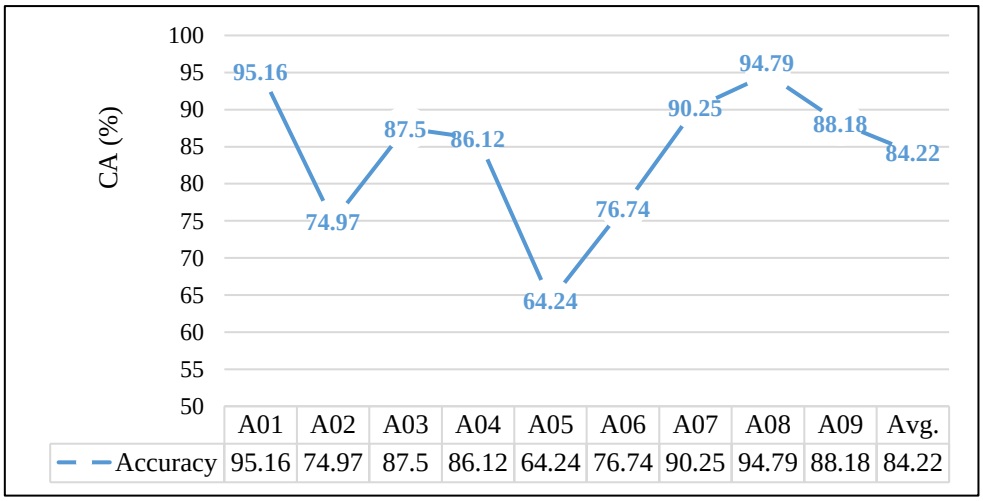

Figure 5.10 CA (%) obtained in the case of 4-class classification

Table 5.4 enlists the K-Scores calculated for all nine subjects for the 2-class classification of all six pairs of classes. It is observed that the highest average K-Score of 0.95 is achieved with subject A08, whereas the lowest average K-Score of 0.52 is obtained by subject A05 when considering all six pairs of classes. The highest average K-Score of 0.93 is obtained in the case of class AB (left hand vs. right hand) for all nine subjects: A01-A09. The lowest average K-Score of 0.68 is obtained for class AC (left hand vs. feet). Figure 5.10 shows the CA obtained in the case of 4-class classification utilizing the E-SVM classifier. The CA is measured

corresponding to all nine subjects: A01-A09. It is analyzed that the highest CA of 95.16% is achieved for subject A01. The lowest CA of 64.64% is attained for subject A05. The average CA of 84.22% is achieved for the 4-class classification. It is analyzed that the methodology classifies the MI-EEG signals well, even for 4-class classification. The highest CA in the 2-class and 4-class classifications is 100% and 95.16%, respectively. It can be concluded that the proposed methodology achieved good CA in both binary and multi-class classification.

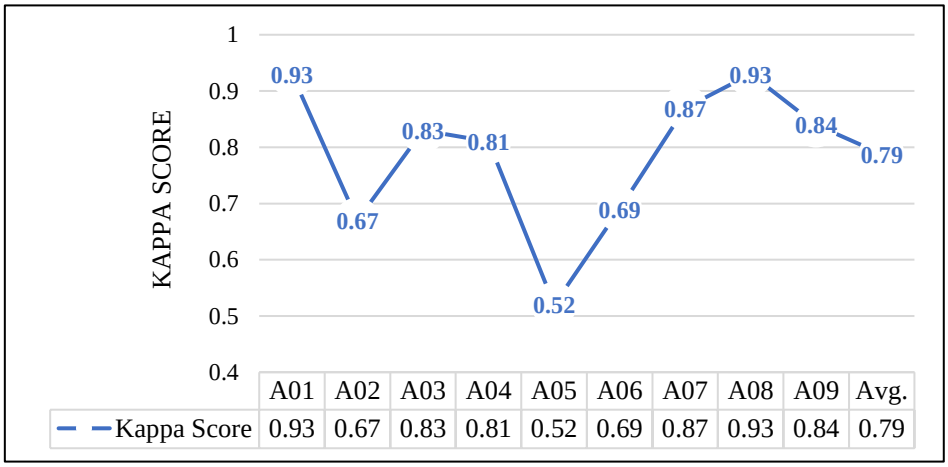

Figure 5.11 K-Score for subjects A01-A09 for 4-class classification

Table 5.5 Evaluation results for 4-class classification for CA (%), K-Score, precision, recall, and F1-score parameters corresponding to all nine subjects

Subjects	CA (%)	K-Score	Precision	Recall	F1-Score
A01	**95.16**	**0.93**	**0.95**	**0.95**	**0.95**
A02	74.97	0.67	0.75	0.75	0.75
A03	87.5	0.83	0.88	0.88	0.88
A04	86.12	0.81	0.86	0.86	0.86
A05	64.24	0.52	0.66	0.64	0.65
A06	76.74	0.69	0.77	0.77	0.77
A07	90.25	0.87	0.90	0.90	0.90
A08	94.79	**0.93**	**0.95**	**0.95**	**0.95**
A09	88.18	0.84	0.89	0.88	0.88
Avg.	84.22	0.79	0.85	0.84	0.84

Figure 5.11 represents the calculated K-Score for subjects A01-A09 in the case of 4-class classification. It can be observed that the maximum K-Score of 0.93 is obtained for subjects A01 and A08. An average K-Score of 0.79 is obtained in the case of the 4-class classification. In order to further assess the proposed methodology for 4-class classification, the precision, recall, and F1- scores are also calculated for all subjects. The precision, recall, and F1-score can be calculated as:

$$Precision = \frac{TP}{TP+FP} \tag{5.11}$$

$$Recall = \frac{TP}{TP+FN} \tag{5.12}$$

$$F1 - Score = \frac{2\ Precision \times Recall}{Precision+Recall} \tag{5.13}$$

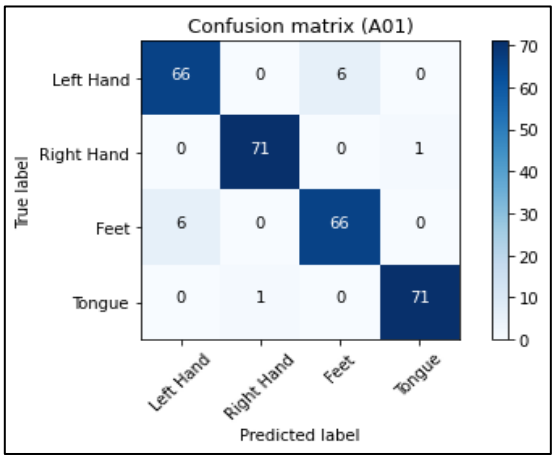

(a)

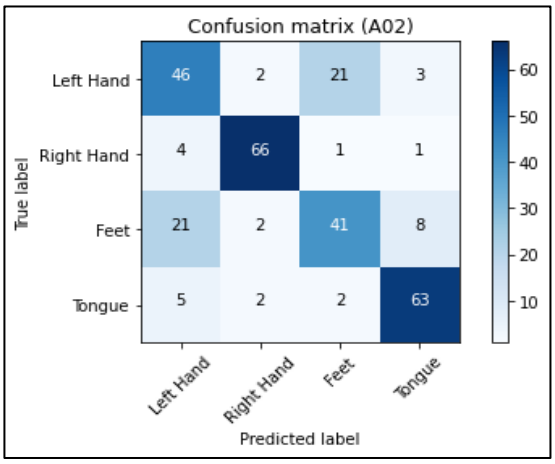

(b)

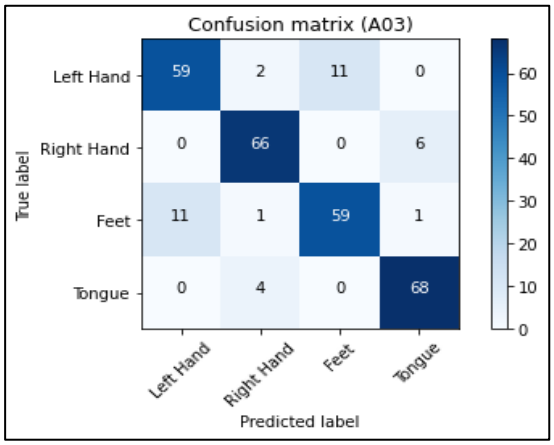

(c)

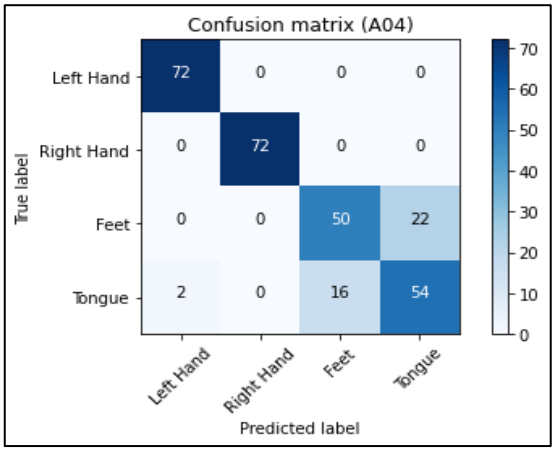

(d)

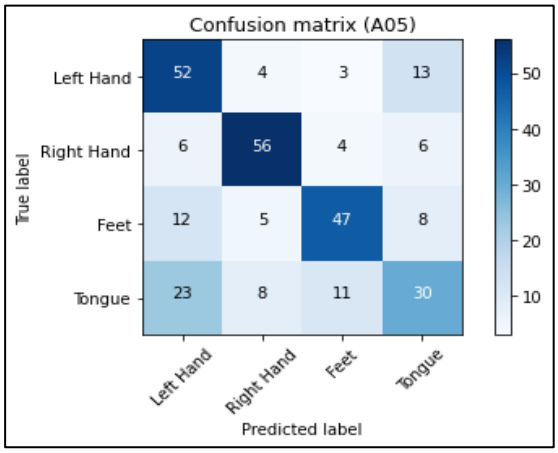

(e)

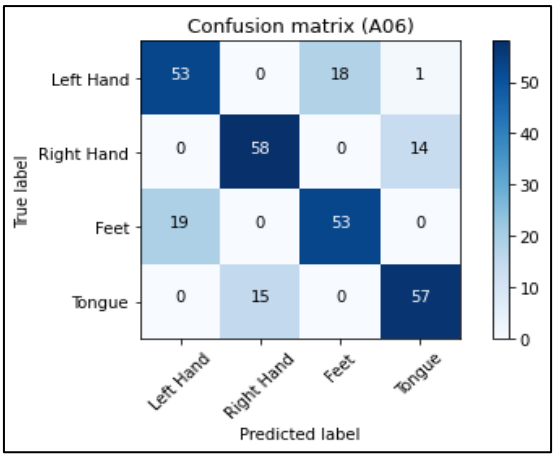

(f)

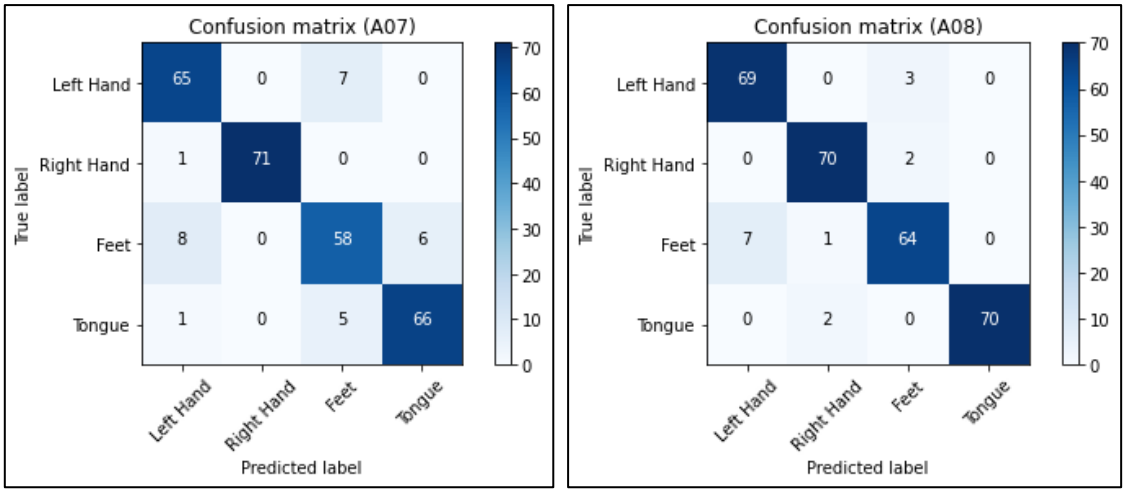

(g) **(h)**

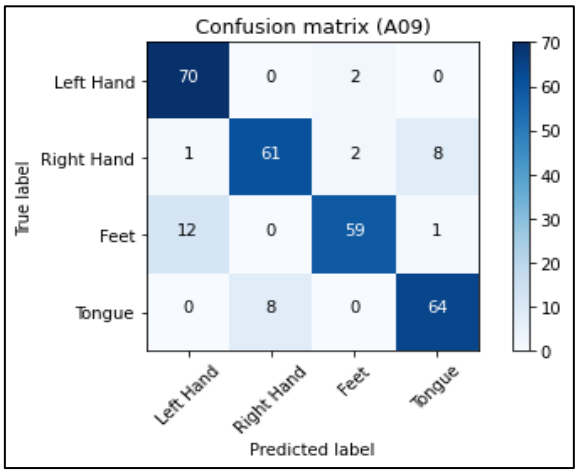

(i)

Figure 5.12 Confusion matrices for subjects **(a)** A01 **(b)** A02 **(c)** A03 **(d)** A04 **(e)** A05 **(f)** A06 **(g)** A07 **(h)** A08 **(i)** A09 for 4-class MI classification

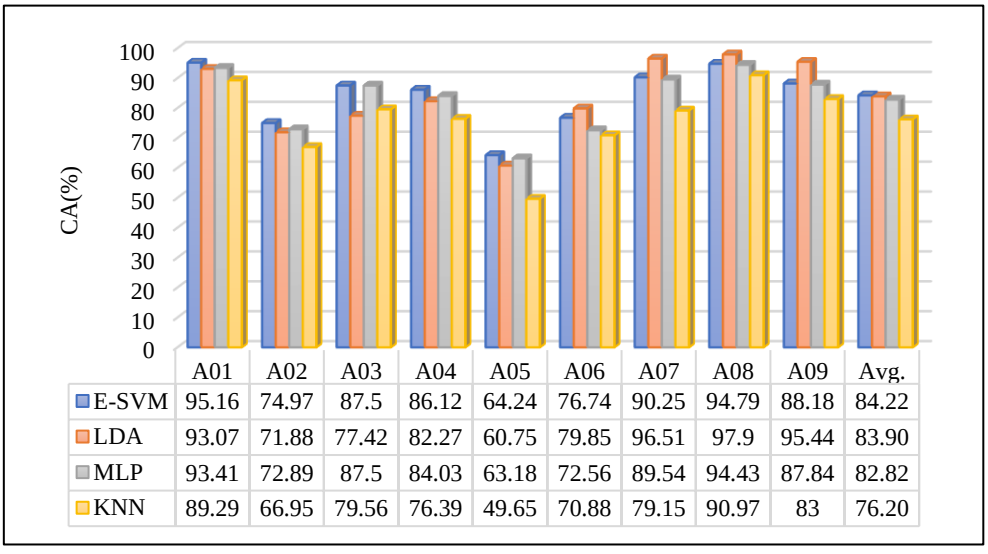

	A01	A02	A03	A04	A05	A06	A07	A08	A09	Avg.
E-SVM	95.16	74.97	87.5	86.12	64.24	76.74	90.25	94.79	88.18	84.22
LDA	93.07	71.88	77.42	82.27	60.75	79.85	96.51	97.9	95.44	83.90
MLP	93.41	72.89	87.5	84.03	63.18	72.56	89.54	94.43	87.84	82.82
KNN	89.29	66.95	79.56	76.39	49.65	70.88	79.15	90.97	83	76.20

Figure 5.13 CA (%) of E-SVM, LDA, MLP, and KNN for 4-class classification

The proposed methodology outperforms the recently suggested methods, with an average CA of 84.22%. Also, it is analyzed that the developed methodology produces better CA for most subjects. A Multiview CNN-based technique proposed by Mane et al. produces better CA in the case of three subjects. However, the average CA of the proposed methodology is 5.09% higher than the Multiview CNN-based technique.

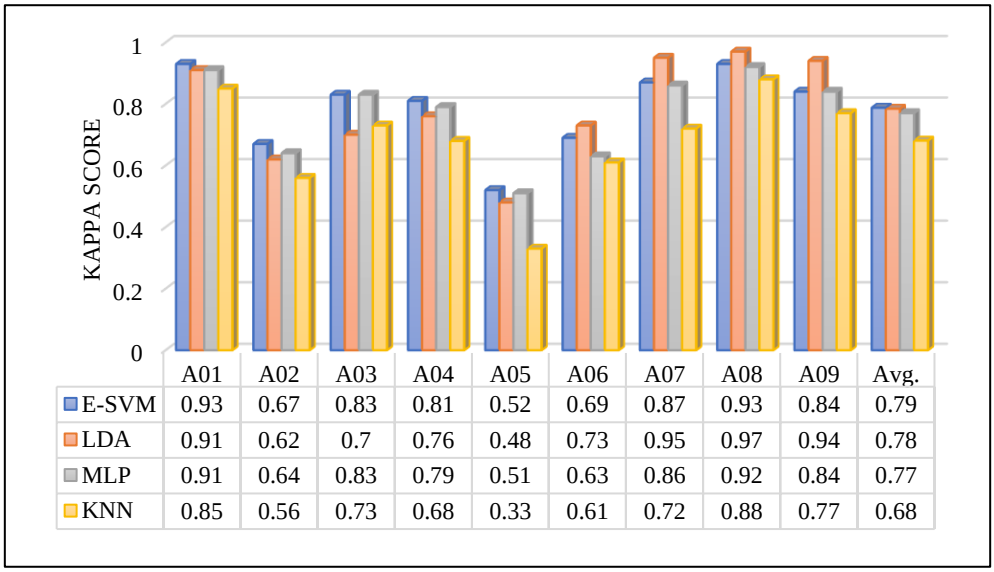

	A01	A02	A03	A04	A05	A06	A07	A08	A09	Avg.
E-SVM	0.93	0.67	0.83	0.81	0.52	0.69	0.87	0.93	0.84	0.79
LDA	0.91	0.62	0.7	0.76	0.48	0.73	0.95	0.97	0.94	0.78
MLP	0.91	0.64	0.83	0.79	0.51	0.63	0.86	0.92	0.84	0.77
KNN	0.85	0.56	0.73	0.68	0.33	0.61	0.72	0.88	0.77	0.68

Figure 5.14 K-score obtained for E-SVM, LDA, MLP, and KNN for 4-class classification

Table 5.7 briefly describes recently suggested FE and classification methods, along with the number of channels used as input for the same MI BCI dataset. It is observed that most recent techniques utilize the input data from all EEG channels for FE of MI-EEG signals. On the other hand, the proposed methodology outperforms the compared methods while utilizing five EEG channels' data. Since the proposed method uses only five EEG channels, it reduces the computational complexity as compared to the recently proposed methods. Also, using a few EEG channels makes the methodology an attractive nominee for practical uses. This implies that information from central EEG channels can be utilized to design an efficient BCI system. This methodology can also be tested and utilized for EEG-based medicinal diagnostics such as Epileptic Seizure, Schizophrenia, and Parkinson's disease. The methodology has a limitation in that the input EEG channels are manually selected. An automatic channel selection criterion can be introduced in order to make the methodology completely automatic. The method proposed in chapter 6 overcomes this limitation by incorporating a channel selection method along with the FE.

Table 5.6 Comparison of subject-wise CA (%) of the proposed methodology with the other recently proposed methods for the classification of MI-EEG signals

Sub.	Deep Conv-net [112]	EEG-Net [108]	FBC-Net [113]	TF-CNN [114]	HSS-ELM [115]	NSL-EEG-Net [109]	Conv-Net [116]	nCSP-TSLR [117]	CSP-LCD [118]	FB-RTS [119]	CWT-FB [110]	Present Work
A01	71.03	72.86	85.76	87.5	82.1	82.29	73.4	89.23	72.4	86.1	87.07	**95.16**
A02	52.05	56.25	61.07	65.28	47.2	51.39	50.2	**76.15**	58.3	65.2	56.17	74.97
A03	82.41	83.39	**94.51**	90.28	80.2	85.07	86.3	90.6	82.1	90	92.97	87.50
A04	58.93	67.54	68.84	66.67	66.2	67.01	55.1	71.38	52.3	63.8	68.67	**86.12**
A05	73.57	76.38	**82.54**	62.5	42.1	58.33	68.7	59.82	62.5	75.6	39.85	64.24
A06	62.5	67.05	58.71	45.49	44.3	56.25	49.3	63.26	61.4	52.4	52	**74.74**
A07	79.33	73.53	**93.08**	89.58	85.6	83.33	73.5	91.7	82.9	91.1	89.85	90.25
A08	82.41	80.27	86.21	83.33	76.4	73.96	86.2	89.18	88.5	89	72.14	**94.79**
A09	87.59	80.94	80.54	79.51	78.3	78.47	77.8	85.26	83.4	86.5	82.56	**88.18**
Avg.	72.2	73.13	79.03	74.46	66.9	70.68	68.9	79.62	71.5	77.7	71.25	**84.22**

Table 5.7 Comparison of the proposed methodology with recently proposed methods of FE and classification of MI-EEG signals

Methods	Description	No. of channels	Average CA (%)
Schirrmeister et al. (2017) [112]	CNN with cropped training (Deep Conv-Net)	22	72.20%
Sakhavi et al. (2018) [114]	Temporal features with FBCSP and CNN	22	74.46%
Lawhern et al. (2018) [108]	CNN with depth and separable convolutions (EEG-Net)	22	69.00%
Olias et al. (2019) [117]	Improved covariance matrix estimators(nCSP-TSLR)	22	79.62%
Ai et al. (2019) [118]	CSP with Local Characteristic-scale Decomposition (CSP-LCD)	22	71.50%
She et al. (2019) [115]	Extreme learning machine	22	66.90%
Raza et al. (2020) [109]	EEG-Net and neural structured learning (NSL-EEG-Net)	22	70.68%
Mane et al. (2021) [113]	Multiview CNN (FBC-Net)	22	79.03%
Mahamune et al. (2021) [110]	Continuous Wavelet Transform with filter bank-based 2D images (CWTFB)	22	71.25%
Fang et al. (2022) [119]	Filter Banks and Riemannian Tangent Space (FBRTS)	22	77.70%
Proposed method	**MVMD-PSR**	**5**	**84.22%**

5.5 Conclusion

A novel MVMD-PSR based FE and classification methodology is proposed for the MI BCI system. The developed methodology is studied on the publicly accessible BCI competition IV(2a) dataset for the classification of binary and multi-class MI-EEG signals. The MI-EEG signals are decomposed by MVMD into a number of modes. The number of decomposition modes is varied, and a detailed analysis is done to select the suitable number of decomposition

modes. The obtained modes are reconstructed into 2D phase space in order to extract meaningful information. Various statistical and non-linear features are extracted and compared for classifying the MI-EEG signals. The proposed methodology is tested on 2-class and 4-class MI-EEG signals. Different evaluation metrics, including CA, K-Score, recall, precision, and F1 score, are calculated to validate the proposed methodology's efficiency. The classification is performed using E-SVM, LDA, MLP, and KNN classifiers for 2-class and 4-class MI-EEG signals. The data training and testing are performed by means of 10-fold cross-validation to avoid any overfitting issues. The results attained by the proposed methodology show its superior performance by achieving an average CA of 96.76 % and 84.22% for 2-class and 4-class classifications, respectively. The proposed methodology outperforms recently suggested methods with only five channels' data as input. The computational complexity of the methodology is reduced as only five input channels are utilized. Hence, the proposed methodology is suitable for designing a real-time BCI system for the MI paradigm. In the future, an automatic channel selection and feature selection method can be introduced in the proposed methodology as an attempt to further reduce the computational complexity. Also, it would be interesting to test the proposed methodology on other EEG datasets.

Chapter 6

LMSST and NMF based MI-EEG task recognition

The present chapter introduces a novel method that effectively extracts features and performs the classification of multi-class MI signals. The method begins by employing an EEG channel selection technique to identify the most relevant channels for each subject to reduce computational complexity. MI-EEG signals from the selected channels are transformed into TF coefficients using the LMSST. This helps in capturing important temporal and spectral information available in the EEG signals. The extracted TF coefficients are treated using NMF for dimensionality reduction and effectively capturing meaningful patterns from the signals. Multiple statistical and nonlinear features are then extracted and classified using seven different classifiers. To evaluate the performance of the method, it is applied to the BCI competition IV (2a) dataset.

6.1 Introduction

The BCI field has witnessed significant advancements in the recent past, yet there are notable research gaps in the realm of MI-EEG signal classification. The variability in EEG signals across individuals, the complexity of MI tasks, and the presence of artifacts and noise pose significant challenges. These gaps hinder the development of more accurate and reliable BCI systems, which can have profound implications for individuals with motor disabilities. Due to these challenges, there lies a need to explore advanced FE methods that can capture the intricate dynamics of MI signals more effectively. Considering the drawbacks of the present FE and classification methods, a novel method for efficiently classifying MI-EEG signals is proposed in the present chapter. Initially, a channel selection technique is introduced to maintain a low computational complexity and remove redundant information. The channel selection technique is based on the ReleifF algorithm and selects the most relevant channels specific to each subject. The TD and FD information is extracted from the MI-EEG signals recorded from the selected channels using the LMSST [21]. The LMSST is an advanced and adaptive TFA method that provides more energy-concentrated representations compared to the STFT and WT methods [21]. This helps in accurately analyzing the input MI-EEG signals and enhancing the FE capability of the method. The TF coefficients obtained with LMSST are then processed using NMF [22] to perform dimension reduction and effectively capture meaningful features. A comprehensive FE and analysis approach is employed in order to identify the most pertinent statistical and nonlinear features, ensuring precise classification of the MI-EEG signals. The classification is carried out using seven different classification algorithms, including LDA, KNN, SVM, Multi-Layer Perceptron (MLP), Extreme Gradient Boosting (XGB), Gradient Boosting (GB), and Cat Boosting (CB) classifiers. To prevent overfitting, a 10-fold cross-validation approach is used for training and testing. The proposed method encompasses both binary and multi-class classification, and the classification results are meticulously evaluated using diverse performance evaluation metrics, including CA, precision, F1-score, and K-Score. The outcomes determine that the method is competent in classifying binary and multi-class MI-EEG signals.

The work proposed in the present chapter brings multiple contributions to the field of MI-EEG FE and classification as outlined below:

- In the present chapter, an innovative method for BCI systems that involves a new approach for FE and classification of MI-EEG signals is proposed. This method utilizes LMSST in conjunction with NMF, showcasing significant advancements in the field of BCI technology.
- In order to decrease computational complexity and eliminate redundant information originating from neighbouring channels, a channel selection technique is implemented. This technique selects the most relevant subject-specific channels, ensuring accurate classification of the MI-EEG signals. Consequently, the suggested method becomes suitable for real-time BCI systems due to the reduced computational complexity.
- The LMSST is employed to extract temporal and spectral information from the MI-EEG signals obtained from the selected channels. By applying the LMSST, the nonlinear MI-EEG signals are transformed into TF representations with high energy concentration and enhanced resolution, thereby facilitating more effective FE.
- The TF coefficients obtained using LMSST are further processed through NMF for capturing meaningful patterns and dimension reduction in order to facilitate accurate classification of MI-EEG signals.
- The processed MI-EEG signals are subjected to FE, incorporating statistical and nonlinear measures. A detailed analysis is carried out to pinpoint the most pertinent features that play a crucial role in precisely classifying the MI tasks.
- Seven different classifiers are employed to assess the efficacy of the designed FE method. The classification results validate the method's efficacy for classifying binary and multi-class EEG signals.
- In-depth analysis is performed to classify both binary and multi-class EEG signals. The results reveal the efficient performance of the method in accurately categorizing the MI-EEG signals. Average accuracies of 98.44% and 90.00% are achieved in binary and multi-class classification, respectively. Furthermore, a comprehensive comparison is conducted with previously proposed FE and classification methods using the same dataset, thereby validating the efficacy of the approach.

The subsequent structure of the chapter is outlined as follows. Section 6.2 provides an exposition of the materials and methods employed, along with a detailed description of the LMSST and NMF techniques. A comprehensive explanation of the proposed FE and classification method is furnished in section 6.3. Section 6.4 demonstrates the execution of the experimental procedures conducted to authenticate the efficacy of the proposed approach,

accompanied by a comprehensive analysis of recently published works within the corresponding domain. The outcomes derived from this research are summarized in section 6.5.

6.2 Materials and Methods

6.2.1 Dataset

The effectiveness of the proposed approach is assessed using the BCI Competition IV(2a) dataset, a widely utilized multi-class MI-EEG dataset [111]. Section 5.2.1 provides a detailed description of the dataset.

6.2.2 LMSST

The LMSST is an advanced technique used in the field of signal processing, specifically for TFA [21]. It offers a highly accurate and localized representation of signals, making it particularly useful in applications such as EEG signal analysis. Traditional TF analysis methods such as STFT or WT often struggle to provide precise information about a signal's time and frequency content, especially when dealing with non-stationary signals like EEG. The LMSST overcomes these limitations by leveraging the concept of synchro-squeezing [21]. The SST is a TFA method that emphasizes the local energy distribution of a signal in the TF plane, resulting in improved time and frequency resolution. This redistribution ensures that critical information related to the frequency and timing of these components is better preserved [21]. The LMSST further enhances the SST by identifying and exploiting local maxima in the TF representation of the input signal. Local maxima correspond to the significant peaks in the TF plane, indicating regions where the signal exhibits strong oscillatory behavior. The LMSST starts by computing the STFT of the input signal $s(t)$ using a window function. The STFT of an input signal $s(t)$ at time t and frequency ω is given by [21]:

$$G(t,\omega) = -\int_{\infty}^{\infty} g(\mu - t)s(\mu)e^{-i\omega(\mu - t)}\,du \tag{6.1}$$

where $g(\mu - t)$ is the window function, which is usually a localized function centered around t and $|G(t,w)|$, is the spectrogram of STFT. A multicomponent amplitude and frequency-modulated signal can be written as [21]:

$$S(t) = \sum_{m=1}^{n} A_m(t)e^{i\varphi_m(t)} \tag{6.2}$$

where $A_m(t)$, $\varphi'_m(t)$ and $\varphi_m(t)$ are instantaneous amplitude, instantaneous frequency, and instantaneous phase, respectively. According to Taylor expansion, the instantaneous amplitude function, $A_m(\mu)$ and instantaneous phase function $\varphi_m(\mu)$ of the m^{th} component at the time point t can be expanded as $A_m(\mu) = A_m(t)$ and $\varphi_m(\mu) = \varphi_m(t) + \varphi'_m(t)(\mu - t)$. Therefore, the signal in Eq. (6.2) can be rewritten as [21]:

$$s(\mu) = \sum_{m=1}^{n} A_m(t) e^{i(\varphi_m(t)) + \varphi'_m(t)(\mu - t)} \tag{6.3}$$

Now, the STFT of Eq. (6.3) can be written as [21]:

$$G(t, \omega) = \sum_{m=1}^{n} A_m(t) e^{i\varphi_m(t)} \hat{g}\big(\omega - \varphi'_m(t)\big) \tag{6.4}$$

where, $\hat{g}$ symbolizes the FT of the window. According to Eq. (6.4), the spectrogram concentrates on the IF energies and can be illustrated as [21]:

$$|G(t, \omega)| = \sum_{m=1}^{n} A_m(t) \hat{g}\big(\omega - \varphi'_m(t)\big) \tag{6.5}$$

The LMSST defines a novel frequency reassignment operator given by [21]:

$$\omega_k(t, \omega) = \begin{cases} argmax_{\omega} |G(t, \omega)|, \omega \in [\omega - \Delta, \omega + \Delta], & if\ |G(t, \omega)| \neq 0 \\ 0, & if\ |G(t, \omega)| = 0 \end{cases} \tag{6.6}$$

It is assumed that there is a substantial frequency separation between the two arbitrary modes, expressed as $\varphi'_{m+1}(t) - \varphi'_m(t) > 4\Delta$ where $m \in \{1, \ldots\ldots\ldots\ldots, n-1\}$ [21]. Additionally, the FT of the window function is maximized at zero, denoted as $\hat{g}(w) \leq \hat{g}(0),\ for\ t \in \mathbb{R}, m \in \{1, \ldots\ldots\ldots\ldots, n\}$. Therefore,

$$w_m(t, W) = \begin{cases} \varphi'_m(t), & if\ w \in [\varphi'_m(t) - \Delta, \varphi'_m(t) + \Delta] \\ 0, & otherwise \end{cases} \tag{6.7}$$

Finally, LMSST can be expressed as [21]:

$$LMSST(t, \eta) = \int_{-\infty}^{\infty} G(t, w) \delta\big(\eta - w_k(t, w)\big) dw \tag{6.8}$$

Also, the original signal can be accurately reconstructed by employing Eq. (6.8) [21]:

$$s(t) = \big(2\pi g(0)\big)^{-1} \int_{-\infty}^{\infty} LMSST\ (t, w) dw \tag{6.9}$$

By focusing on the salient oscillatory features, the LMSST enhances the understanding of the TF dynamics in various signal processing applications, such as the analysis of EEG signals. In

the present work, the LMSST method is implemented to extract TF information from the MI-EEG signals obtained from selected channels.

6.2.3 NMF

NMF is a powerful technique utilized for the analysis of multivariate data, offering valuable applications in pattern recognition and machine learning [22]. It is an unsupervised decomposition technique that effectively captures meaningful patterns and reduces the dimensionality of the data. This makes it a valuable tool in machine learning and data analysis. The main objective of NMF is to decompose a given matrix into two non-negative matrices of significantly lower dimensions: a basis matrix and a coefficient matrix [22]. When applied to an input matrix V of dimension $p \times q$, where p represents the number of features, such as TF coefficients extracted from MI-EEG signals, and q represents the number of samples, i.e., the EEG trails. The objective of NMF is to decompose matrix V into two non-negative matrices, W and H, with dimensions $p \times r$ and $r \times q$, respectively. Therefore, the NMF of the input matrix can be given by [22]:

$$V_{p\times q} = W_{p\times r} H_{r\times q} \tag{6.10}$$

where W is the basis matrix, which captures the essential patterns or features in the input data, H is the coefficient matrix, which contains the weights associated with the basis matrix W, and r represents the desired number of extracted features. The main goal of NMF is to minimize the reconstruction error between V and its approximation WH [22]. The non-negativity constraint in NMF ensures that the basis matrix and coefficient matrix contain non-negative values. This constraint makes the extracted features more interpretable and allows for additive combinations of features. In the present work, NMF is employed for capturing valuable information from the TF coefficients acquired through the LMSST method. The lower dimension non-negative basis and coefficient matrices are obtained from the input TF coefficients, and then multiple features are extracted using the basis matrix.

6.3 Proposed Method

The present work proposes an innovative method for FE and classification of the MI-EEG signals. The cornerstone of the proposed method is the utilization of the LMSST in combination with NMF for effective FE and classification of the MI-EEG signals. The framework portrayed in Figure 6.1 illustrates the sequential process involved in FE and the classification of the MI-

EEG signals. The proposed method comprises three key stages, including EEG channel selection, FE based on the integration of LMSST and NMF, and subsequent classification of the MI-EEG signals using seven different classifiers. An EEG channel selection method is devised to reduce the computational complexity and eliminate redundant information from the neighboring channels. Figure 6.2 illustrates the pipeline of the employed channel selection method. To perform channel selection, TF information is extracted from MI-EEG signals recorded from 22 EEG channels employing the LMSST technique. The extracted TF coefficients undergo dimension reduction through NMF, resulting in the generation of two matrices: W (basis matrix) and H (coefficient matrix).

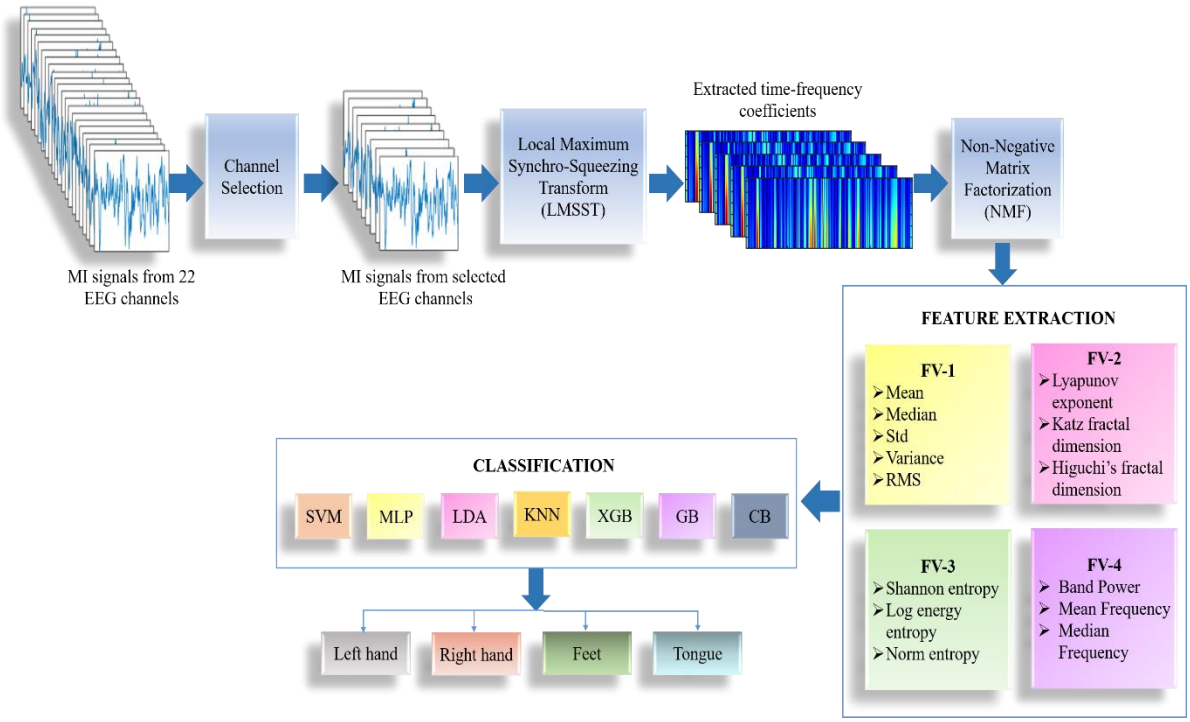

Figure 6.1 Framework of the proposed FE and classification method for MI-EEG signals

6.3.1 Channel Selection

Statistical features, including mean, median, std, variance, and RMS, are computed to form a FV from the basis matrix (W). The weights of these extracted features are determined using the ReleifF algorithm, and the mean weights corresponding to each of the 22 channels are calculated. The channel selection process begins with the channels having the highest mean weights, thereby selecting the channels with the most relevant features. Subsequently, adjacent channels are discarded to eliminate redundant information and reduce computational complexity.

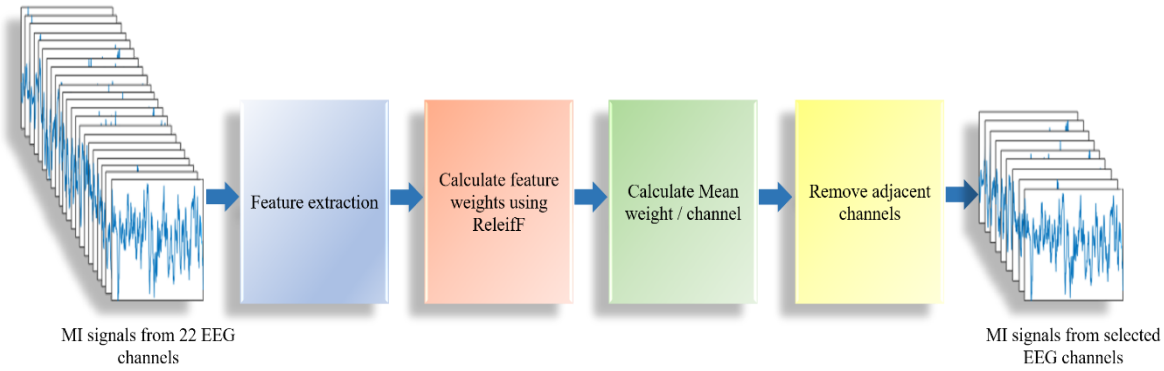

Figure 6.2 Channels selection method

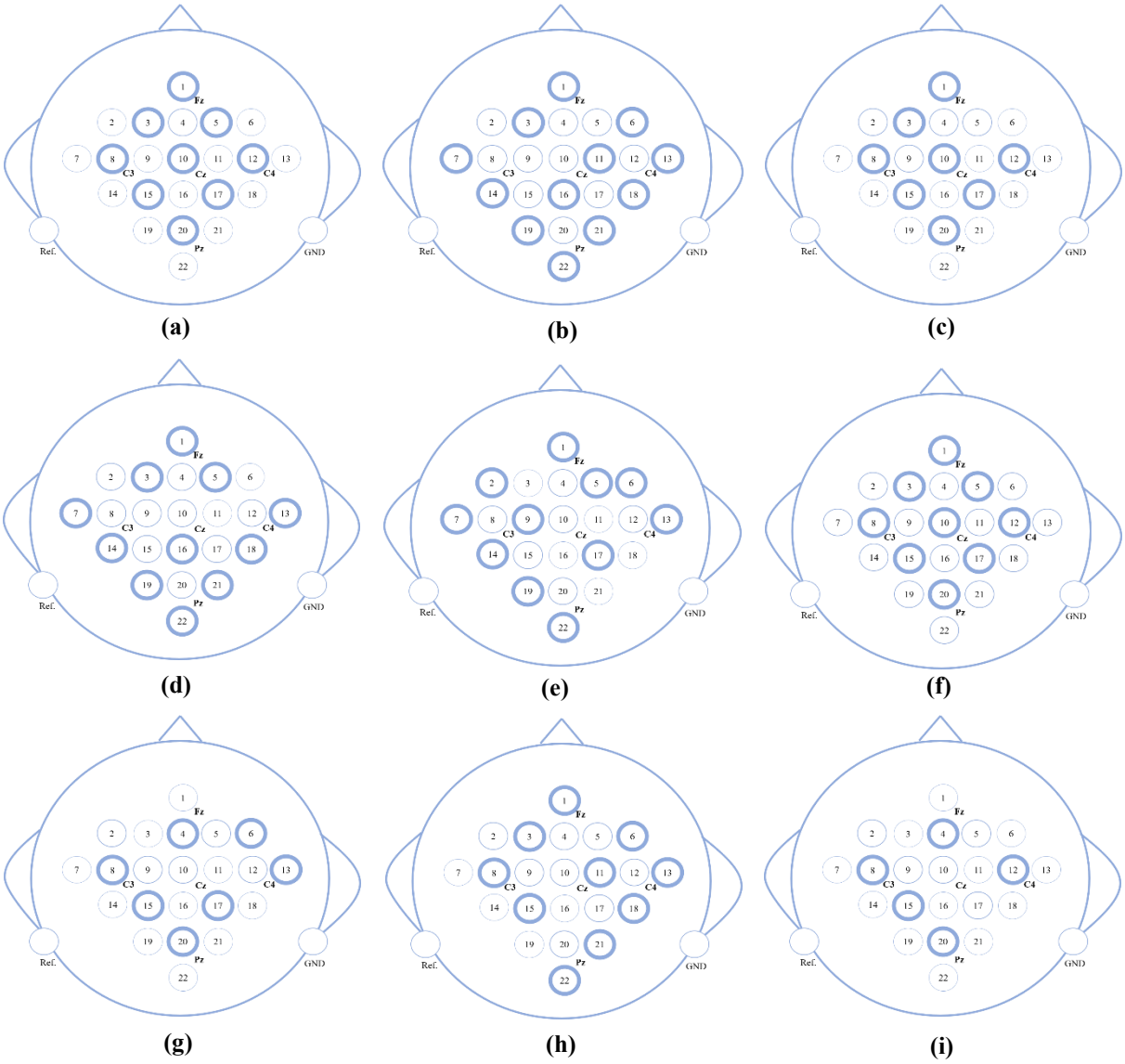

Figure 6.3 Channels selected for subject **(a)** A01 **(b)** A02 **(c)** A03 **(d)** A04 **(e)** A05 **(f)** A06 **(g)** A07 **(h)** A08 **(i)** A09

This channel selection procedure is carried out individually for each subject, resulting in the selection of different channels based on their relevance to each subject. The channels selected from each subject are highlighted in Figure 6.3. The number of selected channels differs for each subject as EEG recordings of each subject exhibit variations due to differences in their brain structure. The proposed technique demonstrates adaptability by selecting relevant channels specific to different subjects and datasets. Furthermore, the proposed channel selection technique eliminates redundant information by removing adjacent channels.

6.3.2 Feature Extraction

After carefully selecting the most relevant channels for each subject, the MI-EEG signals acquired from the selected channels undergo further processing to enable FE and classification. To extract valuable TF information from the MI-EEG signals obtained from the chosen channels of each subject, a specialized technique called LMSST is employed. LMSST serves a vital role in enhancing the comprehension of the TF dynamics during the analysis of the MI-EEG signals. LMSST helps in gaining deeper insights into the temporal and spectral characteristics of the signals. The use of LMSST allows for a more refined exploration of the TF domain, allowing a detailed examination of how the power of neural activity varies over different time intervals and frequency ranges. This enhanced understanding of the TF dynamics is crucial for uncovering patterns and extracting meaningful information from the MI-EEG signals.

LMSST achieves this by transforming the input signals into high-energy concentrated TF representations. Through this transformation, the time and frequency components offer a more comprehensive view of the dynamics occurring in the signals. By localizing the energy of the signals in both TD and FD, LMSST enables to identify important temporal events and frequency modulations within the MI-EEG data. Therefore, by leveraging LMSST in the analysis of MI-EEG signals, the complex interplay between neural oscillations and cognitive processes can be characterized better. It empowers the identification of event-related changes in power, frequency, or phase, providing a deeper understanding of brain dynamics during MI tasks.

The obtained TF coefficient matrix derived from the LMSST undergoes additional processing using NMF. The NMF is an unsupervised decomposition technique that effectively captures meaningful patterns and reduces the dimensionality of the data. It plays a key role in reducing

the dimensionality of the TF coefficient matrix by converting it into two lower-dimensional non-negative matrices. The first resulting matrix is the basis matrix, which captures the essential patterns or features in the input data. These features represent crucial information about the MI-EEG signals that are relevant to the subsequent analysis and classification tasks. The second matrix, the coefficient matrix, encompasses the weights associated with the basis matrix. The non-negativity constraint of NMF makes the extracted features more interpretable and allows for additive combinations of features.

Table 6.1 Multiple features extracted using NMF for forming the four FVs

	FV-1	**FV-2**	**FV-3**	**FV-4**
S. No.		**Features**		
1.	Mean	LE	Shannon entropy	Band Power
2.	Median	KFD	Log energy entropy	Mean Frequency
3.	std	Higuchi's fractal dimension	NE	Median Frequency
4.	Variance			
5.	RMS			

The FE process involves the utilization of multiple statistical and nonlinear features from the basis matrix. Four FVs are created to comprehensively analyze the distinct aspects of the MI-EEG signals, each focusing on different types of features. The extracted features are summarized in Table 6.1, providing an overview of the diverse characteristics incorporated into the four FVs. The first FV encompasses statistical measures like mean, median, std, variance, and RMS. Moving on to the second FV, which comprises nonlinear features including LE, Katz Fractal Dimension (KFD), and Higuchi's Fractal Dimension (HFD), which are computed across the selected channels. These features allow for the exploration of chaotic dynamics, complexity, and self-similarity within the data.

The third FV involves entropy-based features, comprising Shannon entropy, LEE, and NE. By incorporating these measures, the FV captures information regarding the randomness, uncertainty, and significance of rare events present in the MI-EEG data. Lastly, the fourth FV focuses on frequency-based features, including band power, mean frequency, and median frequency. These features delve into the FD characteristics of the data, enabling an analysis of the dominant frequency components and their distribution within the MI-EEG signals. By extracting and organizing these statistical and nonlinear features into four distinct FVs, a comprehensive understanding of the underlying patterns and properties of the MI-EEG signals is obtained. This helps in improving the classification performance of the proposed method.

6.3.3 Classification

To accurately interpret the MI-EEG signals from the extracted features, seven classifiers are employed for classification. These classifiers include SVM, LDA, MLP, KNN, GB, XGB, and CB. SVM is a robust supervised learning algorithm that seeks to identify an optimal hyperplane to effectively distinguish between various classes. It has been successfully applied to MI-EEG signal classification due to its ability to handle high-dimensional data and complex decision boundaries [120]. SVM achieves classification by maximizing the margin between the classes, allowing for robust generalization. LDA, is a statistical method that aims at maximizing the ratio of between-class variance to within-class variance. It is particularly useful when the number of classes exceeds two, as it aims to project the data onto a lower dimensional subspace while preserving class separability [121]. LDA has been broadly employed for MI-EEG signal classification owing to its simplicity and effectiveness in reducing dimensionality. k-Nearest Neighbors (KNN) is another straightforward yet effective classifier that operates by classifying new instances according to their proximity to the closest neighbors in the feature space [120]. It has been extensively utilized for MI-EEG signal classification owing to its simplicity and capability to handle multi-class problems.

MLP, a type of artificial neural network, is a versatile classifier that can capture complex nonlinear relationships between features and classes. It consists of multiple layers of interconnected neurons, enabling it to learn hierarchical representations of the data. MLPs have been extensively used for MI-EEG signal classification, as they can handle large amounts of data and learn intricate patterns [122]. In recent years, boosting algorithms have gained popularity in EEG signal classification. GB, XGB, and CB are all ensemble methods that combine multiple weak classifiers to improve overall performance. They iteratively train classifiers on different subsets of the data and allocate higher weights to misclassified instances, allowing classifiers to focus on the challenging samples. These boosting classifiers have performed well in MI-EEG signal classification tasks, often outperforming traditional classifiers [123]. The extracted features are allocated into four distinct MI tasks: left hand, right hand, feet, and tongue. These tasks are subjected to classification using seven distinct classifiers, and the resulting classifications are thoroughly analyzed. To mitigate the risk of overfitting, the training and testing processes are conducted using a 10-fold cross-validation approach. To assess the overall efficacy of the method, a range of parameters including CA, K-Score, Precision, Recall, and F1-Score are computed and evaluated for both binary and multi-

class classification tasks, utilizing the four FVs. These analytical evaluations are performed across nine different subjects denoted A01 to A09. The classification results are then scrutinized to identify the most pertinent FV and the optimal classifier for both binary and multi-class classification scenarios. Furthermore, a comparative analysis is carried out between these results and previous works on MI-EEG FE and classification to ensure further validation. The calculated outcomes are discussed in the subsequent section.

6.4 Results and Discussion

The proposed MI-EEG FE and classification method involves using LMSST to transform MI-EEG signals into high-resolution and high-energy concentrated TF representations. LMSST is applied to the MI-EEG signals from four different classes: left hand, right hand, feet, and tongue, and the obtained TF representations are shown in Figure 6.4(a), Figure 6.4(b), Figure 6.4(c), and Figure 6.4(d) respectively. It is observed from Figure 6.6 that the transformation by LMSST results in representations with high energy concentration and resolution. This enables effective extraction of both TD and FD information for further classification of the signals into MI tasks. Next, the TF coefficients obtained through LMSST are processed using NMF for dimension reduction, and a non-negative basis matrix is obtained, which captures the important features from the TF coefficient matrix. Multiple features are extracted using the basis matrix, and four different FVs are formed depending upon the type of extracted features. At first, the method is tested for binary classification by employing the LDA classifier. The performance metrics used for evaluation are CA and K-Score.

Table 6.2 provides the CA and K-Score achieved with the LDA classifier for nine distinct subjects (A01-A09) using the four different FVs. All four FVs perform well in binary classification, with FV-1 achieving the highest average CA of 98.44%. FV-2, FV-3, and FV-4 achieve average classification accuracies of 97.76%, 98.38%, and 98.05%, respectively. This indicates that the extracted features are distinguishable, and the proposed FE method is efficient for binary classification. Furthermore, FV-1 yields the highest average CA, suggesting that the extracted statistical features are more relevant compared to the other features. The CA results are further validated with the K-Score. The highest average K-Score of 0.97 is attained with FV-1 and FV-3, while FV-2 and FV-4 also yield a high K-Score of 0.96 each. Figure 6.5 presents a graphical representation of the CA results obtained for the nine subjects using four FVs.

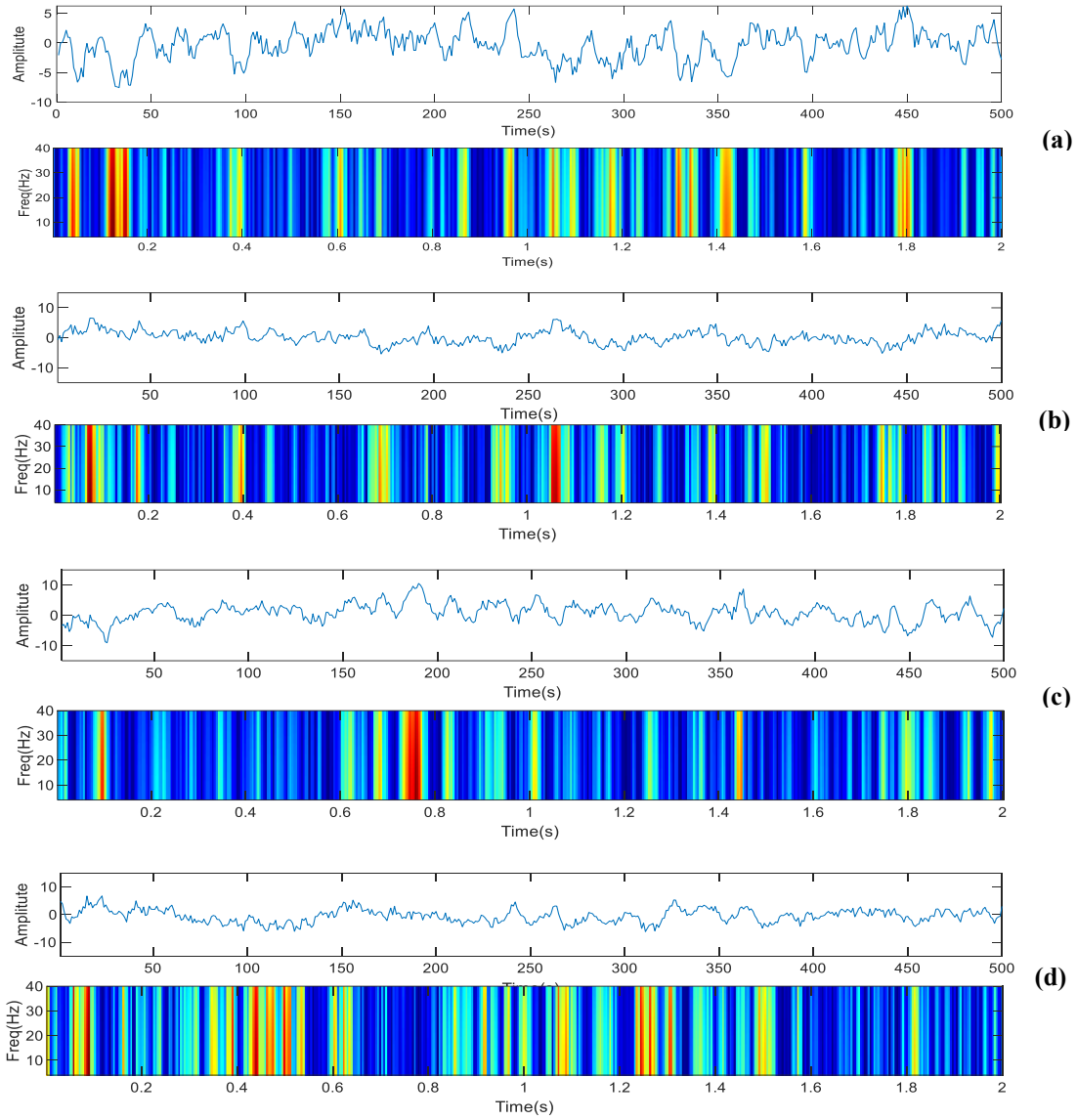

Figure 6.4 TF representation of the MI-EEG signals utilizing LMSST for the **(a)** left hand, **(b)** right hand, **(c)** feet, and **(d)** tongue class, respectively

Table 6.2 CA and K-Score calculated for binary classification using the four FVs

Subjects	**CA (%)**				**K-Score**			
	FV1	**FV2**	**FV3**	**FV4**	**FV1**	**FV2**	**FV3**	**FV4**
A01	100	100	97.95	99.28	1	1	0.96	0.99
A02	98.62	95.24	98.67	96.52	0.97	0.9	0.97	0.93
A03	99.29	97.95	100	98.62	0.99	0.96	1	0.97
A04	98.67	99.28	98.67	98.67	0.97	0.99	0.97	0.97
A05	90.09	90.19	92.95	92.86	0.8	0.8	0.86	0.86
A06	100	99.33	99.28	100	1	0.99	0.99	1
A07	99.28	99.28	99.28	99.28	0.99	0.99	0.99	0.99
A08	100	100	99.33	100	1	1	0.99	1
A09	100	98.57	99.33	97.19	1	0.97	0.99	0.94
AVG.	**98.44**	97.76	98.38	98.05	**0.97**	0.96	**0.97**	0.96

To further validate the suggested method for binary classification, the results are calculated by pairing all other classes. Table 6.3 and Table 6.4 provide the CA and K-Score results for six pairs of classes: class-AB (left hand vs. right hand), class-AC (left hand vs. feet), class-AD (left hand vs. tongue), class-BD (right hand vs. tongue), class-BC (right hand vs. feet), and class-CD (feet vs. tongue). The classification results are calculated using FV-1 due to its superior performance over the other three FVs. The average CA is calculated subject-wise for six pairs of classes and class-wise across all nine subjects. The proposed method efficiently classifies the paired classes, with the highest average CA of 99.06% attained for class-BC (right hand vs. feet).

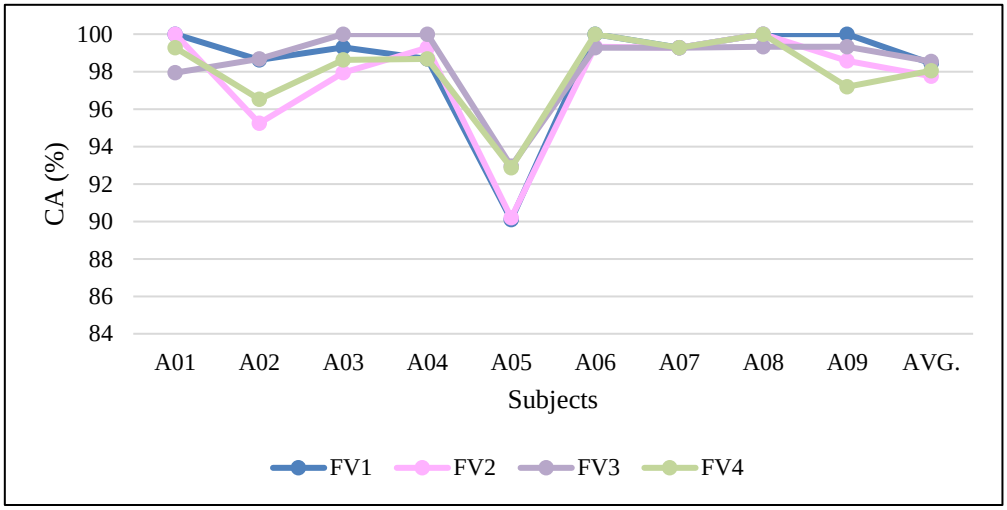

Figure 6.5 CA achieved for 2-class (left hand and right hand) MI-EEG signals for nine subjects (A01-A09) for four different FVs.

Table 6.3 CA (%) calculated using FV-1 for nine subjects corresponding to six pairs of classes.

Subject	Class-AB	Class-AC	Class-AD	Class-BC	Class-BD	Class-CD	Avg.
A01	100	88.24	100	100	98.57	100	97.80
A02	98.62	72.76	100	100	100	98.67	95.01
A03	99.29	88.76	99.28	100	95	99.28	96.94
A04	98.67	97.24	99.33	98.62	99.33	95.14	98.06
A05	90.09	95.81	71.48	96.48	90	96	89.98
A06	100	83.43	99.28	99.33	93.05	99.28	95.73
A07	99.28	84	99.28	98.57	98.57	91	95.12
A08	100	97.86	100	99.28	99.33	100	99.41
A09	100	98.62	68.67	99.28	84.09	99.28	91.66
Avg.	98.44	89.64	93.04	99.06	95.33	97.63	95.52

For all other pairs of classes, the obtained average classification accuracies are 98.44%, 89.64%, 93.04%, 95.33%, and 97.63% for class AB, class AC, class AD, class BD, and class CD, respectively. Subject-wise analysis reveals that subject A08 achieves the maximum average CA of 99.41% across all six pairs of classes. The classification results are also validated

using the K-Score. The highest average K-Score of 0.98 is attained for class-BC when calculated across all subjects. Subject-wise analysis shows that subject A08 achieves the highest K-Score of 0.99. These results demonstrate that the method for MI-EEG FE and classification is highly efficient for binary classification.

Table 6.4 K-Score calculated using FV-1 for six distinct pair of classes

Subject	Class AB	Class AC	Class AD	Class BC	Class BD	Class CD	Avg.
A01	1	0.76	1	1	0.97	1	0.96
A02	0.97	0.46	1	1	1	0.97	0.90
A03	0.99	0.78	0.99	1	0.9	0.99	0.94
A04	0.97	0.94	0.99	0.97	0.99	0.9	0.96
A05	0.8	0.92	0.43	0.93	0.8	0.92	0.80
A06	1	0.67	0.99	0.99	0.86	0.99	0.92
A07	0.99	0.68	0.99	0.97	0.97	0.82	0.90
A08	1	0.96	1	0.99	0.99	1	**0.99**
A09	1	0.97	0.24	0.99	0.68	0.99	0.81
Avg.	0.97	0.79	0.85	**0.98**	0.91	0.95	0.91

To assess the proposed method's efficacy on multi-class MI-EEG signals, the 4-class classification is performed. The CA and K-Score are calculated for all subjects (A01-A09) using four distinct FVs. The outcomes in Table 6.5 illustrate that the maximum average CA of 90.00% is achieved with FV-1. For FV-2, FV-3, and FV-4, the average classification accuracies are 83.39%, 86.81%, and 86.57%, respectively. Although the other FVs produce good classification results, FV-1, which contains statistical features, achieves the best results. The CA results are further validated by calculating the K-Score for all subjects using the four FVs. It is indicated that the maximum average K-Score of 0.87 is attained using FV-1. The FV-2, FV-3, and FV-4 produce the average K-Score of 0.78, 0.82, and 0.80 respectively.

Table 6.5 CA and K-Score calculated with four different FVs for four class classification

Subjects	CA (%)				K-Score			
	FV1	FV2	FV3	FV4	FV1	FV2	FV3	FV4
A01	95.48	92.72	93.77	93.74	0.94	0.9	0.92	0.92
A02	87.47	82.99	83.69	85.42	0.83	0.77	0.78	0.8
A03	88.94	87.23	85.82	85.49	0.85	0.83	0.81	0.8
A04	92.33	84.73	93.4	87.47	0.9	0.8	0.91	0.83
A05	79.85	71.17	72.89	74.99	0.73	0.61	0.64	0.67
A06	90.28	79.54	83.71	79.2	0.87	0.73	0.78	0.72
A07	87.49	80.89	83.64	82.97	0.83	0.74	0.78	0.77
A08	99.65	97.23	98.94	98.94	0.99	0.96	0.99	0.99
A09	88.55	78.48	85.43	79.17	0.85	0.71	0.8	0.72
Avg.	**90.00**	83.89	86.81	85.27	**0.87**	0.78	0.82	0.80

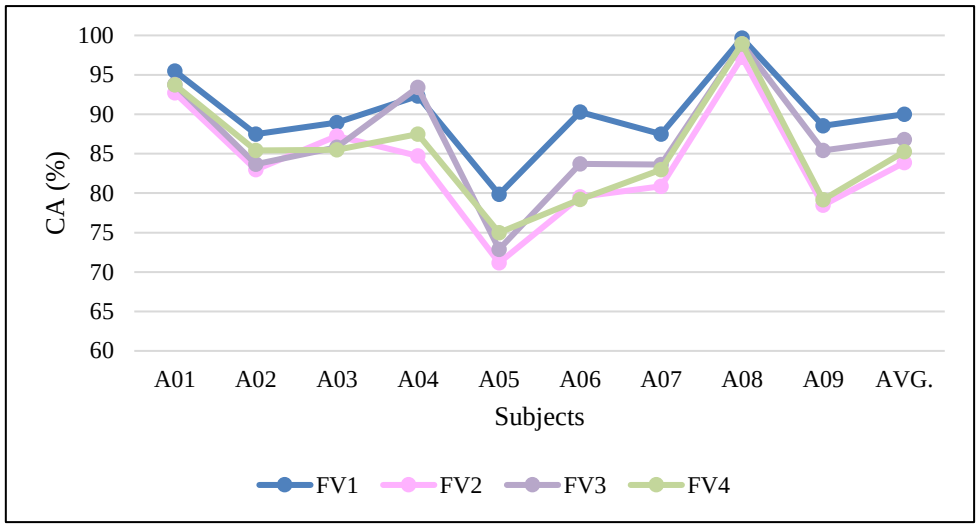

(a)

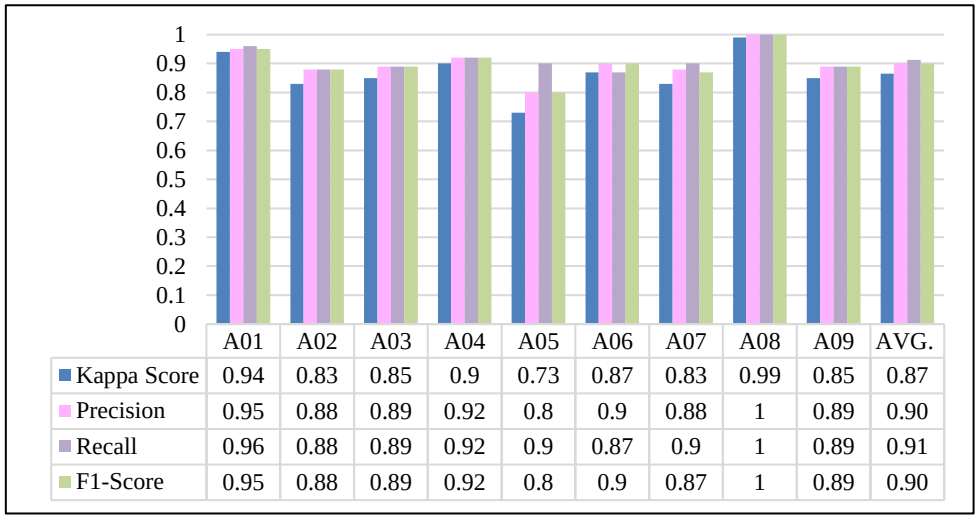

	A01	A02	A03	A04	A05	A06	A07	A08	A09	AVG.
Kappa Score	0.94	0.83	0.85	0.9	0.73	0.87	0.83	0.99	0.85	0.87
Precision	0.95	0.88	0.89	0.92	0.8	0.9	0.88	1	0.89	0.90
Recall	0.96	0.88	0.89	0.92	0.9	0.87	0.9	1	0.89	0.91
F1-Score	0.95	0.88	0.89	0.92	0.8	0.9	0.87	1	0.89	0.90

(b)

Figure 6.6 Evaluated results of multi-class classification for **(a)** CA, **(b)** K-Score, precision, recall, and F1-score for nine distinct subjects.

Figure 6.8 graphically illustrates the classification accuracies achieved for the multi-class classification across nine subjects (A01-A09) utilizing four distinct FVs. The findings indicate that the fractal dimension-based features in FV-2 are the least significant, while the statistical features in FV-1 hold the maximum significance. The classification results suggest that the proposed FE method efficiently classifies binary and multi-class MI-EEG signals. Furthermore, based on the CA and K-Score results, it is concluded that the statistical features demonstrate the most promising performance for both binary and multi-class classification in the suggested method.

To further assess the efficacy of the method, additional performance metrics comprising precision, recall, and F1-score are employed to analyze the classification results. Figure 6.6(a) and Figure 6.6(b) portray the graphical representation of the classification outcomes for the nine subjects. These outcomes are calculated using the FV-1 due to its superior performance compared to the other FVs. The average precision, recall, and F1-score values achieved are 0.90, 0.91, and 0.90, respectively. Furthermore, in order to illustrate the multi-class classification results for subjects A01-A09, the confusion matrices are generated, as depicted in Figure 6.9(a-i). The confusion matrix corresponding to each subject is plotted with true labels on the y-axis and predicted labels on the x-axis. Analyzing the confusion matrices, it is observed that subjects A01, A04, and A08 exhibit accurate predictions for the majority of instances across all four classes, as evident in Figure 6.7(a), Figure 6.7(d), and Figure 6.7(h), respectively.

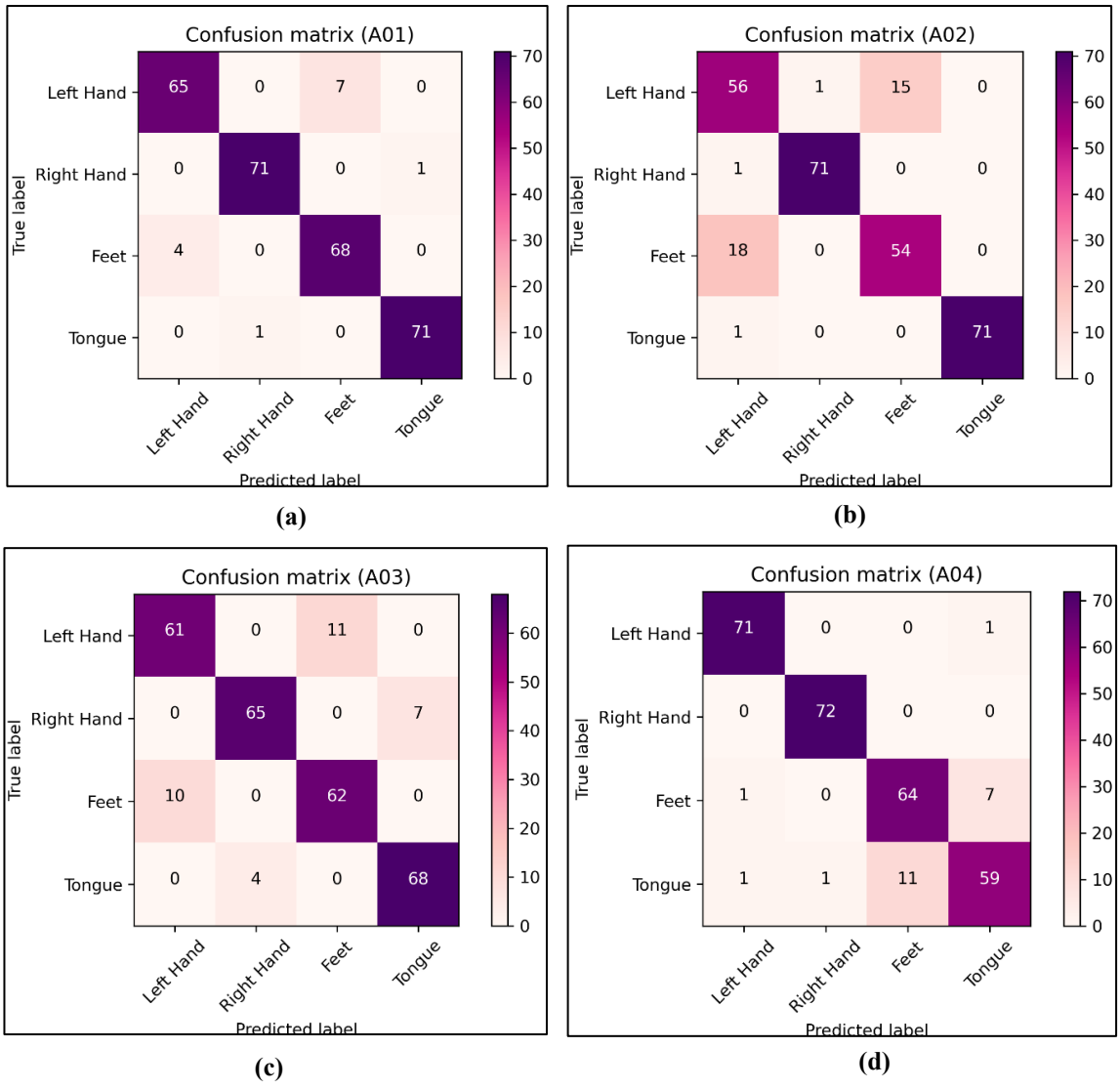

(a) **(b)**

(c) **(d)**

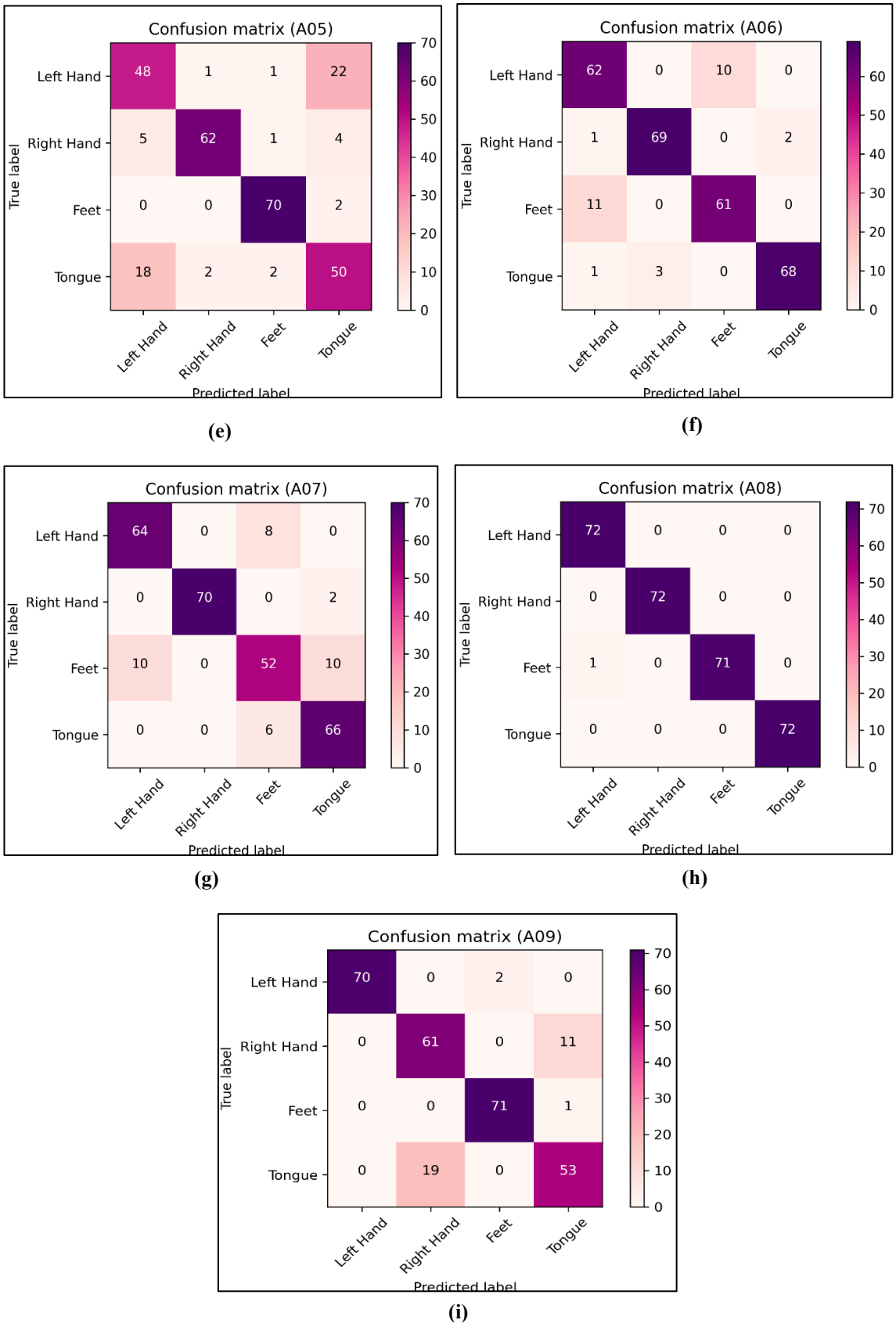

Figure 6.7 Confusion matrices for subjects **(a)** A01 **(b)** A02 **(c)** A03 **(d)** A04 **(e)** A05 **(f)** A06 **(g)** A07 **(h)** A08 **(i)** A09 for classification of multi-class MI-EEG signals

On the other hand, for subjects A02, A03, A06, A07, and A09 the classifier fails to predict some instances correctly. However, for subject A05, numerous instances are misclassified, as indicated in Figure 6.7(e). Consequently, subjects A01, A04, and A08 achieve the maximum average CA, whereas subject A05 demonstrates the lowest average CA. These observations from the confusion matrices successfully validate the classification results portrayed in Figure 6.6.

	A01	A02	A03	A04	A05	A06	A07	A08	A09	Avg.
SVM	99.28	100	100	100	93.14	100	99.28	100	99.28	99.00
MLP	100	100	99.28	100	93.76	100	97.86	100	100	98.99
LDA	100	98.62	99.28	98.67	90.09	100	99.28	100	100	98.44
KNN	100	98.67	100	100	88.9	100	99.28	100	99.28	98.46
XGB	98.57	99.33	98.57	98.62	90.33	100	98.62	97.19	100	97.91
GB	98.57	99.33	98.57	98.62	86.81	100	98.62	97.19	100	97.52
CB	99.28	99.33	99.28	100	87.57	100	98.62	99.28	99.28	98.07

(a)

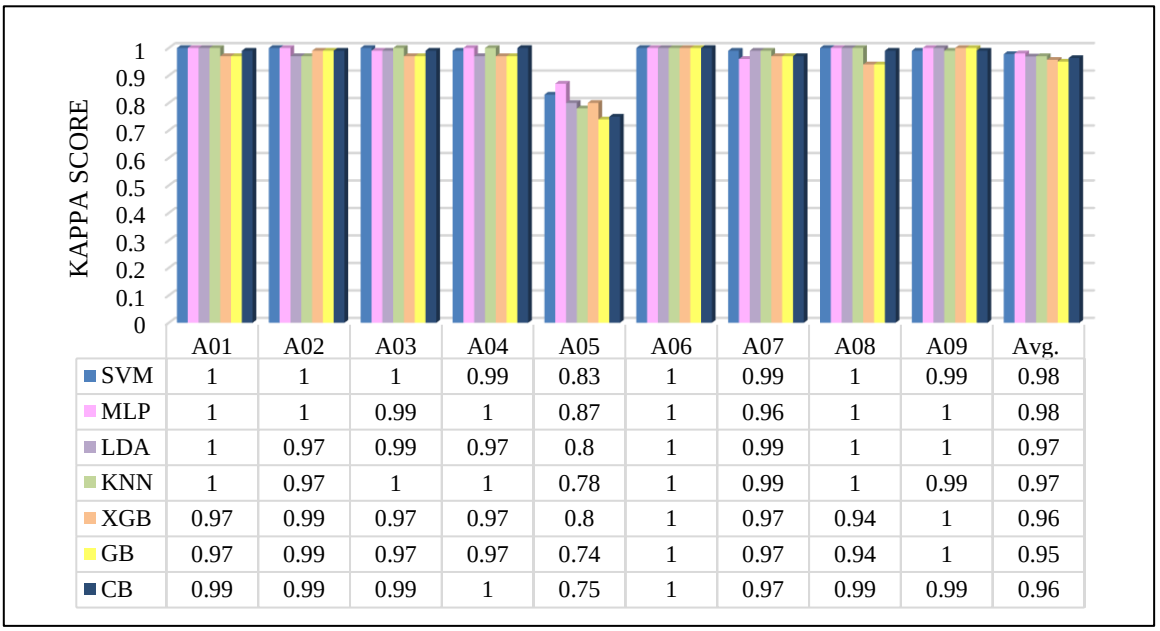

	A01	A02	A03	A04	A05	A06	A07	A08	A09	Avg.
SVM	1	1	1	0.99	0.83	1	0.99	1	0.99	0.98
MLP	1	1	0.99	1	0.87	1	0.96	1	1	0.98
LDA	1	0.97	0.99	0.97	0.8	1	0.99	1	1	0.97
KNN	1	0.97	1	1	0.78	1	0.99	1	0.99	0.97
XGB	0.97	0.99	0.97	0.97	0.8	1	0.97	0.94	1	0.96
GB	0.97	0.99	0.97	0.97	0.74	1	0.97	0.94	1	0.95
CB	0.99	0.99	0.99	1	0.75	1	0.97	0.99	0.99	0.96

(b)

Figure 6.8 (a) CA (%) and **(b)** K-Score achieved with seven different classifiers for binary classification

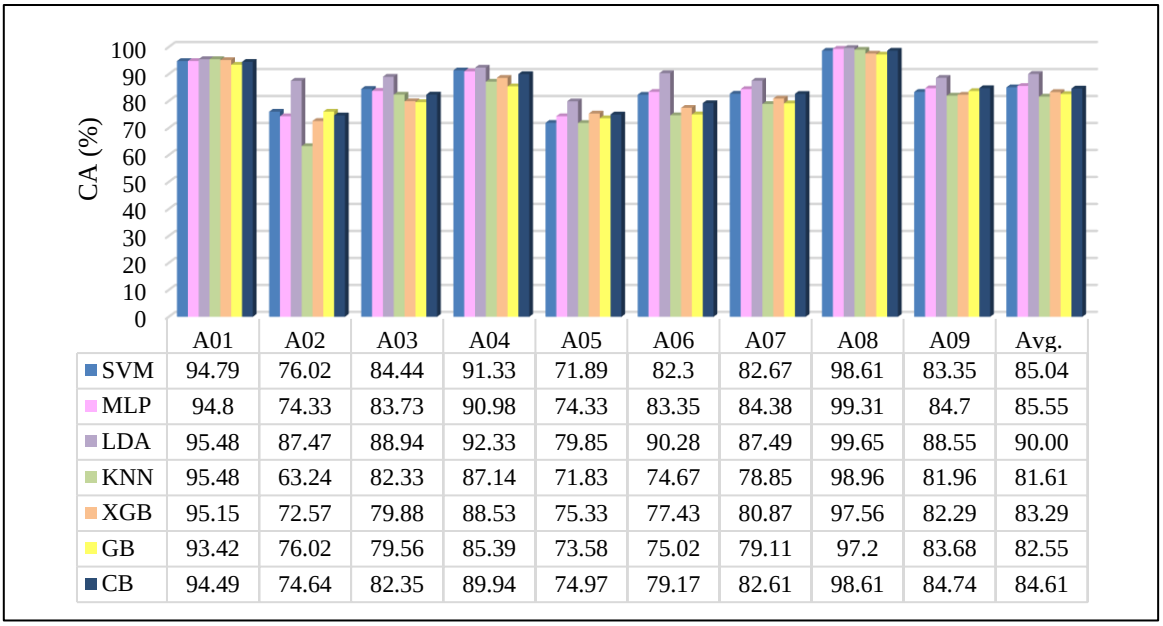

	A01	A02	A03	A04	A05	A06	A07	A08	A09	Avg.
SVM	94.79	76.02	84.44	91.33	71.89	82.3	82.67	98.61	83.35	85.04
MLP	94.8	74.33	83.73	90.98	74.33	83.35	84.38	99.31	84.7	85.55
LDA	95.48	87.47	88.94	92.33	79.85	90.28	87.49	99.65	88.55	90.00
KNN	95.48	63.24	82.33	87.14	71.83	74.67	78.85	98.96	81.96	81.61
XGB	95.15	72.57	79.88	88.53	75.33	77.43	80.87	97.56	82.29	83.29
GB	93.42	76.02	79.56	85.39	73.58	75.02	79.11	97.2	83.68	82.55
CB	94.49	74.64	82.35	89.94	74.97	79.17	82.61	98.61	84.74	84.61

(a)

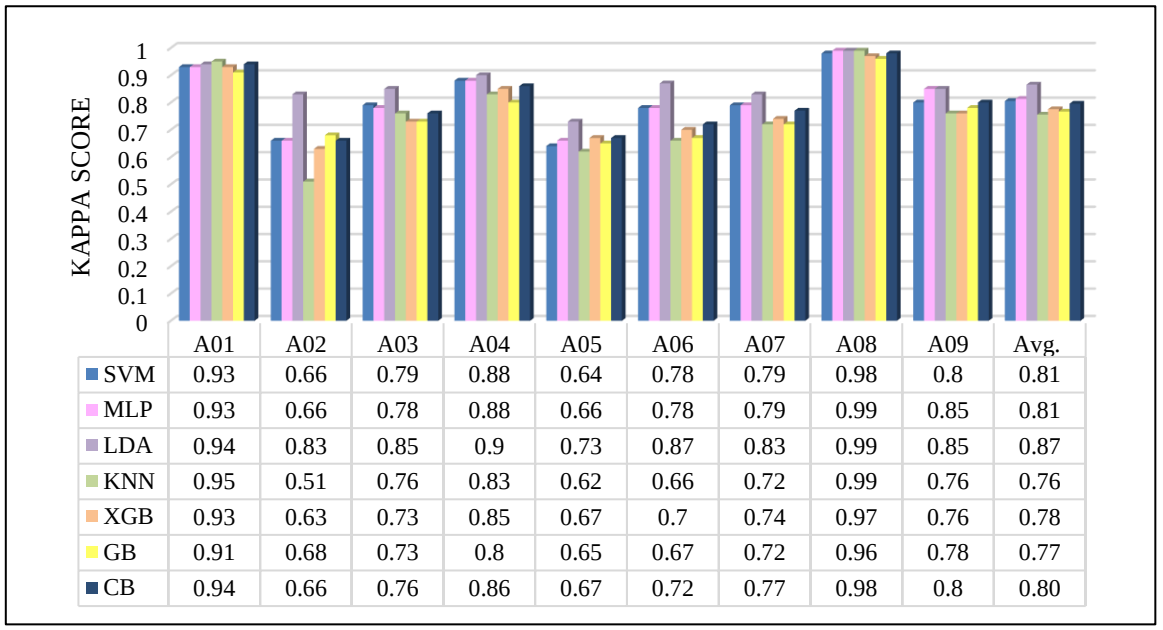

	A01	A02	A03	A04	A05	A06	A07	A08	A09	Avg.
SVM	0.93	0.66	0.79	0.88	0.64	0.78	0.79	0.98	0.8	0.81
MLP	0.93	0.66	0.78	0.88	0.66	0.78	0.79	0.99	0.85	0.81
LDA	0.94	0.83	0.85	0.9	0.73	0.87	0.83	0.99	0.85	0.87
KNN	0.95	0.51	0.76	0.83	0.62	0.66	0.72	0.99	0.76	0.76
XGB	0.93	0.63	0.73	0.85	0.67	0.7	0.74	0.97	0.76	0.78
GB	0.91	0.68	0.73	0.8	0.65	0.67	0.72	0.96	0.78	0.77
CB	0.94	0.66	0.76	0.86	0.67	0.72	0.77	0.98	0.8	0.80

(b)

Figure 6.9 (a) CA (%) and **(b)** K-Score achieved with seven different classifiers for multi-class classification

The classification is performed using seven distinct classifiers, including SVM, MLP, KNN, LDA, XGB, GB, and CB. The CA and K-Score are computed for nine subjects using the FV-1. The obtained CA and K-Score results for binary classification are depicted in Figure 6.8(a) and Figure 6.8(b), respectively. It is demonstrated from Figure 6.8(a) that all seven classifiers were able to accurately classify the MI-EEG signals with high average CA. The SVM classifier attains the highest average CA of 99.00%. The MLP, LDA, KNN, XGB, GB, and CB classifiers also exhibit high average classification accuracies of 98.99%, 98.44%, 98.46%, 97.91%,

97.52%, and 98.07%, respectively. The K-Score is computed using the seven classifiers to validate the CA results. Figure 6.8(b) shows that all seven classifiers achieve a high average K-Score, with SVM and MLP classifiers obtaining the highest average K-Score of 0.98. The LDA and KNN classifiers attain an average K-Score of 0.97, while the XGB, GB, and CB classifiers attain average K-Scores of 0.96, 0.95, and 0.96, respectively. These classification results confirm the efficacy of the proposed method for binary classification.

Subsequently, multi-class classification is conducted using the seven classifiers, and the CA and K-Score results are analyzed for nine subjects (A01-A09). The calculated classification accuracies achieved with the seven classifiers are presented in Figure 6.9(a). It is observed that the LDA classifier attains the highest average CA of 90.00%, while the KNN classifier attains the lowest average CA of 81.61%. However, all classifiers demonstrate considerable success in classifying the multi-class MI-EEG signals using the suggested method, with minimal variation in their classification accuracies. Figure 6.9(b) graphically illustrates the K-Score computed for the nine subjects (A01-A09) across the seven classifiers.

It is noted that the LDA classifier achieves the highest average K-Score of 0.87, while the KNN classifier achieves the lowest average K-Score of 0.76. These K-Score results further validate the effectiveness of the method, showing consistent performance across the seven different classifiers during the multi-class classification process. To further validate the efficacy of the method, a comparative analysis is conducted with several recent approaches that deal with FE and the classification of MI-EEG signals. To ensure a fair assessment, the same dataset (BCI Competition IV (2a)) employed in the present work is utilized for comparison. The performance comparison is based on CA and K-Score calculated for each subject. The compared encompasses various contemporary techniques in the field, spanning various CSP and deep learning based methods.

One notable approach is Channel-wise Convolution with Channel Mixing (C2CM) classification framework by Sakhavi et al. The framework aims to capture temporal information from MI-EEG signals [114]. This approach combined CSP and CNN, utilizing a modified filter bank CSP for temporal representation and a CNN for classification. The C2CM method achieved an average CA of 74.46% and an average K-Score of 0.66. Another study proposed an approach called Filter-Bank Spatial Filtering and Temporal-Spatial Convolutional Neural Network (FBSF-TSCNN) [53]. This method employed an FBSF block to transform MI-EEG signals into appropriate EEG representations, followed by a TSCNN block for

classification. The FBSF-TSCNN approach achieved an average CA of 72.02% and an average K-Score of 0.63. Li et al. suggested a feature fusion network for MI-EEG decoding termed temporal-spectral-based squeeze and excitation feature fusion network (TS-SEFFNet) [124]. The network consisted of two blocks, described as the deep temporal and the multi-spectral convolution blocks. The first block was used to extract temporal representations of the input MI-EEG signals, and the second block was used to extract spectral features. The network achieved an average CA of 74.71% and an average K-Score of 0.66. Musallam et al. proposed another CNN-based fusion network named TCNet-fusion in 2021 [98]. This network integrated temporal convolution, depth-wise convolution, and separable convolution networks. The input MI-EEG signals underwent two 1D convolutions, and the resulting image representations were fed into a temporal convolutional network for classification. The fusion network achieved a high average CA of 83.73%, along with an average K-Score of 0.78.

Table 6.6 Comparison of CA (%) per subject obtained using the proposed method and the recently proposed methods for FE classification of MI-EEG signals

Sub.	C2CM [114]	FBSF-TS-CNN [53]	TS-SEFF-Net [124]	TC-Net [98]	EEG-GE-Net [125]	Sinc-Net [126]	MB-HNN [127]	TSF-STAN [128]	CNN-LSTM [54]	DG-CAN [129]	PGA-CSP [130]	MD-IF [131]	BLRD-LPP [132]	Present work
A01	87.5	85.8	82.29	90.74	82.64	82.67	90.58	88.3	94.1	91.57	86.46	90.04	81.63	**95.48**
A02	65.28	60.1	49.79	70.67	64.58	68.97	75.99	81.7	73.3	75.09	59.03	59.36	63.53	**87.47**
A03	90.28	87.8	87.57	**95.23**	95.14	79.31	93.73	92.2	93.3	92.63	89.24	86.08	83.68	88.94
A04	66.67	64.2	71.74	76.75	74.31	65.52	83.14	77.6	87.7	81.75	69.44	71.05	62.81	**92.33**
A05	62.5	48.6	70.83	82.24	72.92	58.62	73.09	63.3	**86.5**	74.73	63.19	58.33	70.5	79.85
A06	45.49	56.9	63.75	68.83	57.99	48.28	68.15	67.5	88.6	69.52	54.51	54.42	53.77	**90.28**
A07	89.58	83	82.92	94.22	90.97	86.21	**95.82**	90	89.9	95.42	87.15	91.34	88.24	87.49
A08	83.33	81.6	81.53	88.92	87.5	89.66	89.06	95	88.9	89.12	80.21	85.24	84.73	**99.65**
A09	79.51	80.2	81.94	85.98	90.27	89.87	86.24	91.7	86.6	85.61	81.6	79.17	70.46	88.55
Avg.	74.46	72.02	74.71	83.73	79.59	74.35	83.98	83.03	87.66	83.94	74.54	75.00	73.26	**90.00**

In another approach, the authors proposed a feature-level graph embedding network, combining it with the EEGNet method [125]. The average K-Score obtained for nine subjects was 0.73, with an average CA of 79.59%. Lui et al. recently developed a hybrid neural network (NN) for MI-EEG decoding termed SincNet [126]. The input MI-EEG signals were initially mapped into the CSP feature space, followed by automatic data filtering using SincNets. A squeeze-and-excitation module was employed to obtain sparse representations, which were then fed into a CNN for FE [126]. Finally, the extracted features were passed through a gated recurrent unit module and a fully connected layer for classification.

The SincNet method achieved an average CA of 74.34% and an average K-Score of 0.66. Ma et al. designed another hybrid NN that fused TD and FD features extracted by multiple parallel branches combined with a self-attention module [127]. The authors also introduced a novel data augmentation technique called Seg-Swap to expand the EEG dataset. The designed hybrid NN successfully classified the MI-EEG signals with average CA and average K-Score of 83.98% and 0.78, respectively.

Recently, a novel framework called TSF-STAN that used spatial and temporal information for decoding MI-EEG signals was suggested by Jia et al. [128]. The input MI-EEG signals were initially transformed into the spatial-temporal domain using time-contained spatial filtering. Then, a spatial-temporal analysis network was employed to extract spatial and temporal features. An average CA of 83.03, along with an average K-Score of 0.76, was achieved with the TSF-STAN method. Another approach involved feature fusion by connecting CNN and LSTM networks in parallel for the classification of MI-EEG signals [54]. The CNN and LSTM networks were responsible for extracting spatial and temporal features, respectively. All extracted features were merged to enhance CA, resulting in an average CA of 87.66%. Additionally, an average K-Score of 0.82 was achieved using the CNN-LSTM network [54].

Table 6.7 Subject-wise K-Score obtained by the proposed method compared with recently suggested methods of FE and classification of MI-EEG signals

Sub.	C2CM (2018)	FBSF-TS-CNN (2020)	TS-SEFF-Net (2021)	TC-Net (2021)	EEG-GE-Net (2022)	Sinc-Net (2022)	MB-HNN (2022)	TSF-STAN (2022)	CNN-LSTM (2022)	DG-CAN (2023)	MDIF (2023)	Present work
A01	0.83	0.81	0.76	0.87	0.76	0.77	0.88	0.84	0.92	0.86	0.87	**0.94**
A02	0.54	0.47	0.33	0.6	0.53	0.59	0.69	0.75	0.64	0.64	0.46	**0.83**
A03	0.87	0.84	0.83	0.93	0.94	0.75	**0.95**	0.87	0.91	0.92	0.81	0.85
A04	0.56	0.52	0.62	0.68	0.66	0.54	0.71	0.66	0.74	0.73	0.61	**0.90**
A05	0.5	0.31	0.61	0.76	0.64	0.45	0.64	0.54	**0.82**	0.65	0.44	0.73
A06	0.27	0.43	0.52	0.58	0.44	0.35	0.6	0.55	0.85	0.6	0.39	**0.87**
A07	0.86	0.77	0.77	0.92	0.88	0.82	**0.94**	0.86	0.86	0.96	0.88	0.83
A08	0.78	0.75	0.75	0.85	0.83	0.86	0.8	0.92	0.86	0.81	0.8	**0.99**
A09	0.73	0.74	0.76	0.81	0.87	0.85	0.85	0.89	0.82	0.84	0.72	0.85
Avg.	0.66	0.63	0.66	0.78	0.73	0.66	0.78	0.76	0.82	0.78	0.66	**0.87**

Authors Ma et al. recently suggested another NN called DGCAN, which employed graph NN for channel filtering and spatial-temporal domain convolution for MI-EEG classification [129]. The DGCAN method achieved an average CA of 83.94% and an average K-Score of 0.78. In another recently proposed work, a genetic algorithm is combined with CSP for feature selection to better classify the MI-EEG signals [130]. The designed method accomplished an average CA of 74.54%.

In another work, a multi-domain information fusion algorithm was recently suggested by Wang et al., which uses CSP for both channel selection and FE of MI-EEG signals [131]. A classification framework was designed incorporating TF space fusion and discarding irrelevant channels to improve CA. The framework achieved an average CA of 75%, along with an average K-Score of 0.66 [131]. An improved FE method was proposed by Zhu et al. recently, combining Low-Rank Representations (LLR) with Bilinear 2D Discriminant Locality Preserving Projection (B2DDLPP), referred to as BLRDLPP [132]. The BLRDLPP method accomplished an average CA of 72.26% on the BCI dataset. Table 6.6 and Table 6.7 provide an overview of the CA (%) and K-Score obtained through the application of the recently proposed methods and the present work on the nine subjects (A01-A09), respectively. The present work outperforms the previously proposed works, achieving an average CA of 90.00% and an average K-Score of 0.87. Notably, the present method demonstrates superior performance in five out of nine subjects: A01, A02, A04, A06, and A08. These results confirm the efficacy of the method and position it as a suitable contender for developing a real-time BCI system for MI-EEG signal classification.

6.5 Conclusion

The present work proposes a novel approach for FE and the classification of binary and multi-class MI-EEG signals. It introduces a subject-specific channel selection technique to reduce methodological complexity and eliminate redundant information. The method adapts by selecting the most relevant channels for each subject, determined through analysis of classification results. The proposed method combines LMSST and NMF for FE, utilizing LMSST to capture TF information from MI-EEG signals and obtain TF coefficients. These coefficients are then processed using NMF for dimension reduction, resulting in a non-negative basis matrix. Multiple statistical and nonlinear features are extracted, and four different FVs are formed from this matrix. The extracted features are classified into MI tasks using seven different classifiers (SVM, MLP, LDA, KNN, XGB, GB, and CB). Extensive analysis reveals that the statistical features yield the best performance for the proposed method. Furthermore, based on the classification results, the LDA classifier proves to be the most effective in classifying binary and multi-class MI-EEG signals. Various performance metrics, including CA, K-Score, precision, recall, and F1-score, validate the proposed method, which achieves an average CA of 98.44% for binary classification and 90.00% for multi-class classification. The method is evaluated using the widely-used BCI competition IV (2a) dataset, and the outcomes

are compared with other recent MI-EEG FE and classification methods. These comparison results confirm the efficacy of the proposed method in FE and classification. Future enhancements may entail integrating a feature selection method to further reduce computational complexity. Additionally, exploring the application of the method in other domains, such as detecting epileptic seizures, schizophrenia, and sleep disorders, would be intriguing.

Chapter 7
Conclusion and Future Scope

7.1 Conclusion

BCI technology brings hope for individuals grappling with severe motor disabilities, particularly those afflicted by Locked-in Syndrome (LiS), by potentially restoring basic communication capabilities and thereby enhancing their quality of life. The present work addresses the primary objective of advancing pre-processing and FE methodologies in the design of BCI. Delving into the intricacies of the BCI systems, the current work examines state-of-the-art techniques proposed in the past years and presents three innovative methods. The methods presented demonstrate substantial contributions to the field of BCI, in the context of EEG artifact correction and MI-EEG task recognition.

The first method, Hybrid TMSST-Picard based EEG artifact correction, introduces an automated and efficient approach that eliminates the need for manual visual inspection. The methodology, relying on Sparse Entropy and TMSST coefficients, exhibits robust performance with high CA for both 19-channel and 128-channel EEG activity. Comparative analysis underscores its superiority over a state-of-the-art method, and time and frequency domain analysis further validate its effectiveness, suggesting its potential for real-time BCI systems.

The second method, MVMD and PSR based MI-EEG task recognition, presents a novel approach for FE and classification in MI-BCI systems. Evaluated on the BCI Competition IV(2a) dataset, the methodology achieves superior performance in binary and multi-class MI-EEG signal classification. With reduced computational complexity, it is deemed suitable for real-time applications, showcasing its practical significance.

The third method, LMSST and NMF based MI-EEG task recognition, introduces an innovative technique for FE of MI-EEG signals, including subject-specific channel selection to enhance efficiency. This method, utilizing LMSST and NMF, achieves remarkable CA for binary and multi-class MI-EEG tasks, emphasizing its effectiveness through a detailed analysis and comparison with recent methods.

Overall, these methodologies contribute significantly to the development of robust and efficient BCI systems. The findings open avenues for further research and application, with potential implications for real-time BCI implementation and improved disease diagnosis through reduced false classification rates associated with EEG artifacts.

7.2 Future Scope

The methodologies proposed in this work not only aim to exhibit a significant performance compared to current state-of-the-art methods but also aspire to contribute to the establishment of more robust and accurate BCI systems. In future, the potential for developing a BCI system utilizing multi-class MI-EEG activity is expected to grow, with ongoing technological advancements playing a key role in shaping the evolving landscape of this field.

A compelling avenue for future exploration entails incorporating optimal deep learning models, capitalizing on cutting-edge algorithms and computational capabilities. The fine-tuning of various hyperparameters for classifying MI-EEG signals is anticipated to be a focal point, illustrating the intersection of neuroscience and machine learning. Moreover, machine learning algorithms are expected to undergo continual refinement for future studies on feature selection and dimensionality reduction, further optimizing data for training and classification models.

In the future, advanced FE techniques are poised to not only decode specific brain states beyond MI but also incorporate emerging aspects such as emotions, cognitive states, and intentions. This broader scope is set to unlock new dimensions of BCI applications, extending beyond communication, rehabilitation, and cognitive enhancement. The exploration of data from multiple modalities is seen as a significant future aspect, with innovations in this realm expected to lead to more efficient models seamlessly integrating data from various sources, thereby enhancing the adaptability and versatility of BCI systems.

In the realm of multi-class classification methods, the future is expected to witness the development of techniques enabling the simultaneous detection of multiple motor intentions or mental states. This advancement holds the promise of expanding the applications of BCI technology across diverse domains, from healthcare to neuro-engineering. The integration of EEG data with other modalities, such as EMG, fNIRS, or eye movement tracking, is anticipated to create synergies that provide richer insights into brain activity and further improve BCI performance.

Despite these anticipated advancements, the ongoing challenge of tailoring BCI systems to individual users is likely to persist. Future research endeavors are expected to focus on adaptive systems capable of dynamically adjusting to changes in the user's EEG patterns over time, ensuring sustained effectiveness and user satisfaction. The development of personalized BCIs is anticipated to be a crucial element in enhancing user experience and overall system performance, marking a significant stride toward realizing the potential of BCI technology. The application of automated feature engineering through AI algorithms is expected to be a transformative strategy for future studies, identifying and optimizing features specific to different BCI applications and user populations. The anticipated reduction in manual efforts for feature selection is likely to enhance the efficiency and generalizability of BCI systems, making it more accessible for diverse users and tasks.

In conclusion, the anticipated future of FE for MI-EEG signals holds immense potential for advancing BCI technology. By leveraging the capabilities of AI, personalized learning, and multimodal data fusion, future researchers are poised to pioneer the development of sophisticated, user-friendly BCI systems with broad applications. This trajectory of progress underscores the interdisciplinary nature of BCI research, where neuroscience, engineering, and AI converge to unlock new possibilities for communication, rehabilitation, and human-machine interaction.

Bibliography

[1] Selim, S., Tantawi, M. M., Shedeed, H. A., & Badr, A. (2018). A CSP\AM-BA-SVM Approach for Motor Imagery BCI System. IEEE Access, 6, 49192–49208. https://doi.org/10.1109/ACCESS.2018.2868178

[2] Ramadan, R. A., Refat, S., Elshahed, M. A., & Ali, R. A. (2015). Basics of Brain Computer Interface. In A. E. Hassanien & A. T. Azar (Eds.), Brain-Computer Interfaces (Vol. 74, pp. 31–50). Springer International Publishing. https://doi.org/10.1007/978-3-319-10978-7_2

[3] Kumari, N., Anwar, S., & Bhattacharjee, V. (2022a). Automated visual stimuli evoked multi-channel EEG signal classification using EEGCapsNet. Pattern Recognition Letters, 153, 29–35. https://doi.org/10.1016/j.patrec.2021.11.019

[4] Mudgal, S. K., Sharma, S. K., Chaturvedi, J., & Sharma, A. (2020). Brain computer interface advancement in neurosciences: Applications and issues. Interdisciplinary Neurosurgery, 20, 100694. https://doi.org/10.1016/j.inat.2020.100694

[5] Padfield, N., Zabalza, J., Zhao, H., Masero, V., & Ren, J. (2019). EEG-Based Brain-Computer Interfaces Using Motor-Imagery: Techniques and Challenges. Sensors, 19(6), 1423. https://doi.org/10.3390/s19061423

[6] Sharma, N., Sharma, M., Singhal, A., Vyas, R., Malik, H., Afthanorhan, A., & Hossaini, M. A. (2023). Recent Trends in EEG-Based Motor Imagery Signal Analysis and Recognition: A Comprehensive Review. IEEE Access, 11, 80518–80542. https://doi.org/10.1109/ACCESS.2023.3299497

[7] Ketu, S., & Mishra, P. K. (2022). g classification model for eye state detection using electroencephalogram signals. Cognitive Neurodynamics, 16(1), 73–90. https://doi.org/10.1007/s11571-021-09678-x

[8] Upadhyay, R., Padhy, P. K., & Kankar, P. K. (2016). EEG artifact removal and noise suppression by Discrete Orthonormal S-Transform denoising. Computers & Electrical Engineering, 53, 125–142. https://doi.org/10.1016/j.compeleceng.2016.05.015

[9] Hramov, A. E., Maksimenko, V. A., & Pisarchik, A. N. (2021). Physical principles of brain–computer interfaces and their applications for rehabilitation, robotics and control of human brain states. Physics Reports, 918, 1–133. https://doi.org/10.1016/j.physrep.2021.03.002

[10] Tiwari, N., Edla, D. R., Dodia, S., & Bablani, A. (2018). Brain computer interface: A comprehensive survey. Biologically Inspired Cognitive Architectures, 26, 118–129. https://doi.org/10.1016/j.bica.2018.10.005

[11] Wu, D., Jiang, X., & Peng, R. (2022). Transfer learning for motor imagery based brain–computer interfaces: A tutorial. Neural Networks, 153, 235–253. https://doi.org/10.1016/j.neunet.2022.06.008

[12] Nonnekes, J., Arrogi, A., Munneke, M. A. M., Van Asseldonk, E. H. F., Oude Nijhuis, L. B., Geurts, A. C., & Weerdesteyn, V. (2014). Subcortical Structures in Humans Can Be Facilitated by Transcranial Direct Current Stimulation. PLoS ONE, 9(9), e107731. https://doi.org/10.1371/journal.pone.0107731

[13] McFarland, D. J., Daly, J., Boulay, C., & Parvaz, M. A. (2017). Therapeutic applications of BCI technologies. Brain-Computer Interfaces, 4(1–2), 37–52. https://doi.org/10.1080/2326263X.2017.1307625

[14] Mohamed, E. T. A., & Declercq, N. F. (2020). Giga-Hertz ultrasonic microscopy: Getting over the obscurity- A short review on the biomedical applications. Physics in Medicine, 9, 100025. https://doi.org/10.1016/j.phmed.2020.100025

[15] Thompson, T., Steffert, T., Ros, T., Leach, J., & Gruzelier, J. (2008). EEG applications for sport and performance. Methods, 45(4), 279–288. https://doi.org/10.1016/j.ymeth.2008.07.006

[16] Kumari, N., Anwar, S., & Bhattacharjee, V. (2022b). Time series-dependent feature of EEG signals for improved visually evoked emotion classification using EmotionCapsNet. Neural Computing and Applications, 34(16), 13291–13303. https://doi.org/10.1007/s00521-022-06942-x

[17] Ablin, P., Cardoso, J.-F., & Gramfort, A. (2018). Faster Independent Component Analysis by Preconditioning With Hessian Approximations. IEEE Transactions on Signal Processing, 66(15), 4040–4049. https://doi.org/10.1109/TSP.2018.2844203

[18] Yu, G., Lin, T., Wang, Z., & Li, Y. (2021). Time-Reassigned Multisynchrosqueezing Transform for Bearing Fault Diagnosis of Rotating Machinery. IEEE Transactions on Industrial Electronics, 68(2), 1486–1496. https://doi.org/10.1109/TIE.2020.2970571

[19] Sadiq, M. T., Yu, X., Yuan, Z., Aziz, M. Z., Rehman, N. U., Ding, W., & Xiao, G. (2022). Motor Imagery BCI Classification Based on Multivariate Variational Mode Decomposition. IEEE Transactions on Emerging Topics in Computational Intelligence, 6(5), 1177–1189. https://doi.org/10.1109/TETCI.2022.3147030

[20] Kaur, S., Singh, S., Arun, P., Kaur, D., & Bajaj, M. (2020). Phase Space Reconstruction of EEG Signals for Classification of ADHD and Control Adults. Clinical EEG and Neuroscience, 51(2), 102–113. https://doi.org/10.1177/1550059419876525

[21] Yu, G., Wang, Z., Zhao, P., & Li, Z. (2019). Local maximum synchrosqueezing transform: An energy-concentrated time-frequency analysis tool. Mechanical Systems and Signal Processing, 117, 537–552. https://doi.org/10.1016/j.ymssp.2018.08.006

[22] Xu, L., Chavez-Echeagaray, M. E., & Berisha, V. (2022). Unsupervised EEG channel selection based on non-negative matrix factorization. Biomedical Signal Processing and Control, 76, 103700. https://doi.org/10.1016/j.bspc.2022.103700

[23] Azevedo, F. A. C., Carvalho, L. R. B., Grinberg, L. T., Farfel, J. M., Ferretti, R. E. L., Leite, R. E. P., Filho, W. J., Lent, R., & Herculano-Houzel, S. (2009). Equal numbers of neuronal and nonneuronal cells make the human brain an isometrically scaled-up primate brain. Journal of Comparative Neurology, 513(5), 532–541. https://doi.org/10.1002/cne.21974

[24] Hall, John (2011). Guyton and Hall Textbook of Medical Physiology (12th ed.). Philadelphia, PA: Saunders/Elsevier.

[25] Standring, Susan, ed. (2008). Gray's Anatomy: The Anatomical Basis of Clinical Practice (40th ed.). London: Churchill Livingstone.

[26] Freberg, L. (2009). Discovering Biological Psychology. Cengage Learning. pp. 44–46.

[27] https://commons.m.wikimedia.org/wiki/File:Diagram_showing_some_of_the_main_areas_of_the_brain_CRUK_188.svg

[28] Purves, Dale (2012). Neuroscience (5th ed.). Sunderland, MA: Sinauer associates.

[29] Sampaio-Baptista, C., & Johansen-Berg, H. (2017). White Matter Plasticity in the Adult Brain. Neuron, 96(6), 1239–1251. https://doi.org/10.1016/j.neuron.2017.11.026

[30] Pocock, G.; Richards, C. (2006). Human Physiology: The Basis of Medicine (3rd ed.). Oxford: Oxford University Press.

[31] Kawala-Sterniuk, A., Browarska, N., Al-Bakri, A., Pelc, M., Zygarlicki, J., Sidikova, M., Martinek, R., & Gorzelanczyk, E. J. (2021). Summary of over Fifty Years with Brain-Computer Interfaces—A Review. Brain Sciences, 11(1), 43. https://doi.org/10.3390/brainsci11010043

[32] Nicolas-Alonso, L. F., & Gomez-Gil, J. (2012). Brain Computer Interfaces, a Review. Sensors, 12(2), 1211–1279. https://doi.org/10.3390/s120201211

[33] Ramadan, R. A., & Vasilakos, A. V. (2017). Brain computer interface: Control signals review. Neurocomputing, 223, 26–44. https://doi.org/10.1016/j.neucom.2016.10.024

[34] Vallabhaneni, A., Wang, T., & He, B. (2005). Brain—Computer Interface. In B. He (Ed.), Neural Engineering (pp. 85–121). Springer US. https://doi.org/10.1007/0-306-48610-5_3

[35] Castellanos, N. P., & Makarov, V. A. (2006). Recovering EEG brain signals: Artifact suppression with wavelet enhanced independent component analysis. Journal of Neuroscience Methods, 158(2), 300–312. https://doi.org/10.1016/j.jneumeth.2006.05.033

[36] Taran, S., & Bajaj, V. (2019). Motor imagery tasks-based EEG signals classification using tunable-Q wavelet transform. Neural Computing and Applications, 31(11), 6925–6932. https://doi.org/10.1007/s00521-018-3531-0

[37] Selvan, S., & Srinivasan, R. (1999). Removal of ocular artifacts from EEG using an efficient neural network based adaptive filtering technique. IEEE Signal Processing Letters, 6(12), 330–332. https://doi.org/10.1109/97.803438

[38] He, P., Wilson, G., & Russell, C. (2004). Removal of ocular artifacts from electro-encephalogram by adaptive filtering. Medical & Biological Engineering & Computing, 42(3), 407–412. https://doi.org/10.1007/BF02344717

[39] Hagemann, D., & Naumann, E. (2001). The effects of ocular artifacts on (lateralized) broadband power in the EEG. Clinical Neurophysiology, 112(2), 215–231. https://doi.org/10.1016/S1388-2457(00)00541-1

[40] Casarotto, S., Bianchi, A. M., Cerutti, S., & Chiarenza, G. A. (2004). Principal component analysis for reduction of ocular artefacts in event-related potentials of normal and dyslexic children. Clinical Neurophysiology, 115(3), 609–619. https://doi.org/10.1016/j.clinph.2003.10.018

[41] Blum, S., Jacobsen, N. S. J., Bleichner, M. G., & Debener, S. (2019). A Riemannian Modification of Artifact Subspace Reconstruction for EEG Artifact Handling. Frontiers in Human Neuroscience, 13, 141. https://doi.org/10.3389/fnhum.2019.00141

[42] Romero, S., Mañanas, M. A., & Barbanoj, M. J. (2009). Ocular Reduction in EEG Signals Based on Adaptive Filtering, Regression and Blind Source Separation. Annals of Biomedical Engineering, 37(1), 176–191. https://doi.org/10.1007/s10439-008-9589-6

[43] Mammone, N., La Foresta, F., & Morabito, F. C. (2012). Automatic Artifact Rejection From Multichannel Scalp EEG by Wavelet ICA. IEEE Sensors Journal, 12(3), 533–542. https://doi.org/10.1109/JSEN.2011.2115236

[44] Caetano, G., Esteves, I., Vourvopoulos, A., Fleury, M., & Figueiredo, P. (2023). NeuXus open-source tool for real-time artifact reduction in simultaneous EEG-fMRI. NeuroImage, 280, 120353. https://doi.org/10.1016/j.neuroimage.2023.120353

[45] Jafarifarmand, A., Badamchizadeh, M.-A., Khanmohammadi, S., Nazari, M. A., & Tazehkand, B. M. (2017). Real-time ocular artifacts removal of EEG data using a hybrid ICA-ANC approach. Biomedical Signal Processing and Control, 31, 199–210. https://doi.org/10.1016/j.bspc.2016.08.006

[46] Wang, H., Xu, T., Tang, C., Yue, H., Chen, C., Xu, L., Pei, Z., Dong, J., Bezerianos, A., & Li, J. (2020). Diverse Feature Blend Based on Filter-Bank Common Spatial Pattern and Brain Functional Connectivity for Multiple Motor Imagery Detection. IEEE Access, 8, 155590–155601. https://doi.org/10.1109/ACCESS.2020.3018962

[47] Shi, T., Ren, L., & Cui, W. (2020). Feature Extraction of Brain–Computer Interface Electroencephalogram Based on Motor Imagery. IEEE Sensors Journal, 20(20), 11787–11794. https://doi.org/10.1109/JSEN.2019.2939343.

[48] Samek, W., Vidaurre, C., Müller, K.-R., & Kawanabe, M. (2012). Stationary common spatial patterns for brain–computer interfacing. Journal of Neural Engineering, 9(2), 026013. https://doi.org/10.1088/1741-2560/9/2/026013

[49] Wu, W., Chen, Z., Gao, X., Li, Y., Brown, E. N., & Gao, S. (2015). Probabilistic Common Spatial Patterns for Multichannel EEG Analysis. IEEE Transactions on Pattern Analysis

and Machine Intelligence, 37(3), 639–653. https://doi.org/10.1109/TPAMI.2014.2330598

[50] Cheng, L., Li, D., Li, X., & Yu, S. (2019). The Optimal Wavelet Basis Function Selection in Feature Extraction of Motor Imagery Electroencephalogram Based on Wavelet Packet Transformation. IEEE Access, 7, 174465–174481. https://doi.org/10.1109/ACCESS.2019.2953972

[51] Bashar, S. K., & Bhuiyan, M. I. H. (2016). Classification of motor imagery movements using multivariate empirical mode decomposition and short time Fourier transform based hybrid method. Engineering Science and Technology, an International Journal, 19(3), 1457–1464. https://doi.org/10.1016/j.jestch.2016.04.009

[52] Kevric, J., & Subasi, A. (2017). Comparison of signal decomposition methods in classification of EEG signals for motor-imagery BCI system. Biomedical Signal Processing and Control, 31, 398–406. https://doi.org/10.1016/j.bspc.2016.09.007

[53] Chen, J., Yu, Z., Gu, Z., & Li, Y. (2020). Deep Temporal-Spatial Feature Learning for Motor Imagery-Based Brain–Computer Interfaces. IEEE Transactions on Neural Systems and Rehabilitation Engineering, 28(11), 2356–2366. https://doi.org/10.1109/TNSRE.2020.3023417

[54] Li, H., Ding, M., Zhang, R., & Xiu, C. (2022). Motor imagery EEG classification algorithm based on CNN-LSTM feature fusion network. Biomedical Signal Processing and Control, 72, 103342. https://doi.org/10.1016/j.bspc.2021.103342

[55] Khademi, Z., Ebrahimi, F., & Kordy, H. M. (2022). A transfer learning-based CNN and LSTM hybrid deep learning model to classify motor imagery EEG signals. Computers in Biology and Medicine, 143, 105288. https://doi.org/10.1016/j.compbiomed.2022.105288

[56] Chaudhary, S., Taran, S., Bajaj, V., & Sengur, A. (2019). Convolutional Neural Network Based Approach Towards Motor Imagery Tasks EEG Signals Classification. IEEE Sensors Journal, 19(12), 4494–4500. https://doi.org/10.1109/JSEN.2019.2899645

[57] Mall, P. K., Singh, P. K., Srivastav, S., Narayan, V., Paprzycki, M., Jaworska, T., & Ganzha, M. (2023). A comprehensive review of deep neural networks for medical image processing: Recent developments and future opportunities. Healthcare Analytics, 4, 100216. https://doi.org/10.1016/j.health.2023.100216

[58] Azab, A. M., Mihaylova, L., Ang, K. K., & Arvaneh, M. (2019). Weighted Transfer Learning for Improving Motor Imagery-Based Brain–Computer Interface. IEEE Transactions on Neural Systems and Rehabilitation Engineering, 27(7), 1352–1359. https://doi.org/10.1109/TNSRE.2019.2923315

[59] Liang, Y., & Ma, Y. (2020). Calibrating EEG features in motor imagery classification tasks with a small amount of current data using multisource fusion transfer learning. Biomedical Signal Processing and Control, 62, 102101. https://doi.org/10.1016/j.bspc.2020.102101

[60] Lee, D.-Y., Jeong, J.-H., Lee, B.-H., & Lee, S.-W. (2022). Motor Imagery Classification Using Inter-Task Transfer Learning via a Channel-Wise Variational Autoencoder-Based Convolutional Neural Network. IEEE Transactions on Neural Systems and Rehabilitation Engineering, 30, 226–237. https://doi.org/10.1109/TNSRE.2022.3143836

[61] Li, H., Zhang, D., & Xie, J. (2023). MI-DABAN: A dual-attention-based adversarial network for motor imagery classification. Computers in Biology and Medicine, 152, 106420. https://doi.org/10.1016/j.compbiomed.2022.106420

[62] Dong, E., Li, C., Li, L., Du, S., Belkacem, A. N., & Chen, C. (2017). Classification of multi-class motor imagery with a novel hierarchical SVM algorithm for brain–computer interfaces. Medical & Biological Engineering & Computing, 55(10), 1809–1818. https://doi.org/10.1007/s11517-017-1611-4

[63] Fu, R., Tian, Y., Bao, T., Meng, Z., & Shi, P. (2019). Improvement Motor Imagery EEG Classification Based on Regularized Linear Discriminant Analysis. Journal of Medical Systems, 43(6), 169. https://doi.org/10.1007/s10916-019-1270-0

[64] García-Moral, A. I., Solera-Ureña, R., Peláez-Moreno, C., & Díaz-de-María, F. (2007). Hybrid Models for Automatic Speech Recognition: A Comparison of Classical ANN and Kernel Based Methods. In M. Chetouani, A. Hussain, B. Gas, M. Milgram, & J.-L. Zarader (Eds.), Advances in Nonlinear Speech Processing (Vol. 4885, pp. 152–160). Springer Berlin Heidelberg. https://doi.org/10.1007/978-3-540-77347-4_12

[65] Ketu, S., & Mishra, P. K. (2020). Performance Analysis of Machine Learning Algorithms for IoT-Based Human Activity Recognition. In T. Sengodan, M. Murugappan, & S. Misra (Eds.), Advances in Electrical and Computer Technologies (Vol. 672, pp. 579–591). Springer Singapore. https://doi.org/10.1007/978-981-15-5558-9_51

[66] Zhang, Y., Chen, W., Lin, C.-L., Pei, Z., Chen, J., & Chen, Z. (2021). Boosting-LDA algriothm with multi-domain feature fusion for motor imagery EEG decoding. Biomedical Signal Processing and Control, 70, 102983. https://doi.org/10.1016/j.bspc.2021.102983

[67] Dai, M., Wang, S., Zheng, D., Na, R., & Zhang, S. (2019). Domain Transfer Multiple Kernel Boosting for Classification of EEG Motor Imagery Signals. IEEE Access, 7, 49951–49960. https://doi.org/10.1109/ACCESS.2019.2908851

[68] Safieddine, D., Kachenoura, A., Albera, L., Birot, G., Karfoul, A., Pasnicu, A., Biraben, A., Wendling, F., Senhadji, L., & Merlet, I. (2012). Removal of muscle artifact from EEG data: Comparison between stochastic (ICA and CCA) and deterministic (EMD and wavelet-based) approaches. EURASIP Journal on Advances in Signal Processing, 2012(1), 127. https://doi.org/10.1186/1687-6180-2012-127

[69] Croft, R. J., & Barry, R. J. (2000). Removal of ocular artifact from the EEG: A review. Neurophysiologie Clinique/Clinical Neurophysiology, 30(1), 5–19. https://doi.org/10.1016/S0987-7053(00)00055-1

[70] Jung, T., Makeig, S., Humphries, C., Lee, T., McKeown, M. J., Iragui, V., & Sejnowski, T. J. (2000). Removing electroencephalographic artifacts by blind source separation. Psychophysiology, 37(2), 163–178. https://doi.org/10.1111/1469-8986.3720163

[71] Shoker, L., Sanei, S., Wang, W., & Chambers, J. A. (2005). Removal of eye blinking artifact from the electro-encephalogram, incorporating a new constrained blind source separation algorithm. Medical & Biological Engineering & Computing, 43(2), 290–295. https://doi.org/10.1007/BF02345968

[72] Flexer, A., Bauer, H., Pripfl, J., & Dorffner, G. (2005). Using ICA for removal of ocular artifacts in EEG recorded from blind subjects. Neural Networks, 18(7), 998–1005. https://doi.org/10.1016/j.neunet.2005.03.012

[73] Joyce, C. A., Gorodnitsky, I. F., & Kutas, M. (2004). Automatic removal of eye movement and blink artifacts from EEG data using blind component separation. Psychophysiology, 41(2), 313–325. https://doi.org/10.1111/j.1469-8986.2003.00141.x

[74] Nguyen, H.-A. T., Musson, J., Li, F., Wang, W., Zhang, G., Xu, R., Richey, C., Schnell, T., McKenzie, F. D., & Li, J. (2012). EOG artifact removal using a wavelet neural network. Neurocomputing, 97, 374–389. https://doi.org/10.1016/j.neucom.2012.04.016

[75] Wang, Z., Xu, P., Liu, T., Tian, Y., Lei, X., & Yao, D. (2014). Robust removal of ocular artifacts by combining Independent Component Analysis and system identification. Biomedical Signal Processing and Control, 10, 250–259. https://doi.org/10.1016/j.bspc.2013.10.006

[76] Zikov, T., Bibian, S., Dumont, G. A., Huzmezan, M., & Ries, C. R. (2002). A wavelet based de-noising technique for ocular artifact correction of the electroencephalogram. Proceedings of the Second Joint 24th Annual Conference and the Annual Fall Meeting of the Biomedical Engineering Society] [Engineering in Medicine and Biology, 1, 98–105. https://doi.org/10.1109/IEMBS.2002.1134407

[77] Jafarifarmand, A., & Badamchizadeh, M. A. (2013). Artifacts removal in EEG signal using a new neural network enhanced adaptive filter. Neurocomputing, 103, 222–231. https://doi.org/10.1016/j.neucom.2012.09.024

[78] Minguillon, J., Lopez-Gordo, M. A., & Pelayo, F. (2017). Trends in EEG-BCI for daily-life: Requirements for artifact removal. Biomedical Signal Processing and Control, 31, 407–418. https://doi.org/10.1016/j.bspc.2016.09.005

[79] Akhtar, M. T., Mitsuhashi, W., & James, C. J. (2012). Employing spatially constrained ICA and wavelet denoising, for automatic removal of artifacts from multichannel EEG data. Signal Processing, 92(2), 401–416. https://doi.org/10.1016/j.sigpro.2011.08.005

[80] Khatun, S., Mahajan, R., & Morshed, B. I. (2016). Comparative Study of Wavelet-Based Unsupervised Ocular Artifact Removal Techniques for Single-Channel EEG Data. IEEE Journal of Translational Engineering in Health and Medicine, 4, 1–8. https://doi.org/10.1109/JTEHM.2016.2544298

[81] Kumar, P. S., Arumuganathan, R., Sivakumar, K., & Vimal, C. (2008). Removal of Ocular Artifacts in the EEG through Wavelet Transform without using an EOG Reference Channel.

[82] Hyvarinen, A. (1999). Fast and robust fixed-point algorithms for independent component analysis. IEEE Transactions on Neural Networks, 10(3), 626–634. https://doi.org/10.1109/72.761722

[83] Tichavsky, P., Koldovsky, Z., Yeredor, A., Gomez-Herrero, G., & Doron, E. (2008). A Hybrid Technique for Blind Separation of Non-Gaussian and Time-Correlated Sources Using a Multicomponent Approach. IEEE Transactions on Neural Networks, 19(3), 421–430. https://doi.org/10.1109/TNN.2007.908648

[84] Ball, K., Bigdely-Shamlo, N., Mullen, T., & Robbins, K. (2016). PWC-ICA: A Method for Stationary Ordered Blind Source Separation with Application to EEG. Computational Intelligence and Neuroscience, 2016, 1–20. https://doi.org/10.1155/2016/9754813

[85] Koldovsky, Z., Tichavsky, P., & Oja, E. (2006). Efficient Variant of Algorithm FastICA for Independent Component Analysis Attaining the CramÉr-Rao Lower Bound. IEEE Transactions on Neural Networks, 17(5), 1265–1277. https://doi.org/10.1109/TNN.2006.875991

[86] Tichavsky, P., Doron, E., Yeredor, A., & Nielsen, J. (2006). A computationally affordable implementation of an asymptotically optimal bss algorithm for ar sources. Proceedings of the European Signal Processing Conference (EUSIPCO), Florence.

[87] Bandt, C., & Pompe, B. (2002). Permutation Entropy: A Natural Complexity Measure for Time Series. Physical Review Letters, 88(17), 174102. https://doi.org/10.1103/PhysRevLett.88.174102

[88] Higuchi, T. (1988). Approach to an irregular time series on the basis of the fractal theory. Physica D: Nonlinear Phenomena, 31(2), 277–283. https://doi.org/10.1016/0167-2789(88)90081-4

[89] Cardoso, J.-F. (1997). Infomax and maximum likelihood for blind source separation. IEEE Signal Processing Letters, 4(4), 112–114. https://doi.org/10.1109/97.566704

[90] Zima, M., Tichavský, P., Paul, K., & Krajča, V. (2012). Robust removal of short-duration artifacts in long neonatal EEG recordings using wavelet-enhanced ICA and adaptive combining of tentative reconstructions. Physiological Measurement, 33(8), N39–N49. https://doi.org/10.1088/0967-3334/33/8/N39

[91] Azami, H., Fernández, A., & Escudero, J. (2019). Multivariate Multiscale Dispersion Entropy of Biomedical Times Series. Entropy, 21(9), 913. https://doi.org/10.3390/e21090913

[92] Ahmed, M. U., & Mandic, D. P. (2011). Multivariate multiscale entropy: A tool for complexity analysis of multichannel data. Physical Review E, 84(6), 061918. https://doi.org/10.1103/PhysRevE.84.061918

[93] Tu, X., Hu, Y., Li, F., Abbas, S., Liu, Z., & Bao, W. (2019). Demodulated High-Order Synchrosqueezing Transform With Application to Machine Fault Diagnosis. IEEE Transactions on Industrial Electronics, 66(4), 3071–3081. https://doi.org/10.1109/TIE.2018.2847640

[94] He, D., Cao, H., Wang, S., & Chen, X. (2019). Time-reassigned synchrosqueezing transform: The algorithm and its applications in mechanical signal processing. Mechanical Systems and Signal Processing, 117, 255–279. https://doi.org/10.1016/j.ymssp.2018.08.004

[95] Yu, G., & Zhou, Y. (2016). General linear chirplet transform. Mechanical Systems and Signal Processing, 70–71, 958–973. https://doi.org/10.1016/j.ymssp.2015.09.004

[96] Thakur, G., & Wu, H.-T. (2011). Synchrosqueezing-based Recovery of Instantaneous Frequency from Nonuniform Samples. SIAM Journal on Mathematical Analysis, 43(5), 2078–2095. https://doi.org/10.1137/100798818

[97] Daly, I., Scherer, R., Billinger, M., & Muller-Putz, G. (2015). FORCe: Fully Online and Automated Artifact Removal for Brain-Computer Interfacing. IEEE Transactions on Neural Systems and Rehabilitation Engineering, 23(5), 725–736. https://doi.org/10.1109/TNSRE.2014.2346621

[98] Musallam, Y. K., AlFassam, N. I., Muhammad, G., Amin, S. U., Alsulaiman, M., Abdul, W., Altaheri, H., Bencherif, M. A., & Algabri, M. (2021). Electroencephalography-based motor imagery classification using temporal convolutional network fusion. Biomedical Signal Processing and Control, 69, 102826. https://doi.org/10.1016/j.bspc.2021.102826

[99] Lotte, F., & Guan, C. (2011). Regularizing Common Spatial Patterns to Improve BCI Designs: Unified Theory and New Algorithms. IEEE TRANSACTIONS ON BIOMEDICAL ENGINEERING, 58(2), 355.

[100] Zhang, R., Xu, P., Guo, L., Zhang, Y., Li, P., & Yao, D. (2013). Z-Score Linear Discriminant Analysis for EEG Based Brain-Computer Interfaces. PLoS ONE, 8(9), e74433. https://doi.org/10.1371/journal.pone.0074433

[101] Prabhakar, S. K., & Lee, S. W. (2022). Improved Sparse Representation based Robust Hybrid Feature Extraction Models with Transfer and Deep Learning for EEG Classification. Expert Systems with Applications, 198, 116783.

[102] Zhang, Y., Nam, C. S., Zhou, G., Jin, J., Wang, X., Cichocki, A., Zhang, Y., Zhou, G., Jin, J., & Wang, X. (2019). Temporally Constrained Sparse Group Spatial Patterns for Motor Imagery BCI; Temporally Constrained Sparse Group Spatial Patterns for Motor Imagery BCI. IEEE TRANSACTIONS ON CYBERNETICS, 49(9).

[103] Joadder, M. A. M., Siuly, S., Kabir, E., Wang, H., & Zhang, Y. (2019). A New Design of Mental State Classification for Subject Independent BCI Systems. IRBM, 40(5), 297–305.

[104] Usman, M., Zubair, M., Hussein, H. S., Wajid, M., Farrag, M., Ali, S. J., Shiblee, M., & Habeeb, M. S. (2021). Empirical Mode Decomposition for Analysis and Filtering of

Speech Signals. IEEE Canadian Journal of Electrical and Computer Engineering, 44(3), 343–349. https://doi.org/10.1109/ICJECE.2021.3075373

[105] Ahrabian, A., Looney, D., Stanković, L., & Mandic, D. P. (2015). Synchrosqueezing-based time- frequency analysis of multivariate data. Signal Processing, 106, 331–341.

[106] Sadiq M. T., Yu X., Yuan Z., Rehman A.U., Ullah I., Li G., Xiao A.G. (2019). Motor imagery EEG signals decoding by multivariate empirical wavelet transform-based framework for robust brain-computer interfaces. IEEE Access, 7, 171431–171451.

[107] Rehman, N. U., & Aftab, H. (2019). Multivariate Variational Mode Decomposition. IEEE Transactions on Signal Processing, 67(23), 6039–6052.

[108] Lawhern, V. J., Solon, A. J., Waytowich, N. R., Gordon, S. M., Hung, C. P., & Lance, B. J. (2018). EEGNet: A compact convolutional neural network for EEG-based brain-computer interfaces. Journal of Neural Engineering, 15(5).

[109] Raza, H., Chowdhury, A., Bhattacharyya, S., & Samothrakis, S. (2020). Single-Trial EEG Classification with EEGNet and Neural Structured Learning for Improving BCI Performance; Single-Trial EEG Classification with EEGNet and Neural Structured Learning for Improving BCI Performance.

[110] Mahamune, R., & Laskar, S. H. (2021). Classification of the four-class motor imagery signals using continuous wavelet transform filter bank-based two-dimensional images. International Journal of Imaging Systems and Technology, 31(4), 2237–2248.

[111] C. Brunner, R. Leeb, G. Müller-Putz, A. Schl¨ogl, G. Pfurtscheller. BCI Competition 2008_Graz Data Set A. [Online]. Available: http://www.bbci.de/competition/iv/.

[112] Schirrmeister, R. T., Springenberg, J. T., Fiederer, L. D. J., Glasstetter, M., Eggensperger, K., Tangermann, M., Hutter, F., Burgard, W., & Ball, T. (2017). Deep learning with convolutional neural networks for EEG decoding and visualization. Human Brain Mapping, 38(11), 5391–5420.

[113] Mane, R., Chew, E., Chua, K., Ang, K. K., Robinson, N., Vinod, A. P., Lee, S.-W., & Guan, C. (2021). FBCNet: A Multi-view Convolutional Neural Network for Brain-Computer Interface.

[114] Sakhavi, S., Guan, C., & Yan, S. (2018). Learning Temporal Information for Brain-Computer Interface Using Convolutional Neural Networks. IEEE Transactions on Neural Networks and Learning Systems, 29(11), 5619–5629. https://doi.org/10.1109/TNNLS.2018.2789927

[115] She, Q., Hu, B., Luo, Z., Nguyen, T., & Zhang, Y. (2019). A hierarchical semi-supervised extreme learning machine method for EEG recognition. Medical and Biological Engineering and Computing, 57(1), 147–157.

[116] Zhao, D., Tang, F., Si, B., & Feng, X. (2019). Learning joint space–time–frequency features for EEG decoding on small labeled data. Neural Networks, 114, 67–77.

[117] Olias, J., Martin-Clemente, R., Sarmiento-Vega, M. A., & Cruces, S. (2019). EEG signal processing in mi-bci applications with improved covariance matrix estimators. IEEE Transactions on Neural Systems and Rehabilitation Engineering, 27(5), 895–904.

[118] Ai, Q., Chen, A., Chen, K., Liu, Q., Zhou, T., Xin, S., & Ji, Z. (2019). Feature extraction of four-class motor imagery EEG signals based on functional brain network. Journal of neural engineering, 16, 026032.

[119] Fang, H., Jin, J., S., Daly, I., & Wang, X. (2022). Feature Extraction Method Based on Filter Banks and Riemannian Tangent Space in Motor-Imagery BCI. IEEE journal of biomedical and health informatics, 26(6), 2504-2514.

[120] Chatterjee, S., & Byun, Y.-C. (2022). EEG-Based Emotion Classification Using Stacking Ensemble Approach. Sensors, 22(21), 8550. https://doi.org/10.3390/s22218550

[121] Çalişir, D., & Doğantekin, E. (2011). An automatic diabetes diagnosis system based on LDA-Wavelet Support Vector Machine Classifier. Expert Systems with Applications, 38(7), 8311–8315. https://doi.org/10.1016/j.eswa.2011.01.017

[122] Li, C., Shao, C., Song, R., Xu, G., Liu, X., Qian, R., & Chen, X. (2023). Spatio-temporal MLP network for seizure prediction using EEG signals. Measurement, 206, 112278. https://doi.org/10.1016/j.measurement.2022.112278

[123] Dash, S., Tripathy, R. K., Dash, D. K., Panda, G., & Pachori, R. B. (2022). Multiscale Domain Gradient Boosting Models for the Automated Recognition of Imagined Vowels Using Multichannel EEG Signals. IEEE Sensors Letters, 6(11), 1–4. https://doi.org/10.1109/LSENS.2022.3218312

[124] Li, Y., Guo, L., Liu, Y., Liu, J., & Meng, F. (2021). A Temporal-Spectral-Based Squeeze-and- Excitation Feature Fusion Network for Motor Imagery EEG Decoding. IEEE Transactions on Neural Systems and Rehabilitation Engineering, 29, 1534–1545. https://doi.org/10.1109/TNSRE.2021.3099908

[125] Wang, H., Yu, H., & Wang, H. (2022). EEG_GENet: A feature-level graph embedding method for motor imagery classification based on EEG signals. Biocybernetics and Biomedical Engineering, 42(3), 1023–1040. https://doi.org/10.1016/j.bbe.2022.08.003

[126] Liu, C., Jin, J., Daly, I., Li, S., Sun, H., Huang, Y., Wang, X., & Cichocki, A. (2022). SincNet-Based Hybrid Neural Network for Motor Imagery EEG Decoding. IEEE Transactions on Neural Systems and Rehabilitation Engineering, 30, 540–549. https://doi.org/10.1109/TNSRE.2022.3156076

[127] Ma, W., Xue, H., Sun, X., Mao, S., Wang, L., Liu, Y., Wang, Y., & Lin, X. (2022). A novel multi-branch hybrid neural network for motor imagery EEG signal classification. Biomedical Signal Processing and Control, 77, 103718. https://doi.org/10.1016/j.bspc.2022.103718

[128] Jia, X., Song, Y., Yang, L., & Xie, L. (2022). Joint spatial and temporal features extraction for multi-classification of motor imagery EEG. Biomedical Signal Processing and Control, 71, 103247. https://doi.org/10.1016/j.bspc.2021.103247

[129] Ma, W., Wang, C., Sun, X., Lin, X., & Wang, Y. (2023). A double-branch graph convolutional network based on individual differences weakening for motor imagery EEG classification. Biomedical Signal Processing and Control, 84, 104684. https://doi.org/10.1016/j.bspc.2023.104684

[130] Luo, T. (2023). Parallel genetic algorithm based common spatial patterns selection on time–frequency decomposed EEG signals for motor imagery brain-computer interface. Biomedical Signal Processing and Control, 80, 104397. https://doi.org/10.1016/j.bspc.2022.104397

[131] Wang, J., Chen, W., & Li, M. (2023). A multi-classification algorithm based on multi-domain information fusion for motor imagery BCI. Biomedical Signal Processing and Control, 79, 104252. https://doi.org/10.1016/j.bspc.2022.104252

[132] Zhu, J., Zhu, L., Ding, W., Ying, N., Xu, P., & Zhang, J. (2023). An improved feature extraction method using low-rank representation for motor imagery classification. Biomedical Signal Processing and Control, 80, 104389. https://doi.org/10.1016/j.bspc.2022.104389